

**ELECTRICAL DOUBLE LAYER FORMATION IN
NANOPOROUS CARBON MATERIALS**

A Thesis
Presented to
The Academic Faculty

by

Chia-Hung Hou

In Partial Fulfillment
of the Requirements for the Degree
Doctor of Philosophy in the
School of Civil and Environmental Engineering

Georgia Institute of Technology
April 2008

Copyright 2008 by Chia-Hung Hou

**ELECTRICAL DOUBLE LAYER FORMATION IN
NANOPOROUS CARBON MATERIALS**

Approved by:

Dr. Sotira Yiacoumi, Advisor
School of Civil and Environmental
Engineering
Georgia Institute of Technology

Dr. Ching-Hua Huang
School of Civil and Environmental
Engineering
Georgia Institute of Technology

Dr. Costas Tsouris
School of Civil and Environmental
Engineering
Georgia Institute of Technology

Dr. Sankar Nair
School of Chemical and Biomolecular
Engineering
Georgia Institute of Technology

Dr. Spyros G. Pavlostathis
School of Civil and Environmental
Engineering
Georgia Institute of Technology

Date Approved: March 24, 2008

Dedicated to

My Beloved Family, Ying-Chih Hou, Mei-Hua Tsay, Chia-Chi Hou, and Chia-Chueh Hou

ACKNOWLEDGMENT

I would like to express my sincere gratitude to my advisor Dr. Sotira Yiacoumi for her guidance and encouragement that improved the presentation of this thesis. It is a great privilege to work with Dr. Yiacoumi because she gave me not only her advice in academic work but also her friendship on a personal level. I thank Dr. Costas Tsouris, Dr. Spyros G. Pavlostathis, Dr. Ching-Hua Huang, and Dr. Sankar Nair for being my committee members and for providing valuable comments and suggestions in this thesis. I am especially thankful to Dr. Tsouris for his support and for numerous discussions that helped my research forward. I thank Dr. Guangxuan Zhu for his assistance on experimental equipment. My appreciation is also given to Dr. Sheng Dai from the Oak Ridge National Laboratory for his valuable help and for giving me the opportunity to be exposed to nanoporous materials.

I am thankful to my lab mates, Viriya, Patricia, Eunyea, Douglas, and Hyojin, for their friendship during the past few years. I am especially grateful for Patricia, who has helped me enormously throughout my study at Georgia Tech. My thanks also go to my many friends, especially to Yu, Ying, LiLi, Wanru, KJ, Abow, Hunghao, Chunwan, and Vivian, who made my life at Georgia Tech joyful and created a piece of home for me in Atlanta.

I would like to give my deepest appreciation to my parents and sisters for their unselfish support and unconditional love that have enabled me to successfully complete my Ph.D. work.

TABLE OF CONTENTS

	Page
ACKNOWLEDGEMENTS	iv
LIST OF TABLES	ix
LIST OF FIGURES	x
LIST OF SYMBOLS AND ABBREVIATIONS	xvi
SUMMARY	xxi
 <u>CHAPTER</u>	
1 INTRODUCTION	1
1.1 Electrical Double Layer Formation	1
1.2 Scope and Objectives	4
1.3 Organization of Thesis	5
2 BACKGROUND	8
2.1 Application of Structured Carbon Materials for Industrial and Environmental Separations	8
2.2 Classical Electrical Double-Layer Theory	13
2.2.1 Historical Development of the Classical EDL Theory	13
2.2.2 Classical Theory for EDL formation in Nanopores	14
2.3 Monte Carlo Simulation Methods	21
2.3.1 Monte Carlo Integration	21
2.3.2 Canonical and Grand Canonical Ensembles for Electrolyte Systems	24
2.3.3 Monte Carlo Simulations of the Electrical Double Layer	30
2.3.4 Comparison of CMC Simulation Results and GC Theory Predictions	32

3	ELECTROSORPTION OF IONS FROM AQUEOUS SOLUTION USING NANOPOROUS CARBON MATERIALS	37
3.1	Introduction	38
3.2	Experimental Methods	40
3.2.1	Materials	40
3.2.2	Characterization	41
3.3	Model Development	42
3.4	Results and Discussion	45
3.4.1	Characterization of Carbon-Based Materials	45
3.4.2	Electrical Potential Distribution: Modeling Results	50
3.4.3	Effect of Diffuser-Layer and Inner-Layer Capacitances	53
3.4.4	Effect of Pore Size Distribution	56
3.5	Summary	59
4	MONTE CARLO SIMULATION OF ELECTRICAL DOUBLE-LAYER FORMATION FROM MIXTURES OF ELECTROLYTES INSIDE NANOPORES	61
4.1	Introduction	62
4.2	Model and Method	66
4.3	Results and Discussion	69
4.3.1	Comparison of the Classical GC Theory and Monte Carlo Simulation	69
4.3.2	EDL Behavior of a Symmetric Electrolyte in a Nanopore	71
4.3.3	EDL Behavior of an Asymmetric Electrolyte in Nanopores	73
4.3.4	EDL Behavior of Mixtures of Symmetric and Asymmetric Electrolytes in Nanopores at Low Surface Charge Density	75
4.3.5	EDL Behavior of Mixture Electrolytes in Nanopores at High Surface Charge Density	78
4.4	Summary	83

5	SIZE-EXCLUSION EFFECT ON PORE ACCESSIBILITY OF NANOPOROUS CARBON MEMBRANE	85
5.1	Introduction	86
5.2	Materials and Methods	89
5.2.1	Preparation and Characterization of Carbon Materials	89
5.2.2	Permeation Experiment	90
5.2.3	Electrochemical Measurement – Cyclic Voltammetry	92
5.3	Results and Discussion	93
5.3.1	Characterization of Carbon Membranes	93
5.3.2	Molecular-Sieving Effect	93
5.3.3	Ion-Size Effect	102
5.4	Summary	108
6	ELECTROSORPTION SELECTIVITY OF IONS FROM A MIXTURE OF ELECTROLYTES INSIDE NANOPORES	110
6.1	Introduction	111
6.2	Experimental Methods	115
6.2.1	Electrochemical Experiments	115
6.2.2	Equilibrium Experiments of Electrosorption	116
6.3	Grand Canonical Monte Carlo Simulation	118
6.4	Results and Discussion	121
6.4.1	Effects of Ion Properties on Electrosorption Behavior	121
6.4.2	Effects of Counterion Properties on Coion Exclusion of Single Electrolytes	126
6.4.3	Ion-Size Effects on Ion Selectivity in Mixtures of Electrolytes	131
6.4.4	Charge/Size Competitive Effects on Ion Selectivity of Mixture Electrolytes	135

6.5 Summary	141
7 CONCLUSIONS AND RECOMMENDATIONS	143
REFERENCES	149
VITA	159

LIST OF TABLES

	Page
Table 6.1: Experimental data obtained from the batch equilibrium experiments using carbon aerogel. The electrosorption experiments were performed in the following competitive environment of an electrolyte mixture of: (a) KCl and LiCl, and (b) KCl and CaCl ₂ .	124

LIST OF FIGURES

	Page
Figure 2.1: Schematic of the electrosorption process with the nanoporous carbon material to remove ionic species from aqueous solutions. The working principle is to impose an external electric field to force charged species toward oppositely charged electrodes. Cations and anions are then held in the double layer within nanoporous carbon materials.	11
Figure 2.2: Graphical representation of the EDL formation within the two charged solid surfaces of a slit-type nanopore. Counterions are specifically adsorbed at the charged surface and the fully hydrated cations and counterions constitute the inner layer and diffuser layer.	16
Figure 2.3: Schematic representation of the overlapping of two EDLs in a slit-type nanopore. The electrical potential distribution adjacent to an EDL is represented by the dashed line; the solid line is the resulting electrical potential distribution because of the overlapping of the two EDLs. The EDL is composed of the inner layer and diffuse layer. A fully hydrated counterion is held in the EDL without specific adsorption. The surface potential, diffuse potential, midplane potential, and pore width are represented by ψ_o , ψ_d , ψ_m , w , respectively.	19
Figure 2.4: Illustration of the application of the Monte Carlo simulation method for the calculation of the value of π by generating a number of trial shots, in which the ratio of the number of shots inside the circle to the total number of trial shots will approximately approach the ratio of the area of the circle to the area of the square.	23
Figure 2.5: Two-dimensional representation of periodic boundary condition. When an ion moves outside of the central simulation box through a boundary, the image ion is moved into the simulation box through the opposite boundary.	29
Figure 2.6: Schematic of the long-range correction for electrolyte systems, considering only x and y directions. Each ion inside the central simulation box has an associated charged sheet of infinite dimensions (less the square hole corresponding to the central simulation box), which accounts for the electrostatic interactions of the image ions outside the central simulation box.	31

- Figure 2.7: Ion concentration profiles obtained by the classical GC theory and the CMC simulation for 1:1 electrolyte of 0.1 M concentration at a high surface charge density of 0.64 C/m^2 . The local concentration of ion, C , is normalized over the bulk phase concentration C_0 . The classic GC theory fails to describe the second layer of counterions predicted by the CMC simulation. 35
- Figure 2.8: Comparison of ion concentration profiles obtained by the classical GC theory and CMC simulations for a single charged surface at 0.16 C/m^2 immersed in a 2:2 electrolyte at a concentration of 1.0 M. C and C_0 are the local concentration and the bulk concentration of ions, respectively. The CMC simulation results show the occurrence of charge inversion, while the classical GC theory cannot predict charge inversion. 36
- Figure 3.1: Pore size distribution of graphitized carbon, carbon aerogel type A, and carbon aerogel type B, which have specific surface areas of 487, 691, and $431 \text{ m}^2/\text{g}$, respectively. 46
- Figure 3.2: Specific capacitance of graphitized carbon in various NaF solutions measured by cyclic voltammetry at fast (5 mV/s) and slow (1 mV/s) scan rates. (a) NaF concentration: 0.01 M and (b) NaF concentration: 1 M.; (i) high resolution SEM image of the nanopores in the carbon skeleton and (ii) TEM image of the graphite strips within the carbon matrix obtained via STEM. 47
- Figure 3.3: Specific capacitance of carbon aerogel type A and B in a 0.01 M NaF solution measured by cyclic voltammetry at a slow (1 mV/s) scan rate. (i) TEM image of carbon aerogel type A, which is composed of interconnected aerogel particles, and (ii) high resolution SEM image of nanopores in the carbon matrix. 49
- Figure 3.4: Electrical potential distribution of the diffuse layer for a micropore of $10\text{-}\text{\AA}$ diameter for (a) a 0.01 M NaF solution and (b) around the pzc ($\psi_o = 0.01 \text{ V}$). The EDL overlapping effect diminishes with increasing surface potential and solution ionic strength. 51

- Figure 3.5: Effect of diffuse-layer and inner-layer capacitance on the double-layer capacitance in a 0.01 M NaF solution for (a) a mesopore of 100-Å diameter and (b) a micropore of 10-Å diameter. The double-layer capacitance, diffuse-layer capacitance, and inner-layer capacitance are represented by C_d , C_{dl} , and C_1 , respectively. The circles represent the double-layer capacitance without taking into consideration the thickness of the inner layer. 54
- Figure 3.6: The double-layer capacitance in terms of pore size distribution for the micropore region in a 0.01 M NaF solution and at various surface potentials for (a) graphitized carbon, (b) carbon aerogel type A, and (c) carbon aerogel type B. 57
- Figure 4.1: Comparison of ion concentration profiles in a slit-type nanopore of 20-Å diameter derived by the classical GC theory and Monte Carlo simulation techniques for a single 1:1 electrolyte of ionic strength of 1.0 M and a surface charge density of -0.1 C/m^2 . The value of C represents the local concentration of ions inside the pore. The value of C_0 is the average concentration of ions inside the pore in the absence of charge. 70
- Figure 4.2: Counterion and coion concentration profiles in a 20-Å-diameter nanopore for a single 1:1 electrolyte at (a) ionic strength of 0.5 M and surface charge density of -0.05 C/m^2 , (b) ionic strength of 1.0 M and surface charge density of -0.05 C/m^2 , and (c) ionic strength of 1.0 M and surface charge density of -0.1 C/m^2 . 72
- Figure 4.3: EDL structure in a 20-Å-diameter nanopore for an asymmetric 3:1 electrolyte at an ionic strength of 1.0 M and a surface charge density of 0.025 C/m^2 for (a) monovalent coions and trivalent counterions that have diameters of 4.25 Å and (b) monovalent coions and trivalent counterions that have diameters corresponding to 4.25 and 9.0 Å, respectively. 74
- Figure 4.4: EDL structure in a nanopore of 20-Å diameter for a mixture of 1:1 and 3:1 electrolytes at an ionic strength of 1.0 M and a surface charge density equivalent to -0.04 C/m^2 . The sizes of the ions selected are as follows: (a) trivalent and monovalent counterions with equal diameters (4.25 Å), (b) 9.0-Å-diameter trivalent counterions and 4.25-Å-diameter monovalent counterions, and (c) 4.25-Å-diameter trivalent counterions and 9.0-Å-diameter monovalent counterions. 77

- Figure 4.5: EDL structure in a nanopore of 100-Å diameter at a high surface charge density (-0.16 C/m^2) for a mixture containing 1:1 and 3:1 electrolytes at an ionic strength of 5.0 M. The sizes of the ions selected are as follows: (a) trivalent and monovalent counterions with equal diameters (4.25 Å), (b) 9.0-Å-diameter trivalent counterions and 4.25-Å-diameter counterions, and (c) 4.25-Å-diameter trivalent counterions and 9.0-Å-diameter monovalent counterions. 79
- Figure 4.6: EDL structure in a nanopore of 20-Å diameter at a high surface charge density (-0.16 C/m^2) for a mixture containing 1:1 and 3:1 electrolytes at an ionic strength of 5.0 M. The sizes of the ions selected are as follows: (a) trivalent and monovalent counterions with equal diameters (4.25 Å), (b) 9.0-Å-diameter trivalent counterions and 4.25-Å-diameter monovalent counterions, and (c) 4.25-Å-diameter trivalent counterions and 9.0-Å-diameter monovalent counterions. 81
- Figure 5.1: Schematic of the setup for permeation experiments with the carbon membrane. A UV-VIS spectrophotometer was used to measure the concentration of probe molecule in the receiver solution as a function of time. A photograph image reveals the size of our membranes synthesized for our experiments. 91
- Figure 5.2: (a) Nitrogen adsorption/desorption isotherms and (b) the pore size distribution plot of the mesoporous carbon membrane (STP, standard temperature and pressure). 94
- Figure 5.3: Single-component experiment for a source solution of 5 mM anilinium chloride transported through the mesoporous carbon membrane. (a) Absorbance spectra of anilinium recorded at the interval of 10 min. (b) Concentration of anilinium in the receiver solution as a function of time. 95
- Figure 5.4: Single-component experiment for a source solution of 5 mM rhodamine B transported through mesoporous carbon membrane. (a) Absorbance spectra of rhodamine B recorded at the interval of 10 min. (b) Concentration of rhodamine B in the receiver solution as a function of time. 97
- Figure 5.5: Two-component experiment for a source solution of the mixture of 5 mM anilinium chloride and 5 mM rhodamine B transported through mesoporous carbon membrane. (a) Absorbance spectra of anilinium and rhodamine B recorded at the interval of 10 min. (b) Concentration of test molecules in the receiver solution as a function of time. 101

Figure 5.6: Cyclic voltammetry experiments with the mesoporous carbon membrane immersed in various electrolyte solutions, including 0.1 M NaCl, 0.05 M MgCl ₂ , and 0.1 M THACl. The data were obtained at a slow scan rate of 1 mV/s.	103
Figure 5.7: Cyclic voltammetry experiments with the mesoporous carbon membrane immersed in various electrolyte solutions, including 0.1 M NaCl, 0.05 M MgCl ₂ , and 0.1 M THACl. The data were obtained at a fast scan rate of 10 mV/s.	104
Figure 6.1: Schematic of the setup for batch electrosorption equilibrium experiments. The electrosorption unit cell (detailed inset) consisted of: (1) a Plexiglas cover, (2) a titanium plate, (3) a carbon aerogel electrode, (4) a Viton gasket with hole, and (5) a central Plexiglas with hole for spacing between the two electrodes.	117
Figure 6.2: Schematic showing the geometry of the xz cross section of the simulation cell. The dimension of the simulation box is $W \times W \times L$ in the x, y, z directions, respectively. A surface charge density, σ_0 , is located in the xy planes at $z = 0$ and $z = L$. d_i and d_j correspond to the diameters of ions of different sizes. The system is periodic in the x and y directions, and the minimum image convention is employed in the x and y directions.	119
Figure 6.3: Specific capacitance of carbon aerogel measured by cyclic voltammetry using a slow scan rate of 1 mV/s for electrolyte solutions of 1.0 M KCl, 1.0 M LiCl, and 0.5 M CaCl ₂ .	123
Figure 6.4: Percent removal of ions from aqueous solutions obtained via batch equilibrium experiments using carbon aerogel. The study of electrosorption selectivity was based on ion properties in a mixture of electrolytes containing a common anion Cl ⁻ and: (a) monovalent cations K ⁺ and Li ⁺ , and (b) monovalent cation K ⁺ and divalent cation Ca ²⁺ . All experiments were conducted using a three-electrode electrosorption cell.	125
Figure 6.5: Exclusion parameter of coions from nanopores containing a 1:1 symmetric electrolyte: (a) as a function of pore size, and (b) as a function of surface charge density. The bulk electrolyte solution in each case has a concentration of 1 M. All coions and counterions have an equal size of 4.25-Å in all cases.	128

- Figure 6.6: Effects of size and charge asymmetry of counterions on coion exclusion from a 2-nm nanopore for symmetric and asymmetric electrolytes. The bulk electrolyte solutions contained the following species: (1) a 1:1 electrolyte with monovalent counterions and monovalent coions that have diameters corresponding to 3.62 and 4.25 Å, respectively, (2) a 1:1 electrolyte with monovalent counterions and monovalent coions that have diameters of 4.25 Å, or (3) a 1:2 electrolyte with divalent counterions and monovalent coions that have diameters corresponding to 5.8 and 4.25 Å, respectively. The bulk concentration of each of the counterions is 1 M in every case. The size of ions corresponds to: K^+ for 3.62 Å, Li^+ for 4.25 Å, and Ca^{2+} for 5.8 Å. 130
- Figure 6.7: Effect of surface charge density on (a) counterion selectivity and (b) coion exclusion for a mixture of two 1:1 electrolytes inside the pores. The equilibrium bulk electrolyte consists of 0.5 M smaller monovalent counterions of 3.62 Å, 0.5 M larger monovalent counterions of 4.25 Å, and 1.0 M monovalent coions of 4.25 Å. 132
- Figure 6.8: Ion concentration profiles for a mixture of two 1:1 electrolytes inside a slit-type nanopore of 2-nm diameter at surface charge densities of (a) 0 C/m^2 , (b) -0.05 C/m^2 , (c) -0.1 C/m^2 , and (d) -0.32 C/m^2 . The equilibrium bulk electrolyte consists of 0.5 M smaller monovalent counterions of 3.62-Å diameter, 0.5 M larger monovalent counterions of 4.25-Å diameter, and 1.0 M monovalent coions of 4.25-Å diameter. 134
- Figure 6.9: Effect of surface charge density on (a) counterion selectivity and (b) coion exclusion for a mixture of 1:1 and 1:2 electrolytes inside pores. The equilibrium bulk electrolyte consists of 0.5 M smaller monovalent counterions of 3.62-Å diameter, 0.5 M larger divalent counterions of 5.8-Å diameter, and 1.5 M monovalent coions of 4.25-Å diameter. 136
- Figure 6.10: Ion concentration profiles for a mixture of 1:1 and 1:2 electrolytes inside a slit-type nanopore of 2-nm diameter at surface charge densities of (a) 0 C/m^2 , (b) -0.05 C/m^2 , (c) -0.125 C/m^2 , and (d) -0.64 C/m^2 . The equilibrium bulk electrolyte consists of 0.5 M smaller monovalent counterions of 3.62-Å diameter, 0.5 M larger divalent counterions of 5.8-Å diameter, and 1.5 M monovalent coions of 4.25-Å diameter. 139

LIST OF SYMBOLS AND ABBREVIATIONS

a	Diameter of a fully hydrated ion
C_0	Solution concentration in the bulk phase; Solution average concentration in the pore in the absence of charge
C_1	Electrical capacitance of inner layer
C_{dl}	Electrical capacitance of electrical double layer
C_d	Electrical capacitance of diffuse layer
C_i	Average concentration of ion i in the pore
C_j	Average concentration of ion j in the pore
$C_{i,0}$	Concentration of ion i in the bulk solution
$C_{j,0}$	Concentration of ion j in the bulk solution
C_{pore}	Solution average concentration in the pore
D	Diffusion coefficient
D^0	Diffusion coefficient in the bulk solution
D_{pore}	Diffusion coefficient in the pore
d_i	Diameter of a hydrated ion i
dC	Concentration gradient
dx	Diffusion coordinate as the membrane thickness
e	Electrical charge of the electron
F	Definite Integral
f_{ij}	Acceptance probability from state i to j
f_{ji}	Acceptance probability from state j to i

$f(x)$	Generic function
I	Solution ionic strength
k	Boltzmann constant
L	Length of the simulation box
N_i	Number of ion i per unit volume
N_{i0}	Number of ion i per unit volume in the bulk solution
N^+	Number of positive ions in the bulk solution
N^-	Number of negative ions in the bulk solution
N_i^+	Number of positive ions in state i
N_i^-	Number of negative ions in state i
N_j^+	Number of positive ions in state j
N_j^-	Number of negative ions in state j
N_0	Total number of ions in the bulk solution
x	Direction perpendicular to the surface
z_i	Valence of ion i
q_i	Charge of ion i
q_j	Charge of ion j
R	Radius of a circle
R	Ideal gas constant
r	Radius of a molecule
r_{ij}	Distance between the centers of ions i and j
T	Absolute temperature
V	Volume of the simulation box

U_i	Configurational energy in state i
U_j	Configurational energy in state j
v_{LRC}	Long-range correction potential energy
v_1	Single-ion potential energy
v_2	Two-ion potential energy
v_{ij}	Pair interaction potential between ions i and j
v_+	Number of randomly chosen positive ions
v_-	Number of randomly chosen negative ions
v	Sum of v_+ and v_-
W	Width and height of the simulation box
w	Pore width
x	Generic variable; coordinate in the X direction
Y	Dimensionless electrical potential
Y_m	Dimensionless electrical potential at midplane between two surfaces
y	Coordinate in the Y direction
z	Valence of ions; coordinate in the Z direction
z_i	Position of ion i in the Z direction
α	Selectivity factor
β	$(kT)^{-1}$
γ_{\pm}	Mean activity coefficient of the electrolyte in the McMillan–Mayer system
ε	Dielectric constant
ε_0	Vacuum permittivity
ε_r	Relative dielectric permittivity

μ	Chemical potential of the electrolyte
η	Viscosity of water
Γ	Exclusion parameter
σ_0	Surface charge density
σ_1	Surface charge density of the first charged surface of the simulation box
σ_2	Surface charge density of the second charged surface of the simulation box
σ_i	Inner layer charge density
σ_d	Diffuse layer charge density
σ_{ij}	Maximum distance of approach between ions i and j
ζ_i	Random number
τ	Number of trails
ρ	Volume charge density
$\rho(x)$	Arbitrary probability distribution function
ψ	Electrical potential
ψ_0	Surface potential
ψ_d	Diffuse layer potential
ψ_m	Electrical potential at midplane between two surfaces
BET	Brunauer-Emmett-Teller
CMC	Canonical Monte Carlo
EDL	Electrical double layer
EDLC	Electrical double layer capacitor
GC	Gouy Chapman

GCMC	Grand canonical Monte Carlo
IHP	Inner Helmholtz plane
OHP	Outer Helmholtz plane
PB	Poisson-Boltzmann
pzc	Point of zero charge

SUMMARY

Electrical double layer (EDL) formation at the solid/electrolyte interface has many important implications in various physical, chemical, and biological systems. Environmental separation processes such as removal of heavy metals from aqueous solutions, electrosorption in groundwater remediation, capacitive desalination, as well as energy storage are based on the EDL formation inside nanopores. These processes are favored by using nanoporous carbon materials because of high surface area and good electrical conductivity. This research is focused on the microscopic phenomena of EDL formation in a restricted space of nanopores. Combination of experimental data and molecular simulations can improve the current state of knowledge with respect to the fundamental aspects of the EDL formation and its application for the separation of ions via electrosorption by nanoporous carbon materials.

In the first part of this thesis, the electrosorption behavior of nanoporous carbon materials was characterized by measuring the double-layer capacitance using cyclic voltammetry. Double-layer capacitance is much related to both the ion transport rate into pores and the number of ions in the pore solution at equilibrium with the bulk solution. The presence of micropores usually results in the occurrence of EDL overlapping, corresponding to a considerable loss of the double-layer capacitance. EDL overlapping decreases not only the ion transport rate but also the number of ions inside the pores at equilibrium. On the other hand, mesopores are more easily penetrated by ions. Moreover, an EDL model based on the classical Gouy-Chapman theory indicated that pore size distribution plays an important role in determining the double-layer capacitance. It

implies that the EDL formation could dominate ion transport and sorption inside nanopores as well as the pore accessibility.

In the second part of the thesis, molecular modeling based on canonical Monte Carlo (CMC) simulations was developed to quantify the effects of pore size and electrolyte properties on EDL formation in the confined space of nanopores. Simulation results indicated that, when dealing with a mixture of electrolytes, the competition in asymmetries of ion charge and size not only determines the screening of surface charge but also significantly affects the electrolyte distribution within charged pores. When the pore size is reduced, the double layers strongly overlap and the confinement effect enhances the distortion of EDL formation inside nanopores. In this case, multivalent counterions of large size are likely to be distributed in a more concave concentration profile in a restricted space. Furthermore, charge inversion can be found in the central region of the pores because the presence of multivalent counterions causes strong ion-ion interactions and asymmetries in charge and size. These results suggest that considering the ion-size effect is essential to identify the factors affecting EDL formation at the nanoscale.

In the third part of the thesis, laboratory scale experiments were conducted to test the size-exclusion effects on the transport and sorption of ions through nanoporous carbon membranes. The experimental data showed that the diffusion rate of small molecules is faster than that of large molecules because pore accessibility increases as the size of molecule decreases. In a mixture of large and small molecules, the competitive effect of two types of molecules in accessing the pores causes a retardation of diffusive transport of large molecules. By using cyclic voltammetry experiments, the size-

exclusion effects on the electrosorption of ions using nanoporous carbon materials were determined. A larger ion-exclusion volume prevents larger ions from accumulating in the double-layer region of the pores, and then, decreases the double-layer capacitance. This phenomenon implies that selective electrosorption of ions could be achieved inside nanopores under the influence of an electric field.

In the fourth part of the thesis, the electrosorption selectivity of ions involved in the EDL formation inside nanopores was studied via the grand canonical Monte Carlo (GCMC) method. The main advantage of GCMC simulations is that the electrolyte in a nanopore was assumed to be at equilibrium with an external bulk electrolyte solution. Thus, the total number of ions inside a nanopore can be unambiguously determined. As a result, the coion exclusion shows dependence on the proportion of different counterions present in the double-layer region. Moreover, in a mixture of electrolytes, the competitive effects of ion charge and size can determine the pore accessibility. Multivalent counterions with large size have the energetic advantage of screening surface charge. In contrast, small monovalent counterions present “size affinity” to access the pores. Therefore, electrosorption selectivity of counterions with different properties is a result of a counterbalance between minimization of potential energy and size-exclusion effects. Moreover, the data of equilibrium electrosorption experiments using nanoporous carbon materials supported the simulation results that selective electrosorption, imposed by the difference in hydrated ion size, occurs in a competitive environment.

The results obtained in this thesis provide insights into the fundamental mechanisms behind the EDL formation inside nanopores. This research has several

significant implications for the developing of advanced techniques for the selective separation of ions in environmental systems and energy storage in supercapacitors.

CHAPTER 1

INTRODUCTION

1.1 Electrical Double Layer Formation

Electrical double layer (EDL) is the cloud of ions, with high local concentration of counterions and low local concentration of coions, surrounding a charged surface. The thickness of the EDL is typically of a few nanometers (Hunter, 2001). This phenomenon is extremely important in various physical, chemical, and biological systems. For example, EDL formation has several important applications, such as energy storage and capacitive desalination, and is favored by electrode materials of high surface area and high electrical conductivity (Frackowiak and Béguin, 2001; Gabelich et al., 2003; Ying et al., 2002). The basic concept is that a charged porous surface in an aqueous solution leads to a potential difference across the solid/electrolyte interface in which ionic species can be held within the EDL. Moreover, separation of ionic species from aqueous solutions is extremely important in such environmental processes as removal of heavy metals from aqueous streams, water desalination, and ion selectivity of biological membranes.

EDL formation plays a crucial role in determining ion sorption and transport inside nanopores. When pore sizes approach molecular dimensions, EDL formation may be distorted by steric effects. This distortion is much associated with the occurrence of EDL overlapping. Under this condition, EDL extends across the entire pore region where counterions dominate the double-layer region and coions are partially excluded from the pores. This overlapping effect prevents ions from accessing the pores, and as a

consequence electrolyte exclusion is observed (Yang et al., 2001; Ying et al., 2002; Yang et al., 2003; Hou et al., 2006). More specifically, the ion transport rate through membranes that consist of nanopore channels can be determined by the thickness of EDL: only transport of counterions through the pores is expected (Jirage et al., 1997; Kuo et al., 2001). Therefore, selective transport and sorption may be achieved via manipulation of the EDL formation (i.e., electrical potential distribution and double-layer thickness) in the confined space of the pores. Studying such phenomena is very important for the development of technologies for ion separation processes in environmental systems.

The nature of electrolyte solutions such as ionic strength, ion charge, and ion size, has pronounced influence on EDL formation, as well as on electrochemical reactions and electrosorption of ions. For example, electrochemical measurements have shown that the relationship between the pore size of nanoporous electrodes and the ion size can determine the electrosorption behavior of nanoporous materials (Yang et al., 2003; Hou et al., 2006; Salitra et al., 2000; Eliad et al., 2001). In addition, charged platinum nanochannels exhibit molecular-sieving properties for halide ions, whose sorption capacity decreases as the ion size increases (Yang et al., 2002). This finding implies that the size-exclusion effect takes place in the restricted space of the pores and has potential applications in selective separations. In order to perform a realistic approach to the design of a separation process, it is necessary to identify the factors affecting ion transport and sorption from mixtures of electrolytes inside nanopores. This is because ions that have different properties may show competitive behavior to access the pores and to be preferentially sorbed onto the charged surfaces in the double-layer region.

The most-well known method to theoretically describe the EDL formation is based on the classical Gouy-Chapman (GC) theory, in which the electrostatic potential and the ion concentration profiles can be predicted through the solution of the Poisson-Boltzmann (PB) equation (Hunter, 2001). This theory, however, is only applicable to symmetric electrolytes under certain conditions such as low surface charge density, low electrolyte concentration, and for single electrolytes. The key drawback associated with the classical GC theory is the consideration of ions as simple point charges. The fact is that the ion size has a large effect on the EDL formation. Therefore, Monte Carlo simulation methods have shown to be a powerful technique for EDL studies without the simplifications related to the ion size considered in the classical GC theory (Torrie and Valleau, 1979; Torrie and Valleau, 1980). Torrie and coworkers performed a series of Monte Carlo simulations with the primitive model to investigate several interesting aspects of EDL formation next to a single, charged surface such as image effects, unequal ion sizes, and ions with high valences (Torrie et al., 1982; Valleau and Torrie, 1982; Torrie and Valleau, 1982). Their reported simulation results showed the limitations of the classical GC theory under several conditions, such as charge-symmetric (2:2) and charge-asymmetric (2:1) electrolytes or a charged surface immersed in high electrolyte concentrations or high surface charge (Torrie and Valleau, 1982). In addition, the use of the primitive model means that the solvent (water) is treated as a continuum of constant electrical permittivity and ions can be characterized by their hydrated radius. Therefore, Monte Carlo simulation methods using a primitive model are suitable to study the interfacial phenomenon of the EDL formation at the nanoscale because they have

comparative advantages of taking into consideration the ion-size effects and the ion-ion interactions.

Although many studies focused on the microscopic phenomena of sorption of electrolytes have been conducted, more work is needed to better understand the mechanisms behind EDL formation in a confined space in such processes as charging in electrical double layer capacitors (EDLCs), removal of contaminant form aqueous solutions with nanoporous carbon materials, and selective transport of ions through ionic channels and biological membranes. In the present work combination of experimental data and thermodynamic theories provide a more realistic approach to identify the factors (i.e., pore size and properties of electrolytes) affecting the EDL formation inside nanopores.

1.2 Scope and Objectives

This research combines experimental and modeling work (including classical GC theory and molecular simulations) to elucidate the fundamental mechanisms behind the EDL formation inside nanopores, associated with properties of ionic species. The focus is to examine the effects of pore properties (i.e., charge and size) in the presence of mixtures of symmetric and asymmetric indifferent electrolytes confined in nanopores. The hypothesis behind this research is that EDL formation in the confined space of the nanopores depends on the relationship between pore size and the properties of ionic species. Then, ions distributed in nanopores may be determined by several parameters such as pore size, surface charge density, electrolyte concentration, and properties of ionic species present in the double-layer region.

The overall objective of the research presented in this thesis is to understand the fundamental mechanisms behind EDL formation inside nanopores, with respect to selective separation of ions by electrosorption using nanoporous carbon-based materials.

The specific objectives are as follows:

1. Study the electrosorption behavior of nanoporous carbon materials immersed in various types of single electrolytes, including symmetric (1:1), size-asymmetric (1:1), and charge-asymmetric electrolytes, under an external electric field, via cyclic voltammetry experiments.
2. Assess the ability of nanoporous carbon materials to selectively separate ions of different characteristics from a mixture of electrolytes based on the competition between the effects of asymmetries of ion charge and size in the EDL.
3. Study the relationship between pore size and properties of electrolyte involved in the double-layer region in terms of ion sorption and transport in nanoporous carbon materials.
4. Develop theoretical methods using Monte Carlo simulations to investigate the competitive effects of charge and size asymmetries of different counterions on the EDL formation in the confined space of pores, in terms of ion concentration profiles, electrolyte exclusion, and electrosorption selectivity.

1.3 Organization of Thesis

Chapter 1 introduces the EDL formation at the nanoscale and the motivation of this research. Also, the scope and objectives of this work are discussed in this chapter.

A literature review related to the applications of nanoporous carbon materials in environmental systems is described in Chapter 2. Detailed descriptions for EDL studies of the classical GC theory and Monte Carlo simulations can be found in Chapter 2.

Chapter 3 describes a typical electrosorption behavior of structured carbon materials that are mainly composed of micropores (pore width less than 2 nm) and mesopores (pore width between 2 and 50 nm) in an external electric field. Accessibility of nanopores with different sizes is further characterized by measuring the double-layer capacitance via cyclic voltammetry experiments. Moreover, an extended EDL model based on the classical GC theory is developed to predict the electrical potential distribution inside the pores of nanoporous carbon materials. The effect of pore size distribution on the double-layer capacitance of nanoporous carbon materials is also discussed in Chapter 3.

The relationship between pore size and properties of electrolytes may dominate the EDL formation in a restricted space such as nanopores. In Chapter 4, molecular simulations based on canonical Monte Carlo (CMC) methods, using the primitive model, are developed to study EDL formation inside a slit-type nanopore. Through the application of the primitive model, ions are modeled as hard charged spheres in a dielectric continuum (water). Thus, the difference in the hydrated size of ions present in the double-layer region can be taken into account in the presence of mixtures of different counterions. Simulation results are expected to provide insights into the characteristics of EDL (i.e., ion concentration profile and screening of charged surface) inside nanopores, as well as into the size-exclusion effects on the competitive behavior between monovalent and multivalent ions.

In Chapter 5, laboratory scale experiments are performed to investigate the size-sieving properties of a nanoporous carbon membrane with respect to the pore accessibility in terms of transport and sorption of ions. First, we expect to prove that the size-exclusion effects can determine the diffusion behavior of molecules transported through the membrane, via single- and two-component permeation experiments. Second, a series of voltammetry experiments are conducted to study the size-exclusion effect on the electrosorption behavior of ions of different sizes under an externally applied electric field. These experimental data are used to support the theoretical calculations in this research.

Chapter 6 comprises the development of advanced molecular modeling based on grand canonical Monte Carlo (GCMC) simulation that provides deep insight into the EDL formation of mixtures of electrolytes confined in nanopores. In this modeling work, ions distributed in the pore solution are assumed to reach equilibrium with an external bulk electrolyte. This means that the total number of different ions that are present in the double-layer region of the pores can be unambiguously quantified. Based on this comparative advantage, competitive effects of ion charge and ion size on the electrosorption selectivity for a mixture of symmetric and asymmetric electrolytes can be discussed. In addition, batch equilibrium experiments of electrosorption for mixtures of electrolytes are qualitatively compared with the simulation results.

The major conclusions of this research and recommendations for future studies are stated in Chapter 7.

CHAPTER 2

BACKGROUND

2.1 Application of Structured Carbon Materials for Industrial and Environmental Separations

Carbon materials of nanoporous structures such as activated carbon, carbon fiber, carbon aerogel, and graphite are ubiquitous and indispensable in various technologies. These carbon materials usually have high internal surface area and large pore volume. The porous structure is one of the most important characteristics. According to the nomenclature of the International Union of Pure and Applied Chemistry (IUPAC), the pores in a porous carbon material can be classified as micropores (pore width less than 2 nm), mesopores (pore width between 2 and 50 nm), and macropores (pore width larger than 50 nm). Because carbon materials are polarizable, their good electrical conductivity becomes a very desirable electrochemical property. Due to the combination of their high surface area and unique physicochemical properties, nanoporous carbon materials are widely used as molecular sieves for gas separation, as sorbents for separation processes, and as electrode materials for batteries, fuel cells, and supercapacitors (Koresh and Soffer, 1979; Mayer et al., 1993; Frackowiak and Béguin, 2001). Furthermore, many processes have taken advantage of the combination of the physical and electrochemical properties of nanoporous carbon materials in many applications including removal of organic compounds from aqueous solutions (Karanfil et al., 2006; Ania and Béguin, 2007), gas purification (Koresh and Soffer, 1987), groundwater remediation (Farmer et al., 1997),

wastewater treatment (Bán et al., 1998), and water desalination (Gabelich et al., 2002; Ying et al., 2002).

Molecular sieves can be defined as substances containing discrete pore structures that separate the molecules on the basis of their size. Koresh and Soffer (1980) reported that carbon molecular sieving with the pore structure in the range from 0.3 nm to 0.5 nm can serve for estimating the dimensions of gas molecules such as CO₂, O₂, C₂H₂, H₂, N₂, CO, Xe, and SF₆. By selecting a pore size distribution with respect to the target molecules, activated carbons and carbon molecular sieves can be used as separators for gas purification. The mechanism of molecular sieving is based on the fact that molecules of different sizes present differences in their adsorption capacity at equilibrium and diffusion rate. For example, a mixture of methane and hydrogen gases can be successfully separated by using a molecular-sieving carbon because methane molecules with larger size show preferential adsorption and poor permeability through the carbon porous material (Koresh and Soffer, 1987).

Applications of nanoporous carbon materials as electrode materials for electrical double layer capacitors (EDLCs) or supercapacitors have been extensively developed due to the increasing demand for a new kind of storage of electrical energy with high power density and long durability for application in hybrid power sources for electric vehicles (Frackowiak and Béguin, 2001). Consisting of a pair of ideally polarizable carbon electrodes, the energy storage device is associated with a rapid charging/discharging process and to store and release large quantities of energy via the formation of electrical double layer (EDL) across the electrode/electrolyte interface. The mechanism is based on the fact that charges are separated by a very short distance (in the range of nanometers)

within high porous carbon materials, in which the accumulation of charged species is mainly induced by electrostatic forces without phase transformation on the surface. The capacitor performance, which can be characterized via the double-layer capacitance at the interface of the carbon and the electrolyte, is generally proportional to the accessible surface area of an EDLC. A porous carbon material with a higher surface area may contribute to more electrical energy stored in an EDLC. In addition, an ideal double layer capacitance behavior of porous carbon materials represents a rectangular shape of the voltammetry characteristics, where Faradaic reactions do not take place over the potential range of operation, and all the charged species are accumulated in the EDL across the electrode/electrolyte interface. Under this condition, the phenomenon is mainly electrostatic and reversible and the double-layer capacitance is independent of potential (Frackowiak and Béguin, 2001).

Molecular sieving carbons or nanostructured carbons can be potentially applied for electrosorption (defined as potential-induced sorption on the surface) for selective separation of ionic species in aqueous solutions. One of the example applications is water purification. Farmer et al. (1996; 1997) have shown that electrosorption by using carbon aerogel electrodes can effectively remove ions such as sodium, chloride, chromium and ammonium from water. Figure 2.1 shows the working principle of this separation process within an electrosorption cell, which is composed of a pair of porous carbon sheets with opposite charge, referred to as anode and cathode. During the operation, an external electric field is applied across the high porous carbon electrodes to force ionic species toward oppositely charged electrodes: one electrode is positively charged to remove anions, and the other electrode is negatively charged to remove cations.

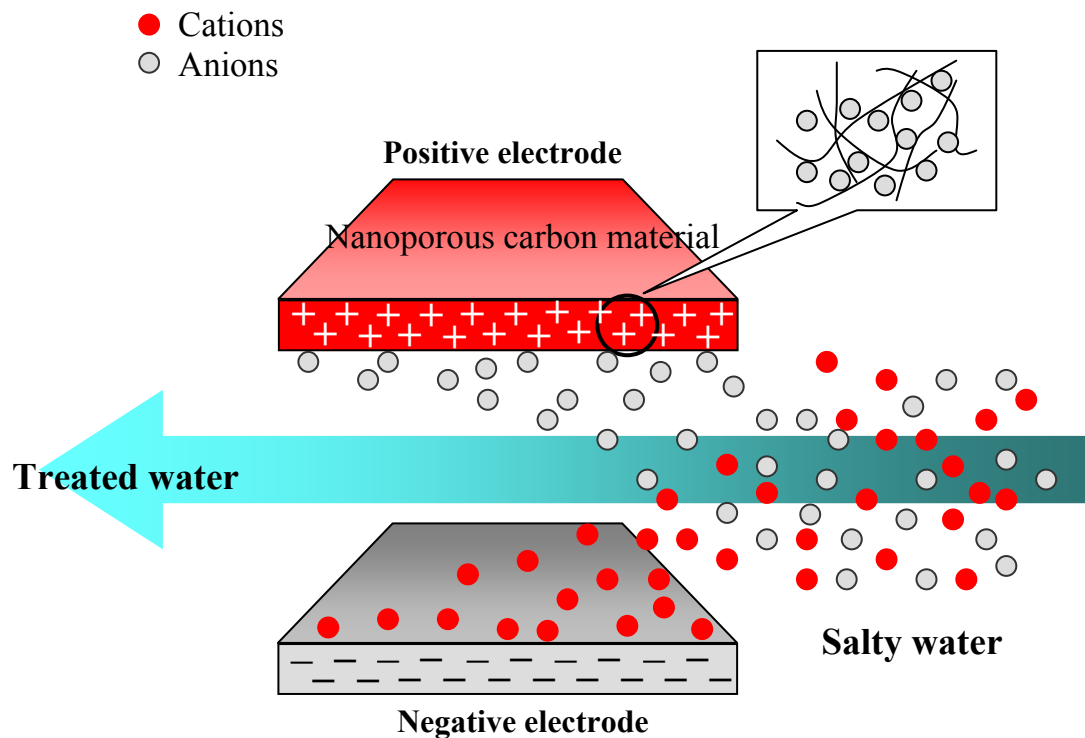


Figure 2.1. Schematic of the electrosorption process with the nanoporous carbon material to remove ionic species from aqueous solutions. The working principle is to impose an external electric field to force charged species toward oppositely charged electrodes. Cations and anions are then held in the double layer within nanoporous carbon materials.

After polarization of the electrodes takes place, charged species (e.g., ionic species and charged organic molecules) are electrostatically removed from water and held in the double layer formed at the carbon surfaces. The thickness of the EDL is typically from 1 to 10 nm, depending on the ionic strength of the solution and the surface charge. Therefore, the water leaving the electrosorption cell has been purified via the removal of the charged dissolved species. After nanoporous carbon electrodes become saturated with charged species, the electrodes are regenerated by electrical discharge and the ions are quickly released to bulk solution. Electrosorption processes have several advantages over existing ion-removal techniques (e.g., reverse osmosis, ion-exchange, and evaporation), including high capacity, no secondary waste, long-term reproducibility, and reversibility.

When the pore size approaches the same order of magnitude as the EDL thickness, the double layers of the inner walls of the pores may overlap. Since high porous carbon materials consist mainly of mesopores and micropores, the effect of EDL overlapping becomes significant and must be taken into consideration. For example, the occurrence of EDL overlapping in micropores may decrease the effective surface area available for electrosorption of ionic species, and then, the electrosorption capacity of carbon materials decreases (Ying *et al.*, 2002). The double-layer capacitance can further be reduced by this overlapping effect (Yang *et al.*, 2003). Additionally, the removal of ionic species can be determined by their molecular size, more specifically, by the ratio of ionic size to pore diameter. It was demonstrated that monovalent ions (e.g., sodium) with smaller hydrated radii were more effectively removed from solution than multivalent ions with larger radii (e.g., calcium) (Gabelich *et al.*, 2002).

In summary, charging of double-layer capacitors and electrosorption process are highly dependent on the EDL formation within nanoporous carbon materials. Therefore, the studies relevant to EDL formation inside nanopores are very important. Applications of the classical theory and Monte Carlo molecular simulations can provide insights into the fundamental mechanism behind EDL formation, associated with properties of ionic species. These methods will be described in the following sections 2.2 and 2.3.

2.2 Classical Electrical Double-Layer Theory

2.2.1 Historical Development of the Classical EDL Theory

When a charged surface is immersed in an aqueous electrolyte solution, a surrounding cloud of counterions forms (i.e., a region where ions bearing opposite charge to that of the surface accumulate). The coions, or ions bearing the same charge as the surface, are driven away from the electrode/electrolyte interfacial region. Therefore, this interfacial region constitutes a well defined capacitor, or parallel fluid layers, where charge separation occurs.

The earliest theoretical studies of the behavior of EDL are usually attributed to Helmholtz, who developed a model describing the EDL over a century ago. He treated the double layer as a capacitor, in which one plate is constituted by a single layer of adsorbed ions on the surface, referred to as the Helmholtz plane, and the second plate constitutes the plane of bulk solution where the net charge is zero (Hamann *et al.*, 1998). The location of the Helmholtz plane is found at a distance coinciding with the plane going through the center of the adsorbed ions (Hamann *et al.*, 1998), which are assumed to be spherical. The Helmholtz layer model was incomplete because it does not take into

account the mobility of the ions, i.e., there is no definite separation of charge into planes, but rather a continuous cloud where charge goes from a finite value at the interface to zero at the bulk solution. Therefore, Gouy and Chapman subsequently extended the EDL model by taking into consideration the effect of thermal motion of ions near a charged surface. A diffuse (Gouy-Chapman) double layer, in which counterions predominate over coions but coions are not completely excluded, was introduced. The electrical potential distribution in this region decreases exponentially, and not linearly as in an electric capacitor. Finally, Stern combined the Helmholtz single-adsorption layer and Gouy-Chapman diffuse-layer models into what is referred to as the classical EDL theory. Another important concept proposed by Stern is that the position of the Helmholtz plane depends on the type of ions attracted to the surface: fully hydrated ions or dehydrated ions that are believed to have undergone specific adsorption (Hamann, 1998).

Consequently, the distribution of ions in the electrode/electrolyte interface can be determined by three factors: (i) electrostatic (Coulombic) forces, (ii) thermal diffusion, i.e., motion due to concentration gradient, and (iii) specific interactions, i.e., physical/chemical adsorption. There are four important approximations adopted by the classical EDL theory: (i) ions are treated as point charges, (ii) the only significant interactions are Coulombic interactions, (iii) ion-ion interactions are not taken into account, and (iv) the electrical permittivity is constant in the double layer.

2.2.2 Classical Theory for EDL Formation in Nanopores

The thickness of EDL usually varies from 100 nm in a dilute solution to a few Angstroms in a concentrated solution (Hunter, 1985). If the distance between a pair of

parallel charged plates decreases towards the nanoscale, such as in a slit-type nanopore, it is expected that the two double layers will overlap. Because the high surface area of porous carbon materials derives from their nanoporous structures (mainly attributed to mesopores and micropores), the overlapping of EDLs may play a very important role to determine their performance under an electric field.

Figure 2.2 shows the schematic representation of EDL formation in a slit-type nanopore, in which the interface can be divided into an inner region (Stern layer) and an outer region (diffuse layer). In the inner layer, the ions are immobilized because they are either strongly attracted to the surface due to electrostatic interactions, or specifically adsorbed onto the charged surface due to van der Waals force, hydrogen bonding, or other mechanisms. By definition, the inner Helmholtz plane (IHP) is assumed to be the locus of the centers of specifically adsorbed dehydrated ions (Hunter, 2001). On the other hand, the outer Helmholtz plane (OHP), in which the diffuse layer begins, is the locus of the closest approach of hydrated counterions. The diffuse layer is composed of the mobile ions and their distribution depends on the electrostatic interaction and on thermal diffusion.

In the region of the diffuse layer, the relationship between the electrical potential drop and the charge density can be described by the Poisson equation for a one-dimensional system:

$$\frac{d^2\psi}{dx^2} = -\frac{\rho}{\varepsilon} \quad (2.1)$$

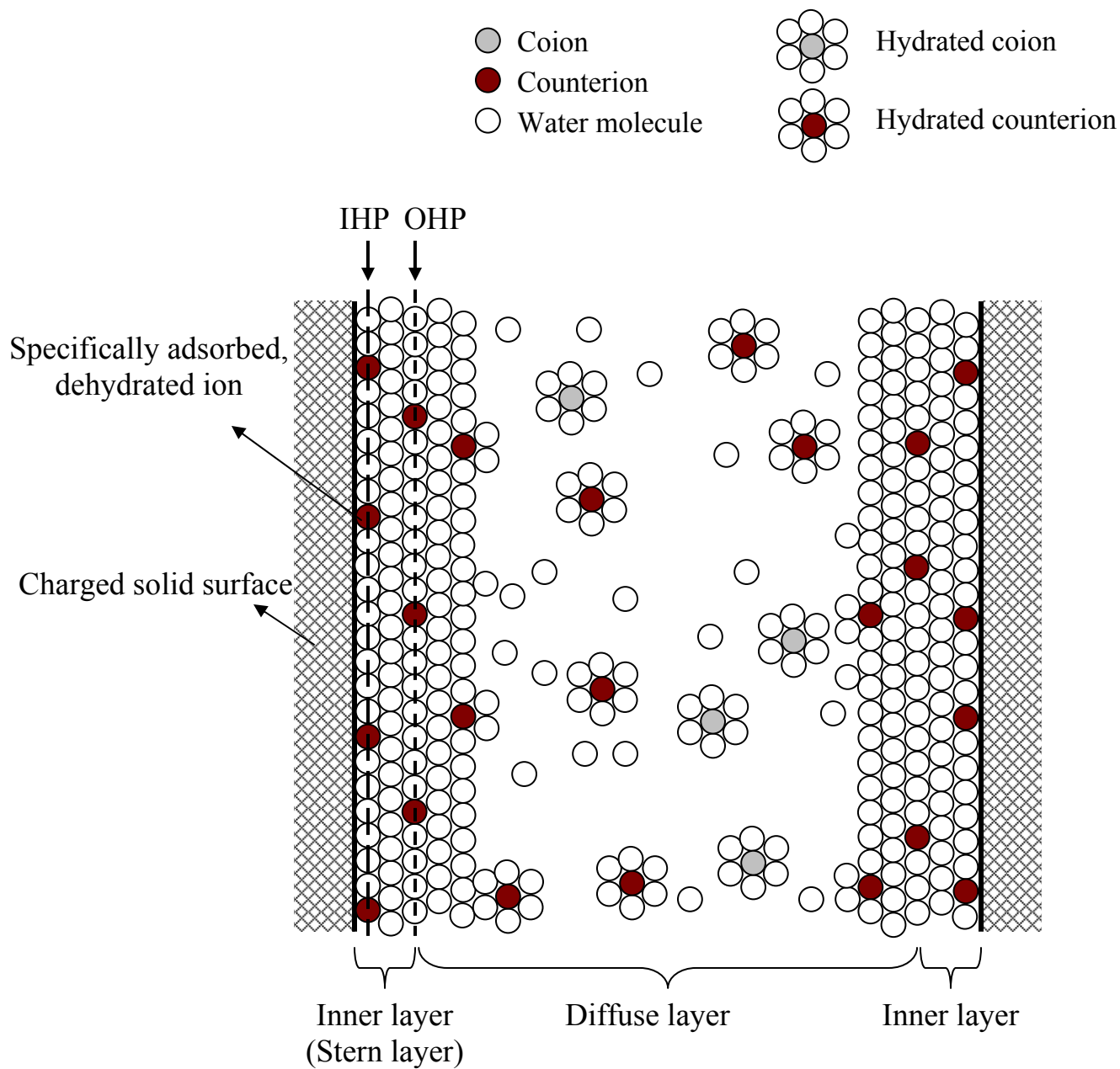


Figure 2.2. Graphical representation of the EDL formation within the two charged solid surfaces of a slit-type nanopore. Counterions are specifically adsorbed at the charged surface and the fully hydrated coions and counterions constitute the inner layer and diffuser layer.

where x is the direction perpendicular to the surface, ψ is the relative electrical potential in the diffuse layer, ρ is the volume charge density in the system, and ε is the dielectric constant of the medium, respectively.

The ion distribution in the region of the diffuse layer is affected by the electrical potential. According to the Boltzmann distribution, the number of ions of type i per unit volume, N_i , is expressed by:

$$N_i = N_{i0} \exp\left(-\frac{z_i e \psi}{kT}\right) \quad (2.2)$$

In this expression, N_{i0} is the bulk concentration of ions, z_i is the valence of ion i , e is the electrical charge of the electron, k is the Boltzmann constant, and T is the absolute temperature.

The volume density of charge is given as follows:

$$\rho = \sum_i N_i z_i e = \sum_i z_i e N_{i0} \exp\left(-\frac{z_i e \psi}{kT}\right) \quad (2.3)$$

By combining equations 2.2 and 2.3, the Poisson-Boltzmann (PB) equation, referred to as one of the most important equations of statistical physics, can be obtained:

$$\frac{d^2 \psi}{dx^2} = \frac{-1}{\varepsilon} \sum_i z_i e N_{i0} \exp\left(-\frac{z_i e \psi}{kT}\right) \quad (2.4)$$

For a symmetric $z : z$ electrolyte system, equation 2.4 can be reduced to the following expression:

$$\frac{d^2\psi}{dx^2} = \frac{2zeN_0}{\varepsilon} \sinh\left(\frac{ze\psi}{kT}\right) \quad (2.5)$$

The classical Gouy-Chapman (GC) theory provides a description of the electrical potential distribution in the diffuse layer, but it is not an accurate representation of the EDL formation in pores because it does not take into account the effect of EDL overlapping. Yang *et al.* (2001) extended the classical EDL theory by considering a double-layer overlapping correction.

As the distance between two charged surfaces decreases, the electrical potentials from the double layers begin to overlap. As shown in Figure 2.3, the net electrical potential in the region of the diffuse layer arises from the contribution of each EDL. If the thickness of the inner (Stern) layer is small compared to the pore width w , it is reasonable to assume that the diffuse layer boundaries are located at $x = +w/2$ and $x = -w/2$. Therefore, the electrical potential profile, ψ , between the two surfaces can be obtained using the PB equation via the application of the following boundary conditions (Yang *et al.*, 2001):

$$\frac{d\psi}{dx} = 0 \quad \text{and} \quad \psi = \psi_m \quad \text{at} \quad x = 0 \quad (2.6a)$$

$$\psi = \psi_d \quad \text{at} \quad x = \pm \frac{w}{2} \quad (2.6b)$$

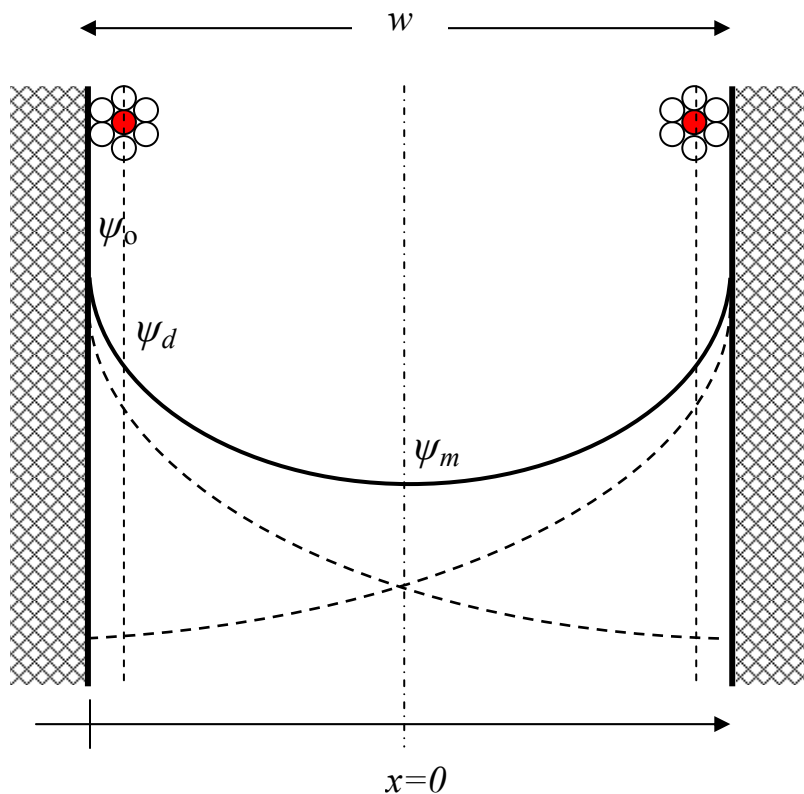


Figure 2.3. Schematic representation of the overlapping of two EDLs in a slit-type nanopore. The electrical potential distribution adjacent to an EDL is represented by the dashed line; the solid line is the resulting electrical potential distribution because of the overlapping of the two EDLs. The EDL is composed of the inner layer and diffuse layer. A fully hydrated counterion is held in the EDL without specific adsorption. The surface potential, diffuse potential, midplane potential, and pore width are represented by ψ_0 , ψ_d , ψ_m , and w , respectively.

where ψ_m is the electrical potential at the midplane and ψ_d is the diffuse layer potential, respectively.

In the double layer, charge balance requires that (Hunter, 2001):

$$\sigma_0 + \sigma_i + \sigma_d = 0 \quad (2.7)$$

where σ_0 , is the surface charge density, σ_i , is the inner layer charge density, and σ_d is the diffuse layer charge density, respectively.

When there is no specific adsorption in the inner layer, only the OHP is considered in the model, and the thickness of the inner layer corresponds to half the diameter of the hydrated counterions. In this case, the charge density in the inner layer is assumed to be zero (Hunter, 2001). Due to electroneutrality, the magnitude of the charge density at the surface is the same as that of the diffuse layer, which is written as (Yang et al., 2001):

$$\sigma_0 = -\sigma_d = (4\varepsilon RTI)^{1/2} \left[\cosh\left(\frac{e\psi_d}{kT}\right) - \cosh\left(\frac{e\psi_m}{kT}\right) \right]^{1/2} \quad (2.8)$$

where R is the ideal gas constant and I is the ionic strength.

If σ_0 is small, the connection between the surface potential (ψ_0) and the diffuse layer potential (ψ_d) is given by the following equation (Yang, 2003):

$$\psi_d = \psi_0 - \frac{\sigma_0}{C_1} \quad (2.9)$$

where C_1 is the inner layer capacitance.

By definition, the double-layer capacitance, C_{dl} , can be expressed as (Hunter, 2001):

$$C_{dl} = \left(\frac{\partial \sigma_0}{\partial \psi_0} \right) \quad (2.10)$$

In general, the EDL behavior can be considered as an electrical capacitor, which behaves as a pair of series combination of diffuse layer and inner layer capacitors. In the case that specific adsorption is absent,

$$\frac{1}{C_{dl}} = \frac{1}{C_d} + \frac{1}{C_1} \quad (2.11)$$

where C_d is the diffuse layer capacitance.

2.3 Monte Carlo Simulation Methods

2.3.1 Monte Carlo Integration

The name “Monte Carlo” was chosen because of the extensive use of random numbers in the calculations (Allen and Tildesley, 1987). One of the better known applications of Monte Carlo simulations consists of the evaluation of integrals by generating suitable random numbers that will fall within the area of integration.

A simple example of how a Monte Carlo simulation method is applied to evaluate the value of π is illustrated in Figure 2.4. By considering a square that inscribes a circle of a diameter R , one can deduce that the area of the square is R^2 , and the circle has an area of $\pi R^2/4$. Thus, the relative area of the circle and the square will be $\pi/4$. A large number of two independent random numbers (with x and y coordinates) of trial shots is generated within the square to determine whether each of them falls inside of the circle or not. After thousands or millions of trial shots, the computer program keeps counting the total number of trial shots inside the square and the number of shots landing inside the circle. Finally, the value of $\pi/4$ can be approximated based on the ratio of the number of shots that fall inside the circle to the total number of trial shots.

As stated earlier, the value of an integral can be calculated via Monte Carlo methods by generating a large number of random points in the domain of that integral. Equation 2.12 shows a definite integral:

$$F = \int_a^b f(x)dx \tag{2.12}$$

where $f(x)$ is a continuous and real-valued function in the interval $[a, b]$. The integral can be rewritten as (Allen and Tildesley, 1987):

$$F = \int_a^b dx \left(\frac{f(x)}{\rho(x)} \right) \rho(x) \cong \left\langle \frac{f(\zeta_i)}{\rho(\zeta_i)} \right\rangle_\tau \tag{2.13}$$

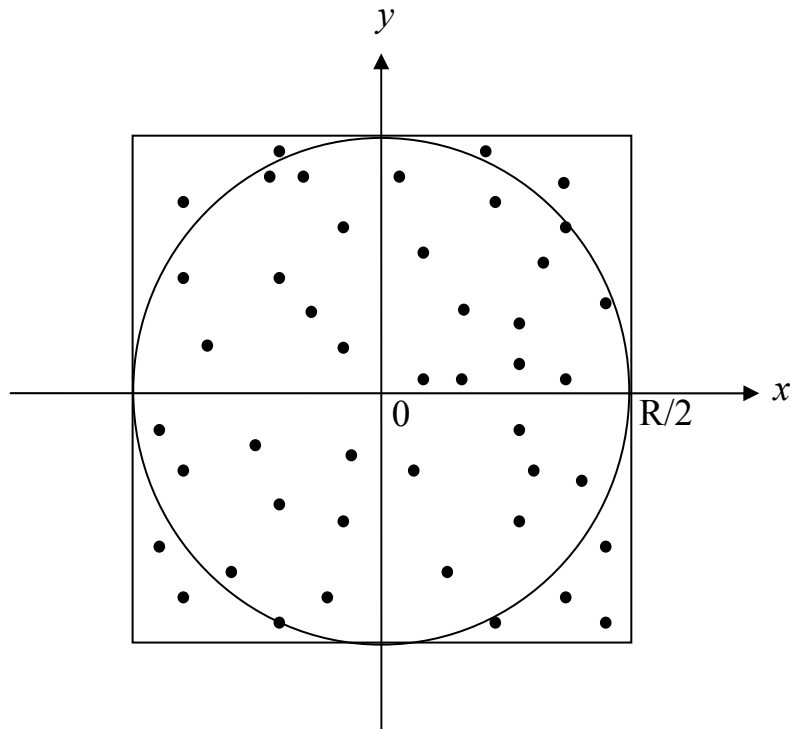


Figure 2.4 Illustration of the application of the Monte Carlo simulation method for the calculation of the value of π by generating a number of trial shots, in which the ratio of the number of shots inside the circle to the total number of trial shots will approximately approach the ratio of the area of the circle to the area of the square.

where $\rho(x)$ is an arbitrary probability distribution function, ζ_i corresponds to the random numbers generated for each trial in the interval $[a,b]$, and τ represents the number of trials. If the probability function is chosen to be a continuous uniform distribution, then:

$$\rho(x) = \frac{1}{(b-a)} \quad a \leq x \leq b \quad (2.14)$$

Subsequently, the integral, F , can be approximated as:

$$F \approx \frac{(b-a)}{\tau} \sum_{i=1}^{\tau} f(\zeta_i) \quad (2.15)$$

In a similar way to the Monte Carlo integration methods, Monte Carlo molecular simulation methods rely on the fact that a physical system can be defined to possess a definite energy distribution function, which can be used to calculate thermodynamic properties. Two important definitions of systems in terms of their distribution functions, i.e, canonical ensemble and grand canonical ensemble, will be introduced in the following section 2.3.2.

2.3.2 Canonical and Grand Canonical Ensembles for Electrolyte Systems

In the present work, Monte Carlo simulations will be used to compute the equilibrium properties of electrolytes using the primitive model, in which ions are treated as charged hard spheres and water is considered as a continuum. The only discrete

entities in the simulation box are the ions. In this case, one must make sure that electroneutrality is maintained inside the simulation box.

For ionic systems, the energy state of the primitive electrolyte system is composed of a hard sphere interaction ($r_{ij} < \sigma_{ij}$) and a Coulombic interaction ($r_{ij} \geq \sigma_{ij}$) (Yang et al., 2002; Taboada-Serrano et al., 2005). The potential energy of interaction v_{ij} between ions, i and j , separated by a distance, r_{ij} , is given by:

$$v_{ij} = \begin{cases} +\infty & r_{ij} < \sigma_{ij} \\ \frac{q_i q_j}{4\pi\epsilon_0\epsilon_r r_{ij}} & r_{ij} \geq \sigma_{ij} \end{cases} \quad (2.16)$$

where q_i and q_j correspond to the charges of ions i and j , σ_{ij} is the maximum distance of approach between ions i and j , and ϵ_0 and ϵ_r are the vacuum and relative permittivity of the dielectric continuum, respectively.

In order to implement the Monte Carlo simulation, the first step is to determine a type of ensemble. In the canonical Monte Carlo (CMC) ensemble, the systems have a fixed number of ions (N) in a given volume (V) and at a fixed temperature (T). The change in potential energy is monitored within a Markov chain composed of trial moves of all the individual atoms or molecules forming the system. Each trial move within the Markov chain involves the displacement of a randomly selected ion along each of the coordinate directions. In the Markov chain, the new state i after each trial move is conditionally independent of every previous state j . The probability associated with the transition from state i to state j is given by the canonical probability distribution function.

The acceptance probability, f_{ij} , of each trial move of an ion is given as (Valleau and Cohen, 1980; Allen and Tildesley, 1987):

$$f_{ij} = \min\{1, \exp[-\beta(U_j - U_i)]\} \quad (2.17)$$

where $\beta = (kT)^{-1}$, and U_i and U_j correspond to the configurational energy of the states i and j . In other words, if the trial move results in a configuration with a lower associated energy, the attempted move is always accepted. If the move results in a configuration with a higher associated energy, the attempted move is accepted with the canonical probability that decreases exponentially with the change in configurational energy.

In the case of the grand canonical Monte Carlo (GCMC) ensemble, the chemical potential (μ) of the system is fixed at a constant volume (V) and a constant temperature (T). By carrying out Monte Carlo simulations of a system at a constant chemical potential, the bulk properties of the electrolyte can be determined unambiguously. The GCMC technique presents comparative advantages for the study of the properties of an electrolyte distributed in the interfacial region or between charged surfaces because the electrolyte system is kept at a constant chemical potential and is allowed to reach equilibrium with an external bulk phase (Valleau and Cohen, 1980; William and Snook, 1980; Vlachy and Haymet, 1989). For each GCMC trial step, there are three different types of moves (Valleau and Cohen, 1980; Allen and Tildesley, 1987):

- (i) An ion is moved to a new position using the method described in the CMC ensemble. The acceptance probability is described by equation 2.17.

(ii) A neutral ion pair is added to the system at a random position. In the system, the electrolyte dissociates into positive ions with ν_+ charge and negative ions with ν_- charge. N^+ and N^- represent the numbers of positive ions and negative ions of the bulk electrolyte solution. In the state i , the numbers of counterions and coions are N_i^+ and N_i^- , respectively. The j^{th} state will consist of N_j^+ positive ions and N_j^- negative ions, in which $N_j^+ = N_i^+ + \nu_+$ and $N_j^- = N_i^- + \nu_-$. Therefore, in order to keep electroneutrality at all times, for each trial move, a pair of neutral ions ν ($\nu \equiv \nu_+ + \nu_-$) are introduced into the system to maintain electroneutrality. The associated probability (f_{ij}) between states i and j , in between which a neutral ion pair has been added, is given as (Valleau and Cohen, 1980):

$$f_{ij} = \min\{1, f_{ij} / f_{ji}\} \quad \text{for addition} \quad (2.18a)$$

$$f_{ij} / f_{ji} = \frac{N_i^+ N_i^-}{N_j^+ N_j^-} \exp[B - \beta(U_j - U_i)] \quad (2.18b)$$

The particular value of B can be defined as (Valleau and Cohen, 1980):

$$\begin{aligned} B &= \beta(\mu - \mu_{ideal}) + \ln N^{+\nu_+} N^{-\nu_-} \\ &= \nu \ln \gamma_{\pm} + \ln N^{+\nu_+} N^{-\nu_-} \end{aligned} \quad (2.19)$$

where γ_{\pm} is the activity coefficient of the electrolyte in the McMillan–Mayer system.

(iii) A neutral pair of ions is randomly selected and removed from the system. The associated probability (f_{ji}) between states j and i , in between which an ion pair has been removed, is given as (Valleau and Cohen, 1980):

$$f_{ji} = \min\{1, f_{ji} / f_{ij}\} \quad \text{for deletion} \quad (2.20)$$

Because computer simulations are usually performed on a limited number of ions, the use of periodic boundary conditions is essential to simulate bulk electrolyte solution. By applying periodic boundary conditions, a small system with a number of ions from 100 to 10000 (e.g., a simulation box) can represent a large system that consists of a large number of ions, on the order of the Avogadro's number (6.023×10^{23}). Figure 2.5 shows the periodic boundary conditions applied in a two-dimensional system, in which the central simulation box is replicated throughout space to form an infinite lattice. There are no walls at the boundary of the central box. When an ion moves in the central box, its periodic image in the neighbor boxes has the exactly same movement.

In the case of electrolytes, the implementation of the minimum image technique for the determination of the system's energy enables the simulation results to be independent of the dimension of the simulation boxes (Torrie and Valleau, 1980; Van Megan and Snook, 1980). Therefore, the minimum image technique is highly recommended when dealing with electrolyte solutions. The most important interaction to be taken into consideration when implementing the minimum image technique is the long-range corrections in the directions where periodic boundary conditions are applied. The long-range corrections account for the contribution to the potential energy by the

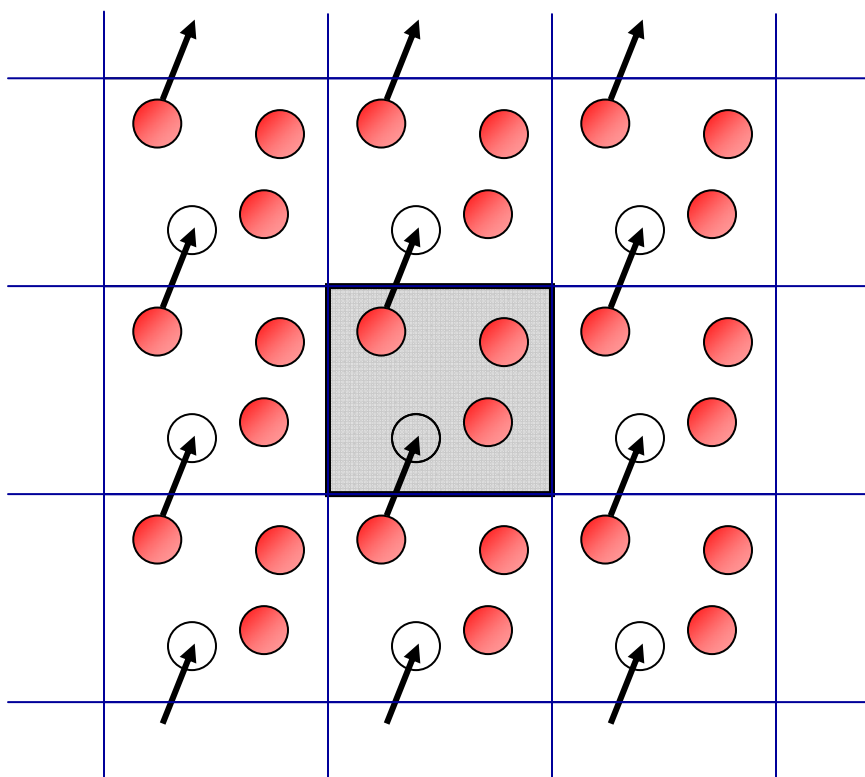


Figure 2.5 Two-dimensional representation of periodic boundary conditions. When an ion moves outside of the central simulation box through a boundary, the image ion is moved into the simulation box through the opposite boundary.

image ions outside the central simulation box. Figure 2.6 presents the concept behind the implementation of long-range corrections: each ion inside the central simulation box interacts with a set of charged sheets of infinite dimensions, associated to each ion inside the simulation box, minus the central square hole corresponding to the charge of the ion in the central box (Torrie and Valleau, 1980; Boda et al., 1998). Each infinite charged sheet represents the image electrostatic interactions of each ion outside the central simulation box.

2.3.3 Monte Carlo Simulations of the Electrical Double Layer

The properties of bulk electrolytes (i.e., configurational energies and activity coefficients) for Coulombic systems with equal ion sizes have been described in the literature by Valleau and Cohen (1980). Monte Carlo simulations were carried out for one planar charged surface with a single symmetric 1:1 electrolyte (Torrie and Valleau, 1979; Torrie and Valleau, 1980; Van Megan and Snook, 1980). The simulation results compare very well with those obtained by the classical theory at the conditions at which the GC theory applies (Torrie and Valleau, 1980; Van Megan and Snook, 1980). Furthermore, Torrie and coworkers used Monte Carlo simulations to examine several interesting aspects related to EDL, including the effects of image force (Torrie et al., 1982) and the effects of an asymmetric electrolyte (Torrie and Valleau, 1982). It is very important to note that Monte Carlo simulation results revealed the limitations of the classical GC theory, specifically in the presence of asymmetric electrolytes in the solution (Torrie and Valleau, 1982).

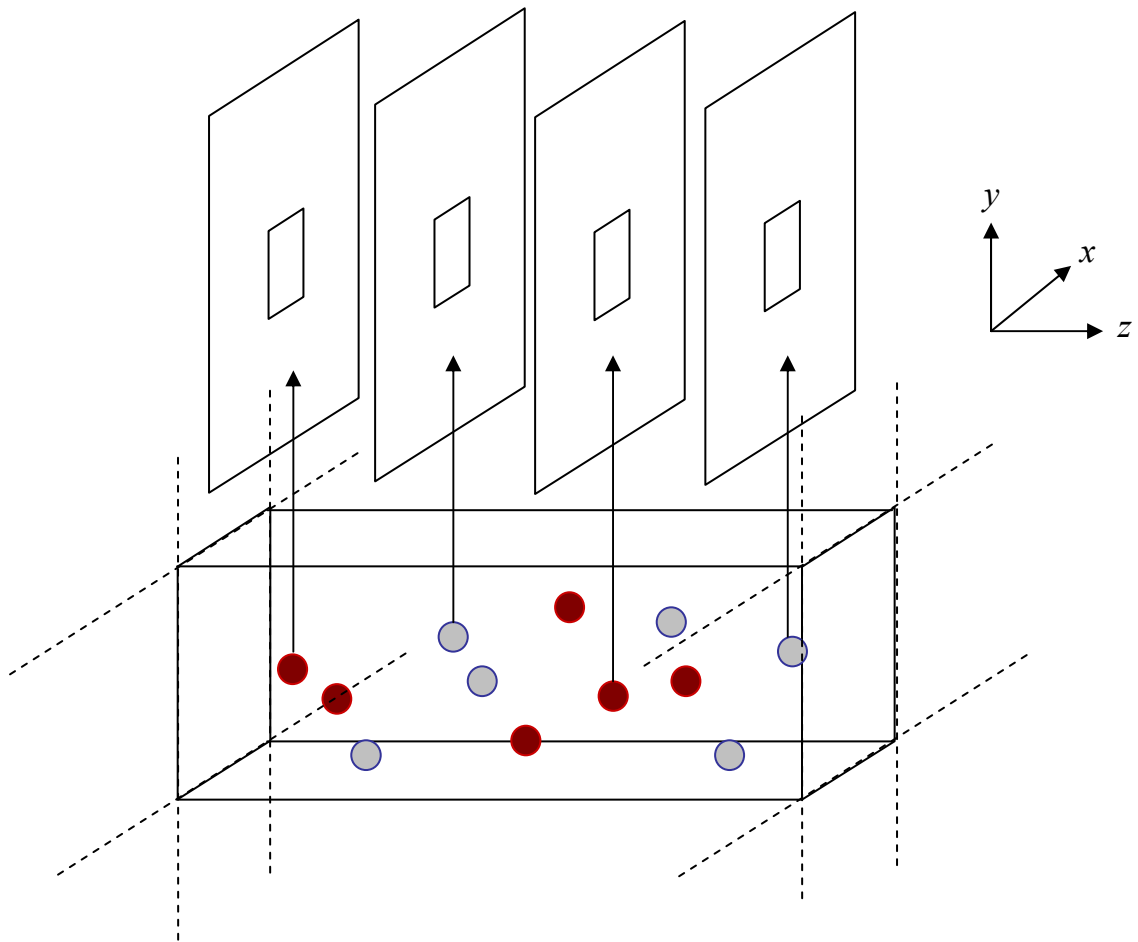


Figure 2.6 Schematic of the long-range correction for electrolyte systems, considering only x and y directions. Each ion inside the central simulation box has an associated charged sheet of infinite dimensions (less the square hole corresponding to the central simulation box), which accounts for the electrostatic interactions of the image ions outside the central simulation box.

Another important interfacial phenomenon, the problem of electrolyte distribution between a porous phase and a bulk solution was studied using GCMC simulations. In these studies, it was observed that exclusion of electrolytes from charged cylindrical pores increases, reaches a maximum, and then decreases with increasing surface charge density (Vlachy and Haymet, 1989; Vlachy and Haymet, 1990; Jamnik and Vlachy, 1993). It has been found that GCMC simulations show a significantly qualitative and quantitative difference with the classical GC theory (i.e, the PB equation) for predicting the behavior of EDL with divalent counterions present in the solution (e.g., 2:2 or 1:2 electrolyte) (Jamnik and Vlachy, 1993; Hibar et al., 2000). In recent studies, the EDL formation with a 1:1 electrolyte confined within a slit-type nanopore of 20-Å diameter and charged internal walls was successfully simulated by applying the CMC and GCMC methods (Yang et al., 2002). However, most Monte Carlo studies do not take into consideration ion-size effects on the electrolyte distribution in the double layer, specifically for confined electrolytes. The size of ions involved in the EDL formation is very important because competition mechanisms between counterions of different sizes and charges were identified (Taboada-Serrano et al., 2005). This topic of counterions of unequal sizes is quite important because it plays a key role in the determination of ion selectivity through channels of molecular dimensions.

2.3.4 Comparison of CMC Simulation Results and GC Theory Predictions

The classical EDL theory based on the GC model, as described in section 2.3, is the widely known method to predict the formation of the double layer through the solution of the PB equation. The classical theory has been proven successful for 1:1

electrolyte solutions of moderate concentration near a single plane charged surface associated with a moderate surface charge (Torrie and Valleau, 1980). However, the classical theory shows less success under several conditions such as high electrolyte concentration, high surface charge, asymmetric electrolytes, mixture of symmetric and asymmetric electrolyte solutions, etc.

The basic disadvantage of the classical GC model is that the ions present in the EDL are considered to be point charges, and that these point charges do not interact with each other. For instance, Figure 2.7 shows a comparison between ion concentration profiles obtained by the classical GC theory and by molecular simulation via the CMC technique (described in section 2.3.2) for a single plane surface associated with a higher surface charge density (0.64 C/m^2) at a 1:1 electrolyte solution of concentration 1.0 M. The ion concentration obtained by molecular simulations is calculated as the number of ions per volume of the simulation box. It is found that the classical theory fails to describe the oscillation of the ion concentration profiles in the interfacial region of the double layer. In the CMC simulation, the ions were assumed to be fully hydrated with a diameter of 4.25 \AA , and one can see that under these conditions, steric excluded-volume effects become significant. It is noticeable on Figure 2.7 that the counterion profiles present a second layer of high local concentration of ions close to the surface, due to the high packing density in the interfacial region. This effect cannot be predicted by the classical GC theory because the ions are considered point charges, and therefore, do not occupy any space.

Figure 2.8 presents the comparison of ion concentration profiles by the GC theory and CMC simulations for a 2:2 electrolyte at an 1.0 M concentration and a surface charge

density of 0.16 C/m^2 . Because of the short-range correlations between ions, oscillation in ion concentration profiles can be observed in the CMC simulation. The CMC-calculated distribution of multivalent counterions exhibits a minimum after the maximum counterion concentration, whereas the coion distribution presents a maximum at the same location of the counterion-concentration minimum. Such phenomenon cannot be predicted by the classical theory because ion-ion interactions are neglected.

Consequently, the classical EDL theory based on the GC model has several limitations under certain conditions. It is more questionable whether the classical EDL theory can be applied to describe the behavior of EDL formation at a small scale, such as electrolytes confined into charged nanopores. Therefore, it is essential to develop molecular modeling approaches using Monte Carlo simulation methods to overcome the simplifications of the classical theory.

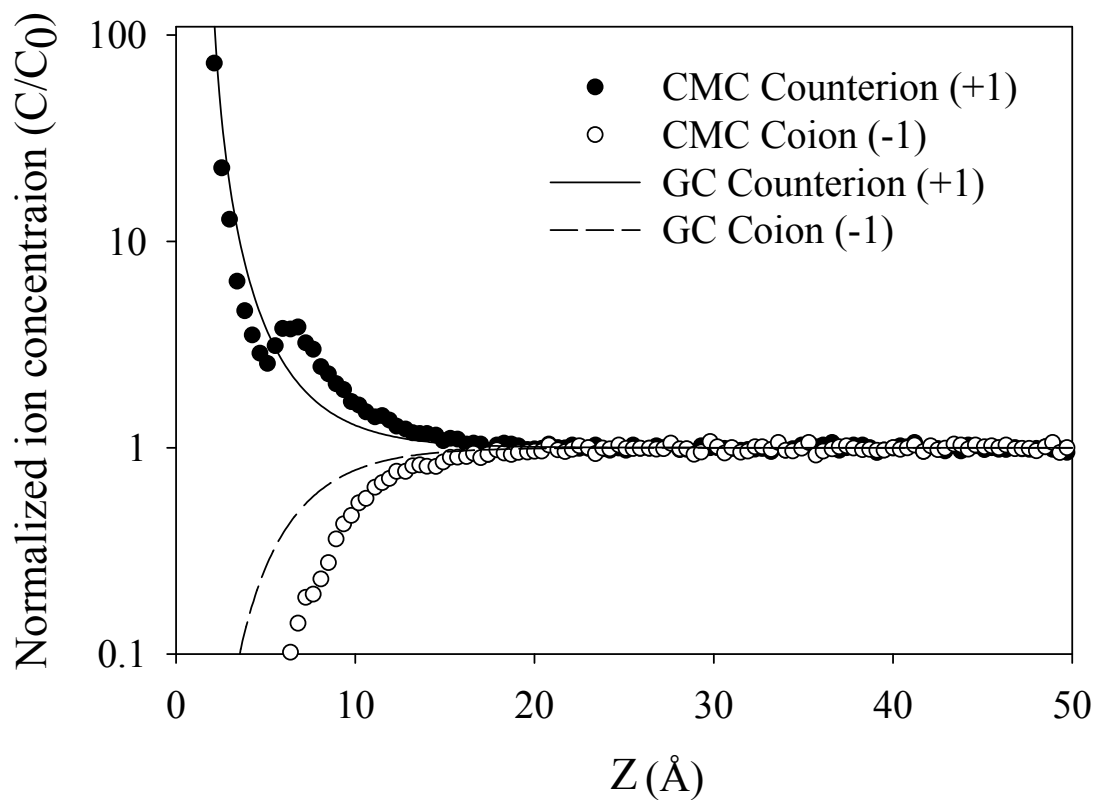


Figure 2.7 Ion concentration profiles obtained by the classical GC theory and the CMC simulation for 1:1 electrolyte of 0.1 M concentration at a high surface charge density of 0.64 C/m^2 . The local concentration of ion, C , is normalized over the bulk phase concentration C_0 . The classic GC theory fails to describe the second layer of counterions predicted by the CMC simulation.

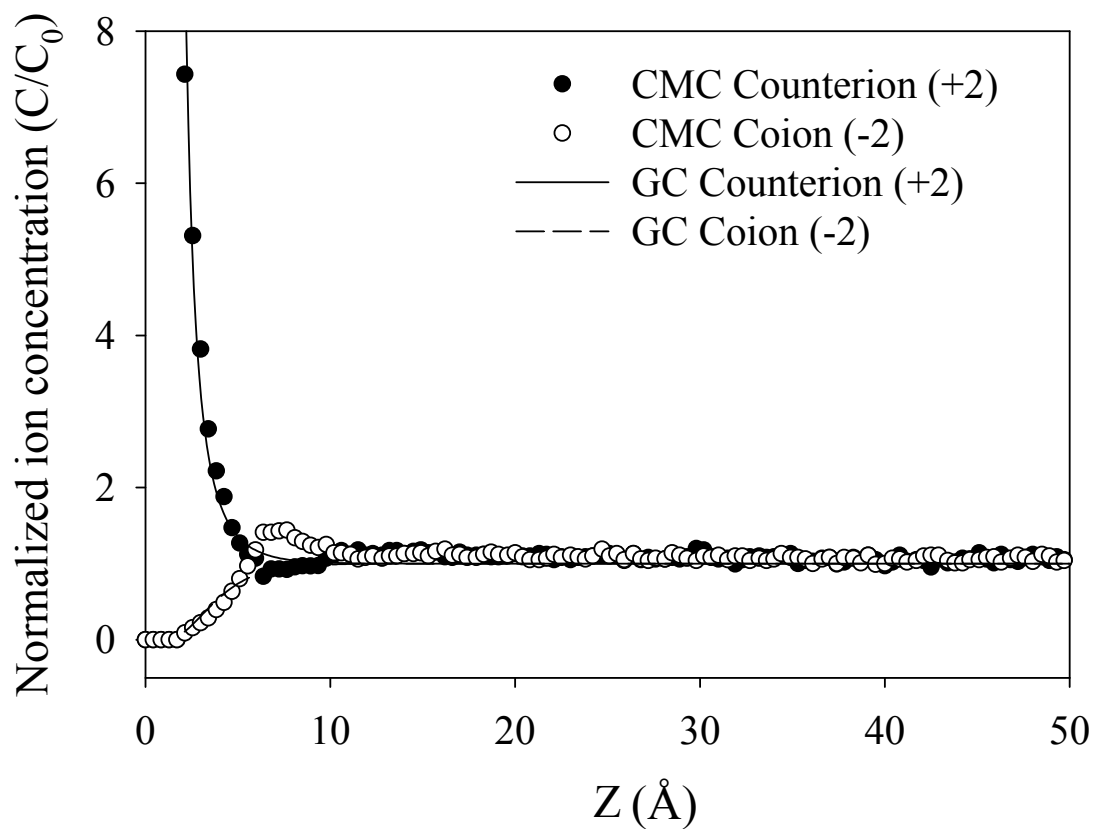


Figure 2.8 Comparison of ion concentration profiles obtained by the classical GC theory and CMC simulations for a single charged surface at 0.16 C/m^2 immersed in a 2:2 electrolyte at a concentration of 1.0 M. C and C_0 are the local concentration and the bulk concentration of ions, respectively. The CMC simulation results show the occurrence of charge inversion, while the classical GC theory cannot predict charge inversion.

CHAPTER 3

ELECTROSORPTION OF IONS FROM AQUEOUS SOLUTIONS USING NANOPOROUS CARBON MATERIALS

In this chapter, the fundamental mechanism of ion electrosorption, in which an electrical double layer develops inside nanopores, was studied via a combination of experimental and theoretical studies. Using nanoporous carbon materials, the electrosorption process can be characterized via a double-layer capacitance, which is determined by the pore accessibility in terms of transport rate of ions and number of ions at equilibrium with the bulk solution. An extended electrical double-layer model, based on the classical Gouy-Chapman theory, indicated that the pore size distribution plays a key role in determining the double-layer capacitance. Because of the occurrence of double-layer overlapping in narrow pores, mesopores and micropores present different behaviors in the electrosorption process; mesopores show good electrochemical accessibility, and micropores present a slow mass transfer of ions and a considerable loss of the double-layer capacitance associated with a shallow potential distribution inside pores. The effect of double-layer overlapping can be reduced by increasing the pore size, electrolyte concentration, and applied potential. Consequently, electrical double-layer formation inside nanopores can significantly affect ion sorption and transport in nanoporous carbon materials.

3.1 Introduction

Electrosorption has been developed as a potential technology for removing inorganic ions from aqueous solutions (Johnson and Newman, 1971; Oren and Soffer, 1983; Matlosz and Newman, 1986; Gabelich et al., 2002; Ying et al., 2002). The working principle of electrosorption is based on imposing an external electric field in order to force charged species such as ions to move towards oppositely charged electrodes. The charged species can then be held within the electrical double layer (EDL) associated with the electrodes. The application of electrosorption processes offers several advantages: high capacity, no secondary waste, and reversibility.

Carbon materials of porous structure, such as activated carbon, carbon fibers, and carbon aerogel, constitute very attractive electrodes for electrosorption processes because of their high specific surface area and their good electrical conductivity (Wang et al., 1993; Pekala et al., 1998; Qu and Shi, 1998; Frackowiak and Béguin, 2001).

Experimental results have shown that electrosorption using carbon aerogels as adsorbents can effectively remove ions such as sodium, chloride, and chromium from aqueous solutions (Farmer et al., 1996; Framer et al., 1997; Gabelich et al., 2002; Ying et al., 2002). These porous materials can be treated as electrical double-layer capacitors (EDLCs), characterized via a double-layer capacitance at the interface of the carbon and the electrolyte. The electrosorption capacitance is a good indicator of the performance of porous materials in the removal of ions.

High specific surface area, a determining factor in the performance of EDLCs, is determined mainly by the contribution of the surface area of mesopores (pores of width between 20 and 500 Å) and micropores (pores of width smaller than 20 Å) present in the

carbon material. Some studies have shown that the EDLCs can be divided into mesoporous and microporous capacitors, because the two pore size ranges have distinct contributions to the total specific double-layer capacitance (Shi, 1996; Yang et al., 2003; Gryglewicz, 2005). It is believed that the micropores with diameters larger than 5 Å are available for the electrosorption of simple hydrated ions (Shi, 1996; Yang et al., 2003). However, Lin et al. (1999) indicated micropores with diameter smaller than 8 Å may not contribute significantly to the EDL capacitance. Therefore, the EDL capacitance performance is limited because a significant fraction of micropores have poor electrochemical accessibility. The effect of pore size distribution extends beyond the surface area available for sorption. Pore size distribution affects not only the surface area available for sorption but also the formation of the EDL inside porous carbon materials and thus the electrochemical performance of these materials (Qu and Shi, 1998; Gryglewicz et al., 2005).

When the pore size is comparable to the EDL thickness, the EDLs of the inner walls of the pores overlap. The transport rate of ions is also determined by the thickness of the EDL and the electrical potential distribution inside pores. Since the nanostructured carbon materials consist of mesopores and micropores, EDL overlapping becomes a key factor in ion transport and EDL capacitance can then be reduced by the overlapping effect (Ying et al., 2002; Yang et al., 2003). More specifically, the occurrence of EDL overlapping can be used to explain the mechanism that membranes containing channels in molecular dimensions can show selective ion transport, mimicking biological transport processes (Nishizawa et al., 1995; Schmuhl et al., 2004). A model describing the formation of the EDL inside pores was developed by taking into consideration a double-

layer overlapping correction (Yang et al., 2001). The EDL model was based on the classical Gouy-Chapman theory and provided a good agreement with Monte Carlo simulations of fully hydrated ions inside pores for simple 1:1 electrolyte solutions (Yang et al., 2002; Taboada-Serrano et al., 2005). For sufficiently small pores, the thickness of the inner layer of the EDL is considered to be comparable to the pore width. In our earlier work (Yang et al., 2001), the thickness of the inner layer was assumed to be small compared to the pore width. In that case, the double-layer capacitance will probably be overestimated, especially for micropores.

Deionization based on electrosorption by using nanostructured carbon materials is a complicated process. The present work combines experimental and modeling work to examine the fundamental mechanism of the EDL formation inside nanopores. A novel graphitized carbon material, which is believed to be suitable for application in electrosorption processes, is investigated. The EDL model is further developed and solved with realistic boundary conditions to better represent a real system.

3.2 Experimental Methods

3.2.1 Materials

A novel graphitized-carbon monolithic column, prepared at Oak Ridge National Laboratory (Liang et al., 2003), was tested because of its low hydraulic resistance, nanostructured porosity, and high potential for electroseparations. Two types of carbon aerogels were obtained from Marketech (Port Townsend, WA) for the purpose of comparison with the novel graphite material.

The preparation of the graphitized carbon consisted of the following three steps: (i) preparation of the precursor rod, (ii) carbonization and removal of the silica beads and the catalyst, and (iii) graphitization. The phenolic resin rod with embedded 10- μm silica beads was prepared by acid-catalyzed polymerization of a resorcinol/ iron (III) complex and formaldehyde. Subsequently, this rod was carbonized under inert atmosphere with a programmed temperature cycle that ran from room temperature to 1250°C. The silica beads along with iron catalysts were removed, leaving porous carbon rods that were loaded into a graphitization furnace, heated to 800°C, and held at this temperature overnight with helium gas flow of 10 mL/min. The temperature was then raised to 2800°C at 10°C/min and kept at 2800°C for 2 hrs. The furnace was allowed to cool naturally to room temperature after the graphitization.

3.2.2 Characterization

The specific surface area and pore size distributions for the materials were obtained via nitrogen gas adsorption (Micromeritics Gemini 128). The data were derived from the Brunauer-Emmett-Teller (BET) isotherm by using the supporting software for the instrument. Cyclic voltammetry experiments were performed using a Bioanalytical Systems (BAS, West Lafayette, IN) voltammetric analyzer (CV-50W) connected to a BAS C2 cell stand. The working electrode was a platinum wire attached to a small piece of carbon material in the aqueous solution. The counter electrode was a large piece of carbon material clipped to another platinum wire, and the reference electrode was a Ag/AgCl electrode immersed in a 3.0 M NaCl electrolyte solution. All aqueous solutions were prepared by using triply distilled 18-M Ω deionized water and sodium fluoride

(Mallinckrodt Baker, Inc., Phillipsburg, NJ). The voltammetry experiments were conducted with solution concentrations of NaF ranging from 1.0 mM to 1.0 M. Fluoride ions were chosen as counterions due to their insignificant specific adsorption (Golub et al., 1989; Ying et al., 2002). Prior to each experiment, the solution was purged with nitrogen gas, which was also blown continuously over the top of the solution during the experiment. All measurements were performed at room temperature.

3.3 Model Development

Based on the Gouy-Chapman-Grahame theory, the EDL is composed of a diffuse layer and an inner (Stern) layer. The electrical potential distribution of a symmetric $z:z$ electrolyte solution in the diffuse layer inside a pore can be described by the Poisson-Boltzmann (PB) equation as follows:

$$\frac{d^2\psi}{dx^2} = \frac{2zeN_0}{\varepsilon} \sinh\left(\frac{ze\psi}{kT}\right) \quad (3.1)$$

where x corresponds to the distance between the walls of the pore, ψ is the electrical potential, z is the valence of the ions, e is the electrical charge of the electron, N_0 is the total number of ions in the bulk solution, ε is the dielectric constant of the medium, k is the Boltzmann constant, and T is the absolute temperature.

In the inner layer, the interface can be further divided into the inner Helmholtz plane (IHP) and the outer Helmholtz (diffuse-layer) plane (OHP). Only the OHP is considered in the model because of the absence of specific adsorption and the width of the inner layer is half the diameter of hydrated ions (Hamann et al., 1998). Moreover, the

diameter of the fully hydrated ions becomes comparable to the width of some pores, especially that of micropores. The solution of the PB equation for the system was obtained via the application of the following boundary conditions:

$$\frac{d\psi}{dx} = 0 \quad \text{and} \quad \psi = \psi_m, \quad \text{at} \quad x = 0 \quad (3.2a)$$

$$\psi = \psi_d, \quad \text{at} \quad x = \pm \frac{w-a}{2} \quad (3.2b)$$

$$\psi = \psi_s, \quad \text{at} \quad x = \pm \frac{w}{2} \quad (3.2c)$$

where ψ_m is the electrical potential at the midplane, ψ_d is the diffuse-layer potential, ψ_0 is the surface potential, w is the pore width, and a is the diameter of a fully hydrated counterion (e.g., $\sim 4.25 \text{ \AA}$ in most cases).

The relationship between the surface potential and the diffuse-layer potential is given by the following equation (Hunter, 2001):

$$\psi_d = \psi_0 - \frac{\sigma_0}{C_1} \quad (3.3)$$

where C_1 and σ_0 correspond to the inner-layer capacitance and to the surface charge density, respectively. When specific adsorption is not considered, C_1 can be assumed to be constant over the low-voltage range (Grahame, 1954).

The surface charge density can be obtained via the integration of equation 3.1 with the boundary conditions defined in equations 3.2a and 3.2b. For a single symmetric electrolyte solution, the surface charge density can be expressed as

$$\sigma_0 = (4\varepsilon\varepsilon_0RTI)^{1/2} \left[\cosh\left(\frac{e\psi_d}{kT}\right) - \cosh\left(\frac{e\psi_m}{kT}\right) \right]^{1/2} \quad (3.4)$$

where R is the gas constant and I is the ionic strength.

The double-layer capacitance C_{dl} can then be defined as (Hunter, 2001)

$$C_{dl} = \frac{d\sigma_0}{d\psi_0} \quad (3.5)$$

Because iteration techniques were required for the solution of equations 3.4 and 3.5, modeling results were obtained by the application of a program developed in MATLAB 7.0.

The EDL composed of the diffuse and inner layers can be modeled as a parallel-plate capacitor. The double-layer capacitance C_{dl} can be calculated from the following equation (Hunter, 2001):

$$\frac{1}{C_{dl}} = \frac{1}{C_d} + \frac{1}{C_1} \quad (3.6)$$

where C_d is the diffuse-layer capacitance.

3.4 Results and Discussion

3.4.1 Characterization of Carbon-Based Materials

The experimental characterization of the nanostructured carbon materials consisted of the determination of pore size distributions and specific double-layer capacitances. Figure 3.1 presents the pore size distribution of the graphitized carbon and the two different carbon aerogels, referred to as type A and type B. The BET surface area for the graphitized carbon was determined to be $487 \text{ m}^2/\text{g}$, 94% of which is attributed to micropores and only 6% attributed to mesopores. The surface area of carbon aerogel type A was $691 \text{ m}^2/\text{g}$, 85% of which can be attributed to micropores and 15% to mesopores. For the BET surface area of carbon aerogel type B ($431 \text{ m}^2/\text{g}$), 77 and 23% were attributed to micropores and mesopores, respectively. Moreover, carbon aerogel type A exhibits the highest surface area, which is associated with considerable contribution from small micropores less than 5 \AA in width.

In previous work (Yang et al., 2003), the specific capacitance of carbon aerogel was investigated via cyclic voltammetry. Results indicated that the electrolyte concentration and scan rate play important roles in the characterization of nanoporous materials. The EDLCs can be classified as mesoporous and microporous capacitors. Figure 3.2(a) presents the cyclic voltammogram of the graphitized carbon in a 0.01 M NaF solution with low (1 mV/s) and high (5 mV/s) scan rates. The shape of the cyclic voltammogram is distorted because of the contribution of the equivalent series resistance associated with the low electrolyte concentration. When a fast scan rate is used, the specific capacitance depends only slightly on the applied potential after the transient response. It is also found that the mesoporous capacitance is about 30 F/g and that the

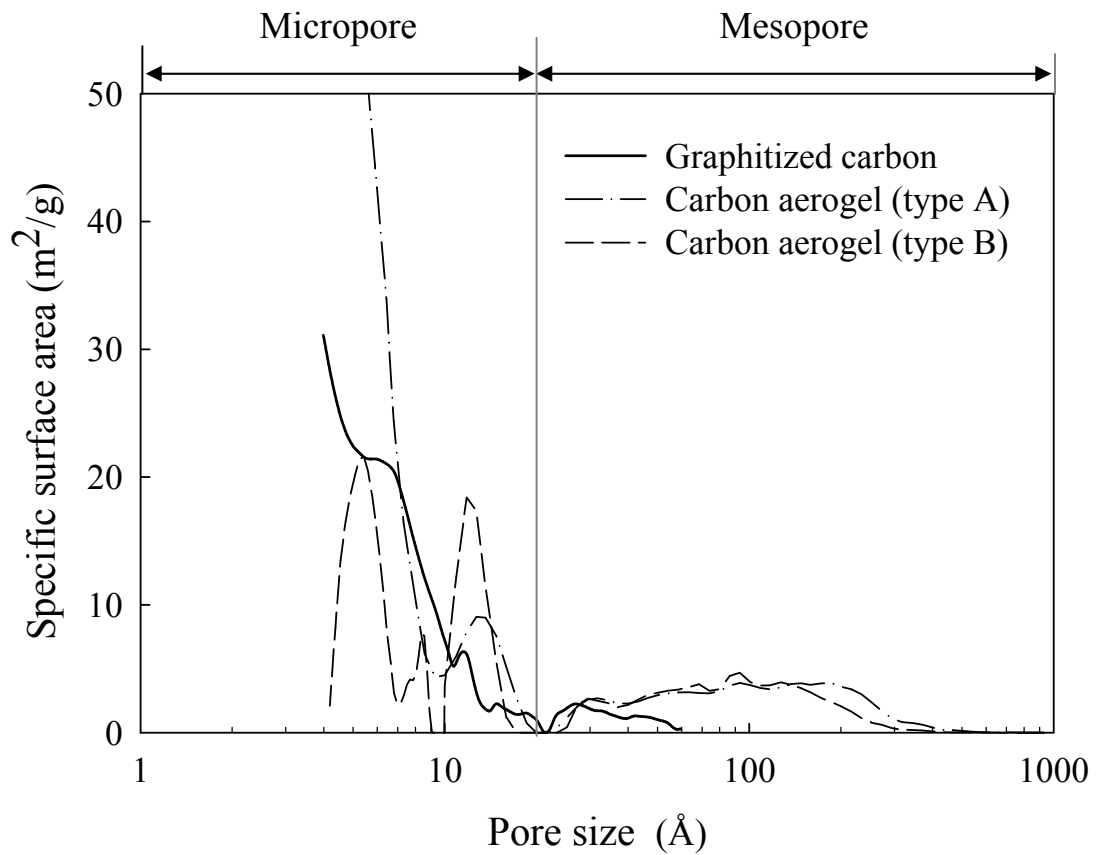


Figure 3.1 Pore size distribution of graphitized carbon, carbon aerogel type A, and carbon aerogel type B, which have specific surface areas of 487, 691, and 431 m²/g, respectively.

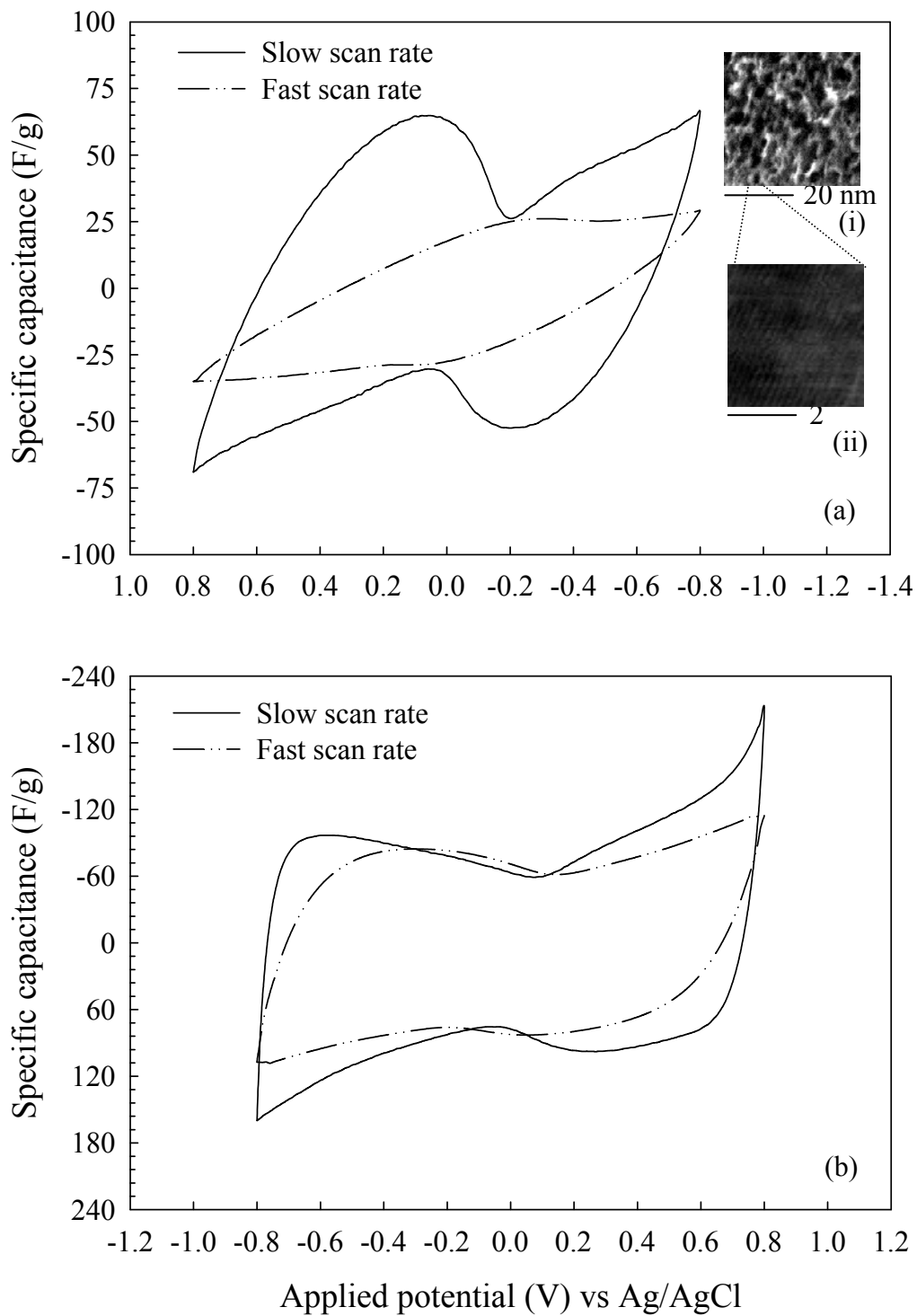


Figure 3.2 Specific capacitance of graphitized carbon in various NaF solutions measured by cyclic voltammetry at fast (5 mV/s) and slow (1 mV/s) scan rates. (a) NaF concentration: 0.01 M and (b) NaF concentration: 1 M.; (i) high resolution SEM image of the nanopores in the carbon skeleton and (ii) TEM image of the graphite strips within the carbon matrix obtained via STEM.

micropores are unavailable for electrosorption due to the slow electrolyte penetration (Yang et al., 2003). When a slow scan rate is used, the specific capacitance is a result of the contribution of mesopore and micropore capacitances. Hence, microporous capacitors have an important contribution to the total capacitance at lower scan rates. Furthermore, the cyclic voltammogram shows a deep minimum of the specific capacitance (28.5 F/g) around the point of zero charge (pzc), indicating that the presence of micropores results in the occurrence of double-layer overlapping. Figure 3.2(b) presents the cyclic voltammogram in a concentrated electrolyte solution (1.0 M NaF). The difference in measured specific capacitance during slow and fast scan rates becomes less pronounced than that detected in a 0.01 M NaF solution. The explanation for this finding is the decrease in EDL overlapping and the high concentration gradient at the carbon/electrolyte interface. Figure 3.3 presents the cyclic voltammograms of carbon aerogel types A and B measured in a 0.01 M NaF solution. The specific capacitance of carbon aerogel type A is higher than that of type B. For example, at -0.4 V, the specific capacitances are 73.6 F/g for carbon aerogel A and 42.4 F/g for carbon aerogel B. This difference is mainly the result of differences in the specific surface areas of the two carbon aerogels. At lower potentials, the presence of micropores plays a stronger role. At 0.1 V for example, the difference in the specific capacitance of the two materials is smaller because the material with the low surface area has a lower percentage in the micropore region than the material of the high surface area.

Based on the characterization experiments, the micropore region constitutes a large portion of the total specific surface area, and double-layer overlapping will thus

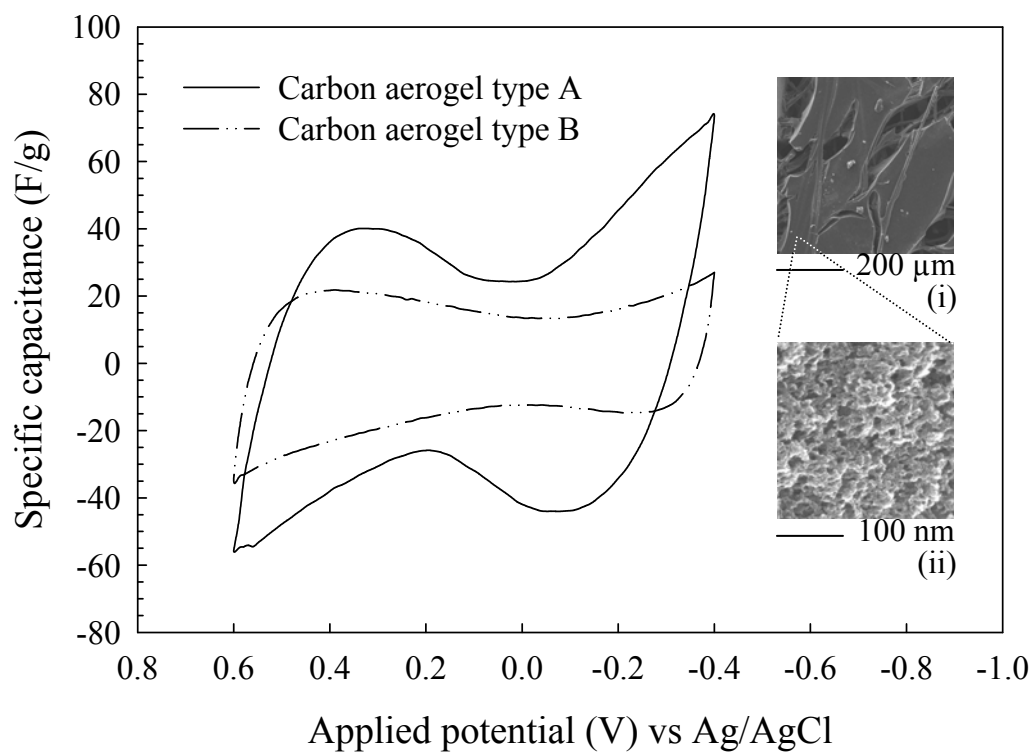


Figure 3.3 Specific capacitance of carbon aerogel type A and B in a 0.01 M NaF solution measured by cyclic voltammetry at a slow (1 mV/s) scan rate. (i) TEM image of carbon aerogel type A, which is composed of interconnected aerogel particles, and (ii) high resolution SEM image of nanopores in the carbon matrix.

have a pronounced effect on electrosorption capacitance. Under these conditions, the presence of micropores can become a determining factor in the effectiveness of EDLCs.

3.4.2 Electrical Potential Distribution: Modeling Results

The modified EDL model was employed to study the formation of the electrical double layer inside the pores of nanostructured materials. In this model, the inner-layer capacitance C_1 was considered to be a constant with a value of $20 \mu\text{F}/\text{cm}^2$, which is equal to the double-layer capacitance of clean graphite (Kinoshita, 1998). To compare the electrical potential in different cases, new variables, Y and Y_m , are defined as follows:

$$Y = \frac{\psi - \psi_d}{\psi_0} \quad \text{and} \quad Y_m = \frac{\psi_m - \psi_d}{\psi_0} \quad (3.7)$$

where Y is a dimensionless potential that represents the potential drop at any point with respect to the diffuse-layer potential. If there is no potential drop in the diffuse layer, then $\psi = \psi_d$ and $Y = 0$ at any point. If the potential drops to zero at any point (e.g., in the middle of the pore), $Y = -\psi_d / \psi_0$. In equation 3.7, Y_m constitutes a dimensionless midplane potential. The lower the absolute value of Y_m , the larger is the effect of EDL overlapping.

Figure 3.4(a) shows the electrical potential distribution for a 0.01 M solution of NaF inside a micropore of $10\text{-}\text{\AA}$ diameter. A very strong double-layer overlapping effect is observed in the micropore region, which can be visualized through the small difference between the diffuse-layer potential and the midplane potential ($Y - Y_m$). This behavior results from what is called the ion-exclusion effect (Vlachy et al., 1990). For example,

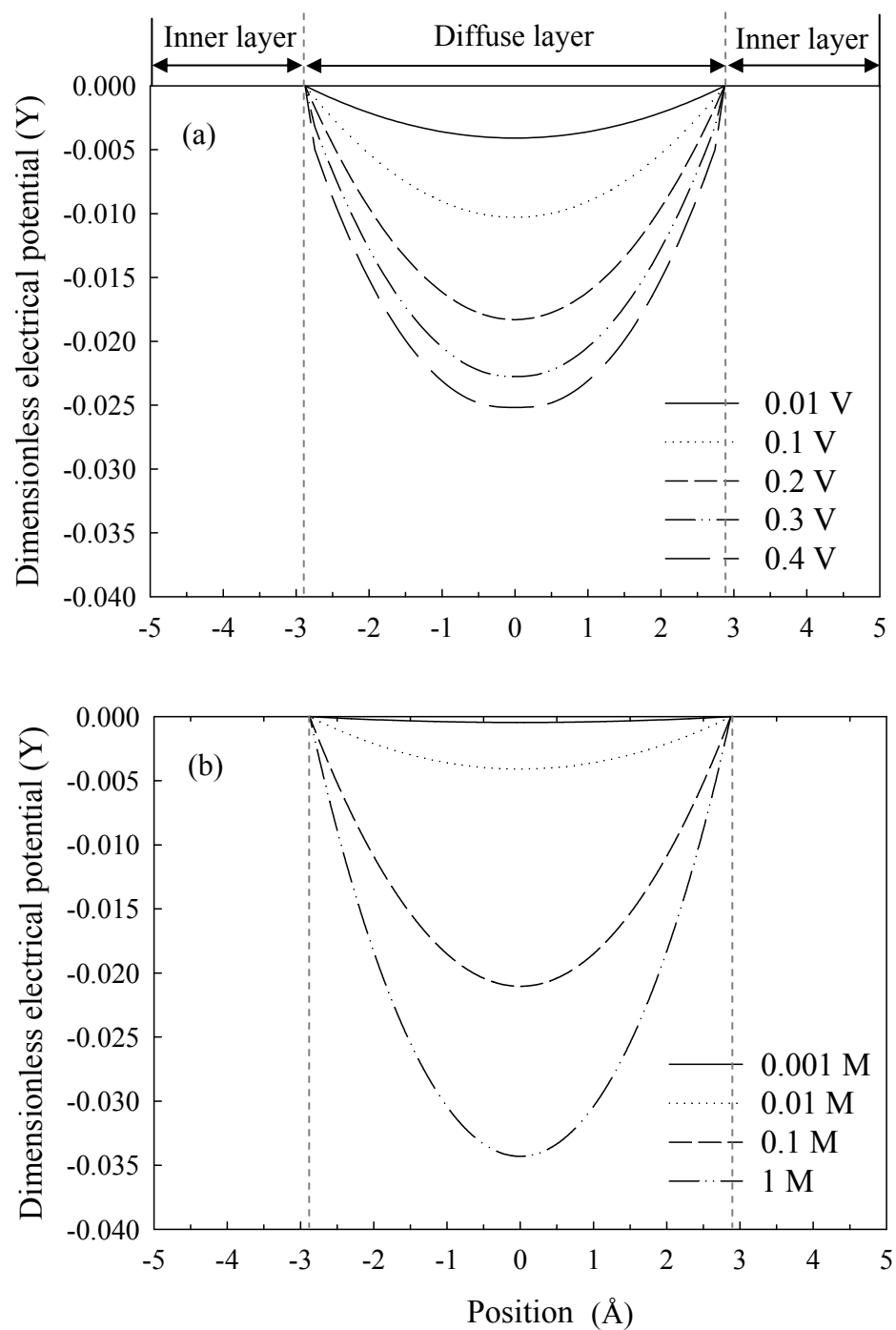


Figure 3.4 Electrical potential distribution of the diffuse layer for a micropore of 10-Å diameter for (a) a 0.01 M NaF solution and (b) around the pzc ($\psi_0 = 0.01$ V). The EDL overlapping effect diminishes with increasing surface potential and solution ionic strength.

when the surface potential is near the pzc, the potentials at the diffuse layer (ψ_d) and at the midplane (ψ_m) are 9.00 and 8.96 mV, respectively. These values correspond to a Y_m of -0.004 . On the other hand, values of $\psi_d = 4.665$ mV, $\psi_m = 0$ mV, and $Y_m = -0.467$ correspond to a mesopore of diameter 100 Å. In this case, according to the Debye-Hückel approximation, the thickness of the double layer is calculated to be 30.5 Å and the double layer is fully developed inside the mesopore. It is obvious that the micropore has a shallow potential distribution compared with that of the mesopore. A shallow potential distribution is associated with a high counterion concentration at the midplane and a large osmotic pressure, which have a negative effect on ion transport inside the micropores. As seen in Figure 3.4(a), the electrical potential profile is a function of the surface potential. For example, when the surface potential changes from the pzc to 0.4 V, the absolute values of Y_m increase from 0.004 to 0.025, thus, leading to a sharper potential drop and a higher concentration gradient. Higher surface potentials or applied potentials reduce the occurrence of double-layer overlapping. Figure 3.4(b) shows that the electrolyte concentration also plays an important role in the occurrence and extent of EDL overlapping. For instance, the potential drop between the surface and the midplane for an electrolyte solution of concentration 1.0 M is much larger than that for an electrolyte solution of 0.001 M concentration, and the absolute value of Y_m increases from 0.004 to 0.034. This observation can be used to explain the characteristics of the voltammograms depicted in Figure 3.2, in which, when a fast scan rate is used, the microporous capacitor cannot be accessed by ions unless in high electrolyte concentration solutions (Yang et al., 2004). The specific capacitance is less dependent on the scan rate at a higher electrolyte concentration. This phenomenon occurs because the mass transfer

rate of ions inside the micropores can be enhanced by larger concentration gradients while the overlapping effect is reduced at the same time. Therefore, at higher electrolyte concentrations, ions can diffuse into electrochemically accessible micropores in a shorter period of time.

3.4.3 Effect of Diffuse-Layer and Inner-Layer Capacitances

Figures 3.5(a) and 3.5(b) illustrate the electrosorption capacitances as a function of surface potential at an electrolyte concentration equal to 0.01 M. The model prediction is based upon the assumption that ions are able to reach equilibrium inside both mesopores and micropores. If the thickness of the inner layer is not taken into account, the EDL model overestimates the double-layer capacitance, especially for micropores at low surface potentials. In Figure 3.5(a), the mesoporous capacitance is determined by the contribution of the diffuse-layer and the inner-layer capacitances near the pzc, where the values of C_{dl} , C_d , and C_1 are obtained from the model as 10.7, 22.9, and 20 $\mu\text{F}/\text{cm}^2$, respectively. As the surface potential increases, the diffuse layer becomes small due to EDL compression and its capacitance becomes large. Under these conditions, the values of the EDLCs are determined by the inner layer. On the other hand, the double-layer capacitance of micropores (10 Å in diameter) shows a quite different electrosorption behavior, as shown in Figure 3.5(b). The diffuse layer determines the value of the double-layer capacitance around the pzc. In the case of an electrolyte concentration of 0.01 M, the values of C_{dl} , C_d , and C_1 correspond to 2.0, 2.2, and 20 $\mu\text{F}/\text{cm}^2$, respectively. However, high surface potential leads to a substantial accumulation of ions in the EDL. This accumulation then results in a few angstroms of double-layer thickness and the

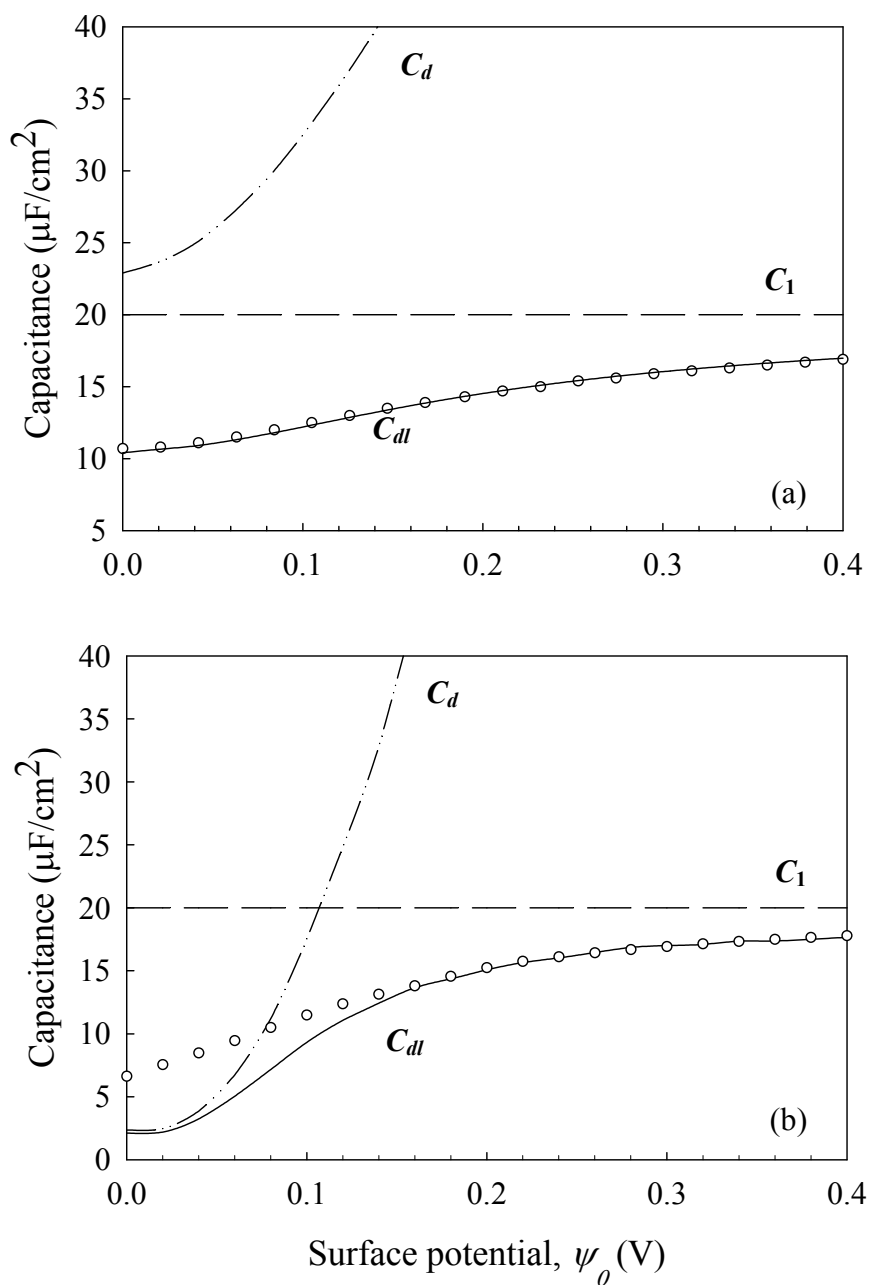


Figure 3.5 Effect of diffuse-layer and inner-layer capacitance on the double-layer capacitance in a 0.01 M NaF solution for (a) a mesopore of 100-Å diameter and (b) a micropore of 10-Å diameter. The double-layer capacitance, diffuse-layer capacitance, and inner-layer capacitance are represented by C_d , C_{dl} , and C_1 , respectively. The circles represent the double-layer capacitance without taking into consideration the thickness of the inner layer.

dominance of the double-layer capacitance by the inner layer. For example, when the surface potential is 0.4 V and the electrolyte concentration is 0.01 M, the model predicts that $C_{dl} = 18 \mu\text{F}/\text{cm}^2$, $C_d = 151 \mu\text{F}/\text{cm}^2$, and $C_1 = 20 \mu\text{F}/\text{cm}^2$. In general, during electrosorption, the diffuse layer inside micropores plays a more important role than the diffuse layer inside mesopores. The importance of the diffuse layer decreases with increasing electrolyte concentration and surface potential.

The microporous capacitance strongly depends on the surface potential. For example, as shown in Figure 3.5(b), when a 0.01 M electrolyte concentration is used, the microporous capacitance decreases from $17.7 \mu\text{F}/\text{cm}^2$ at a surface potential of 0.4 V to $2.0 \mu\text{F}/\text{cm}^2$ at the pzc, leading to a considerable loss in double-layer capacitance. Therefore, double-layer overlapping can diminish the efficiency of the microporous capacitor, explaining the sharp decrease in specific capacitance observed in the cyclic voltammograms in Figure 3.2(a).

Consequently, mesopores and micropores manifest significantly different behaviors in the electrosorption process (Qu and Shi, 1998; Lin et al., 1999; Yang et al., 2001; Yang et al., 2003; Gryglewicz et al., 2005). Mesopores are much more easily and rapidly penetrated by ions because less overlapping occurs inside the pores. In contrast, a shallow electrical potential distribution exists inside micropores, leading to a smaller driving force for transport and a larger osmotic pressure. EDL overlapping decreases not only the mass transfer rate of ions but also the number of ions inside the pores at equilibrium. Under these conditions, the diffuse layer dominates the EDL formation and a considerable loss of the double-layer capacitance takes place. The effect of the diffuse

layer on the EDL capacitance can be reduced by increasing pore size, electrolyte concentration, or surface potential.

3.4.4 Effect of Pore Size Distribution

The double-layer capacitances of micropores based on the actual pore size distributions are illustrated in Figures 3.6(a), 3.6(b), and 3.6(c) for 0.01 M NaF solutions at various surface potentials. The results indicate that the double-layer capacitance of porous carbon materials is strongly correlated to the pore size distribution. For instance, as shown in Figure 3.6(a), at a high surface potential, the capacitance curve of the graphitized carbon presents behavior and shape similar to that of the pore size distribution of materials depicted in Figure 3.1. The capacitance curve becomes increasingly flat as the surface potential decreases, becoming almost zero around the pzc.

For carbon aerogel type A, 40% of the total surface area is attributed to the micropores with diameters less than 5 Å and only 15% of the total surface area is attributed to the mesopores. As seen in the modeling results in Figure 3.6(b), near the pzc, the micropores with size less than 5 Å have insignificant contribution to the total capacitance. On the other hand, 74% of the capacitance is determined by the mesopores, because the capacitance per unit surface area of mesopores is much higher than that for micropores. In contrast, because the overlapping decreases with increasing surface potential, the microporous capacitance will control the total double-layer capacitance. Accordingly, the double-layer capacitance per unit microporous surface area can be different from that per unit mesoporous surface area. Due to the EDL overlapping, the porous carbon with higher surface area may not yield higher electrosorption capacitance.

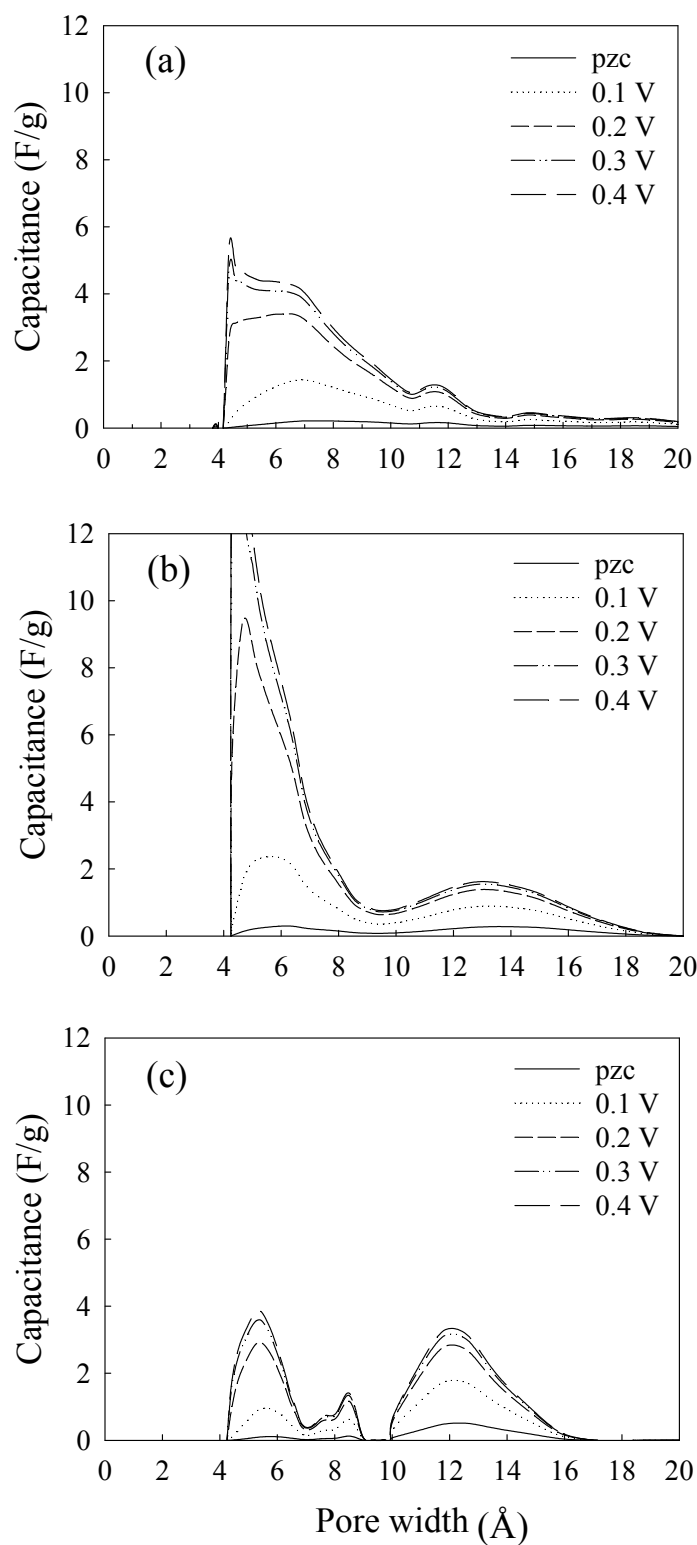


Figure 3.6 The double-layer capacitance in terms of pore size distribution for the micropore region in a 0.01 M NaF solution and at various surface potentials for (a) graphitized carbon, (b) carbon aerogel type A, and (c) carbon aerogel type B.

Figure 3.6(c), depicting carbon aerogel type B, provides a good means to discuss the contribution of larger (8- to 20-Å-diam) and smaller (5- to 8-Å-diam) micropores to the double-layer capacitance, since each contributes 35% to the total surface area. When the surface potential is close to the pzc, 20% of the total capacitance is attributed to larger micropores and only 9% to smaller micropores. This finding indicates that the main contribution to the total capacitance comes from larger micropores and a significant loss in capacitance occurs in smaller micropores.

The modeling results are consistent with the experimental characterizations. As shown in Figure 3.3, the two different carbon aerogels have similar values for specific capacitance near the pzc, although carbon aerogel type A has a much higher surface area attributed to smaller micropores. Smaller micropores do not seem to make a significant contribution to the double-layer capacitance around the pzc. Moreover, the cyclic voltammogram of carbon aerogel type A has a sharper decrease than that of type B because, for this material, the loss in the double-layer capacitance can be reduced by increasing the applied potential.

Pore size distribution plays a key role in the determination of the EDLCs. Three factors could explain this behavior: (i) specific surface area, (ii) pore accessibility by ions, and (iii) EDL formation. The specific surface area can be determined by the pore size distribution. In general, a higher specific surface area results in a higher electrosorption capacitance. However, electrosorption capacitance is also a function of pore size distribution. Accessibility by ions determines the number of ions inside pores at equilibrium and the rate of ions diffusing inside pores. A shallow potential observed inside a narrow pore causes ion exclusion, which prevents ions from penetrating inside

pores and leads to a slow mass transfer rate of ions. Finally, the occurrence of EDL overlapping is accompanied by a significant loss in electrosorption capacitance.

3.5 Summary

The present work demonstrates the fundamental aspects of EDL formation at the nanoscale level that is important to many interfacial phenomena occurring in physical, chemical, and biological systems. EDL formation plays a crucial role in determining ion sorption and transport inside nanopores. Throughout this study, a novel graphitized carbon and two different type carbon aerogels have been proven to be good EDLCs due to their high specific areas and high specific capacitances. The experimental characterization demonstrated that high specific capacitance has an effect on double layer capacitance, which results from contribution of mesopores and micropores. Transfer of ions in mesopores is faster and easier than transfer in micropores. However, the occurrence of mesopores may reduce the double-layer capacitance due to an overall decrease in the specific surface area. In contrast, most of the specific surface area is derived from microporous surface area. Micropores show a slow charging process and cause a substantial loss of the double-layer capacitance.

When low electrolyte concentrations or low electric fields are used, the diffuse layer of micropores plays an essential part in the determination of the double-layer capacitance. Double-layer overlapping can be reduced by increasing the pore size, electrolyte concentration, and electric field. A balanced surface-area ratio of micropores to mesopores is necessary for an effective EDLC under various operating conditions of electrolyte concentration and applied potential. The results of this work may be used to

provide valuable information needed for the synthesis and utilization of nanostructured materials for electrosorptive separation processes, as well as energy-storage devices.

CHAPTER 4

MONTE CARLO SIMULATION OF ELECTRICAL DOUBLE-LAYER FORMATION FROM MIXTURES OF ELECTROLYTES INSIDE NANOPORES

As shown in Chapter 3, the electrochemical experiments and the classical Gouy-Chapman theory have demonstrated that electrosorption of ions inside nanopores highly depends on the formation of the electrical double layer (EDL). In this chapter, molecular modeling based on the canonical Monte Carlo (CMC) simulation method was used to study the EDL formation in the presence of trivalent and monovalent ions inside a slit-type nanopore. In large pores, the distribution of ionic species is similar to that observed in an isolated planar double layer. Screening of surface charge is determined by the competitive effects between ion size and charge asymmetry of the counterions. On the other hand, as the pore size approaches the dimension of the ionic species, phenomena such as EDL overlapping are enhanced by ion-size effects. Simulation results demonstrate that EDL overlapping is not only a function of such parameters as ionic strength and surface charge density, but also a function of the properties of the ionic species involved in the EDL. Furthermore, charge inversion can be observed under certain conditions when dealing with mixtures of asymmetric electrolytes. This phenomenon results from strong ion-ion correlation effects and the asymmetries in size and charge of ionic species, and is most significant in the case of trivalent counterions with larger diameters. The simulation results provide insights into the fundamental

mechanisms behind the formation of EDL within nanopores as determined by pore size and by the properties of ionic species present in solution.

4.1 Introduction

The electrical double layer (EDL) is the cloud of ions with high local concentrations of counterions and low local concentrations of coions surrounding a charged surface. The thickness of the EDL is typically on the order of a few nanometers (Hunter, 2001). The EDL has proven to be extremely important in various physical, chemical, and biological systems. The formation of the EDL may involve the electrosorption of ions in aqueous solutions. During electrosorption, ions accumulate next to the charged surface without triggering electrochemical reactions. Electrosorption has several important applications, such as energy storage and water purification, and is favored by electrode materials of high surface area and high electrical conductivity (Frackowiak and Béguin, 2001; Gabelich et al., 2002; Yang et al., 2002). Some widely used electrodes include nanoporous carbon-based materials, in which the pore size distribution plays a key role in the determination of electrosorption capacitance associated with ion accessibility and ion accumulation inside the EDL (Yang et al., 2003; Hou et al., 2006). In addition, ion transport and selectivity occur according to the electrical potential distribution and the double-layer thickness via manipulation of the EDL structure inside membranes containing channels of molecular dimensions (Nishizawa et al., 1995; Kemery et al., 1998).

The classical Gouy-Chapman (GC) theory has been the best-known method to describe the EDL structure, in which the electrostatic potential and the ion concentration

profile can be predicted through the solution of the Poisson-Boltzmann (PB) equation (Hunter, 2001). This theory, however, is applicable only to single symmetric electrolytes under certain conditions such as low surface charge density and low electrolyte concentration. The key drawback associated with the classical GC theory is the consideration of ions as simple point charges. Therefore, various theoretical approaches such as molecular dynamics (Lo et al., 1998), hypernetted chain approaches (Lozada-Cassou and Henderson, 1981; Lozada-Cassou et al., 1982; Lozada-Cassou et al., 1996), and Monte Carlo methods (Torrie and Valleau, 1979; Torrie and Valleau, 1980) have been employed to study the EDL formation without the simplification of considering ions as point charges. Torrie and Valleau performed a series of Monte Carlo simulations to examine different aspects of EDL formation next to a single charged planar surface, such as image effects, unequal ion sizes, and ions with higher valences (Torrie et al., 1982; Valleau and Torrie, 1982; Torrie and Valleau, 1982). Their simulation results indicated that the classical GC theory is less accurate for the cases of 2:2 and 2:1 electrolytes, high electrolyte concentrations, or high surface charges (Torrie and Valleau, 1982). Moreover, the point of zero charge shows a dependence on electrolyte concentration that is not predicted by the GC theory (Valleau and Torrie, 1982). Recently, the consideration of multivalent ions within the EDL and ion-size effects has been the focus of computer simulations (Boda et al., 2002; Lamperski and Bhuiyan, 2003; Quesada-Pérez et al., 2004; Valiskó et al., 2004; Taboada-Serrano et al., 2005).

The behavior of the EDL of one charged surface immersed in a mixture of electrolytes of monovalent and multivalent ions has been the subject of many studies (Martín-Molina et al., 2003; Quesada-Pérez et al., 2005; Taboada-Serrano et al., 2005;

Martín-Molina et al.; 2006). When dealing with multivalent ions of large diameters, ion-size correlations play a fundamental role in determining the concentration profiles of electrolyte mixtures near charged surfaces (Taboada-Serrano et al., 2005; Quesada-Pérez et al., 2005; Martín-Molina et al.; 2006). For example, under conditions of high ionic strength or high surface charge density, monovalent counterions can displace larger multivalent counterions from the first layer of the EDL because smaller monovalent counterions can approach closer to the charged surface (Taboada-Serrano et al., 2005; Quesada-Pérez et al., 2005). Furthermore, during the formation of the EDL with either a single electrolyte or a mixture of electrolytes with multivalent counterions, overcharging phenomena as well as charge inversion may take place (Boda et al., 2002; Martín-Molina et al.; 2003; Quesada-Pérez et al., 2004; Quesada-Pérez et al., 2005; Martín-Molina et al.; 2006). The mechanism behind these phenomena is overcompensation of surface charges in a layer of strong attraction of multivalent counterions. Larger size differences of ions present in solution lead to a more pronounced charge inversion (Quesada-Pérez et al., 2004; Quesada-Pérez et al., 2005; Greberg and Kjellander, 1998).

When two charged plates approach one another, the EDL structure may be distorted by steric effects. The most interesting distortions occur under conditions of low surface charge, where EDL overlapping can take place (Ying et al., 2002; Yang et al., 2003; Hou et al., 2006). Vlachy and coworkers studied ion distributions in charged pores for single 1:1, 2:2, 1:2, and 2:1 symmetric or asymmetric electrolytes (Vlachy and Haymet, 1989; Vlachy and Haymet, 1990; Jamnik and Vlachy, 1993; Hribar et al., 2000). Calculations of the thermodynamic parameters of electrolytes were also reported. One important aspect of electrolytes confined to a nanopore is the exclusion of ions as a

function of surface charge density (Vlachy and Haymet, 1990; Jamnik and Vlachy, 1993). The topic of EDL structure inside nanopores of mixed symmetric and asymmetric electrolytes has been scarcely addressed in the literature. One study that has reported the behavior of mixtures of electrolytes between a charged micropore and external electrolyte solution is that by Jamnik and Vlachy (1995), who used Monte Carlo methods. Additionally, Boda and coworkers (2006; 2007) studied the behavior of a mixture of electrolytes inside a pore channel using a cylindrical simulation cell. They found that the charge/space competition mechanism results in selectivity for divalent ions in the confined space. This selectivity increases with decreasing pore size (Boda et al., 2006; Boda et al., 2007). Electrochemical measurements on the other hand have shown ion-sieving effects within the EDL, in which the relationship between the pore size of nanoporous electrodes and the ionic dimensions can determine the electrosorption behavior of nanoporous materials (Salitra et al., 2000; Eliad et al., 2001). The modeling studies mentioned above were focused on mixtures of ions of similar size and different valence. Thus, there is still a need to investigate the effect of ion size on the EDL formation in nanopores.

In previous work (Yang et al., 2002; Taboada-Serrano et al., 2005), we performed Monte Carlo simulations to investigate the EDL structure of a single 1:1 electrolyte inside a charged nanopore and of mixtures of electrolytes adjacent to a charged planar surface. The present work combined and expanded those studies through the application of the canonical Monte Carlo (CMC) simulation method to examine the EDL structure of symmetric and asymmetric electrolytes enclosed within charged nanopores. Our main objective was to elucidate the fundamental mechanisms behind the electrolyte

distribution within charged nanopores when a single electrolyte or a mixture of electrolytes containing monovalent and trivalent counterions was present in solution. Specifically, the effect of ion size was studied through the consideration of asymmetry in the hydrated diameters of the ionic species. The simulation results obtained in this work provide valuable information on the characteristics of the EDL inside nanopores, which leads to a better understanding of such phenomena as ion sorption and transport inside nanostructured materials.

4.2 Model and Method

Molecular simulations were carried out within a canonical ensemble (N, V, T), in which the configuration states are sampled at constant number of ions, volume, and temperature. A simulation box of dimensions $W \times W \times L$ in the x, y , and z directions, respectively, was used to represent a slit-type nanopore with two impenetrable walls at $z = 0$ and $z = L$ (i.e., W is the width and the height of the square charged surface and L is the distance between its walls). The walls were modeled as two uniformly charged planar surfaces. Periodic boundary conditions were applied in the x and y directions, and the minimum image convention was employed in the x and y directions (Allen and Tildesley, 1987). The primitive model was used, in which the ions were considered as hard charged spheres in a dielectric continuum (water). In some cases, the difference in hydrated diameters of the ionic species present was accounted for by considering two different hydrated ion diameters: 4.25 Å (which was used as the baseline) and a larger diameter of 9.0 Å (Taboada-Serrano et al., 2005).

The potential energy was calculated as the sum of single-ion (ion–wall) potential energies and two-ion (ion–ion) potential energies. Multi-body interactions were not considered in the calculation because their contributions to the total potential energy are negligible in light of the large computational demands for their consideration (Allen and Tildesley, 1987). The potential energy of interaction between the i th ion and the two charged walls was calculated from the expression (Boda et al., 1998; Yang et al, 2002):

$$v_1 = \begin{cases} +\infty, & z_i < d_i/2 \quad \text{and} \quad z_i > L - d_i/2 \\ -\frac{q_i}{2\epsilon_0\epsilon_r}(\sigma_1|z_i| + \sigma_2|L - z_i|), & d_i/2 \leq z_i \leq L - d_i/2, \end{cases} \quad (4.1)$$

where v_1 is the single-ion energy; z_i is the z coordinate of the center of hydrated ion i , whose diameter is d_i ; ϵ_0 and ϵ_r are the vacuum and relative permittivity of the dielectric continuum, respectively; q_i is the charge of ion i ; and σ_1 and σ_2 correspond to the surface charge densities of the two charged surfaces.

The interaction energy between two mobile ions (two-ion energy), v_2 , was calculated via the application of Coulomb's law:

$$v_2 = \begin{cases} +\infty, & r_{ij} < \sigma_{ij}, \\ \frac{q_i q_j}{4\pi\epsilon_0\epsilon_r r_{ij}}, & r_{ij} \geq \sigma_{ij}, \end{cases} \quad (4.2)$$

where q_j is the charge of ion j , r_{ij} is the distance between the centers of ions i and j , and σ_{ij} is the maximum distance of approach between ions i and j .

Because of the long-range nature of electrostatic interactions, long-range corrections were necessary. In the present work, we used the method employed by Boda et al (1998). Each ion was considered to possess an associated charged sheet of infinite dimensions minus the central square hole occupied by the simulation box. Each infinite charged sheet represented the image charge of each ion outside the central simulation box.³⁸ Thus, the potential energy resulting from the long-range correction between the j th ion above a center charged sheet and the i th ion, v_{LRC} , was expressed as:

$$v_{LRC} = \frac{1}{4\pi\epsilon_0\epsilon_r} \frac{q_i q_j}{W^2} [\phi(z_{ij}, \infty) - \phi(z_{ij}, W)], \quad z_{ij} \geq \sigma_{ij}, \quad (4.3)$$

$$\phi(z_{ij}, \infty) = -2\pi|z_{ij}|, \quad (4.4)$$

$$\phi(z_{ij}, W) = \left\{ 4W \ln\left(\frac{0.5 + r_1}{r_2}\right) - |z_{ij}| \left[2\pi - 4 \tan^{-1} \frac{4|z_{ij}|r_1}{W} \right] \right\}, \quad (4.5)$$

$$r_1 = \sqrt{0.5 + \left(\frac{z_{ij}}{W}\right)^2}, \quad (4.6)$$

$$r_2 = \sqrt{0.25 + \left(\frac{z_{ij}}{W}\right)^2}, \quad (4.7)$$

where $|z_{ij}| = |z_i - z_j|$

All the CMC simulations were performed by an upgraded version of a code developed in FORTRAN 90/95 (Taboada-Serrano et al., 2005), which was adapted for its application to nanopores. Each simulation began with an initial random configuration of

confined ions. The length of the simulations was 500,000 cycles. After the initial equilibration period, the final 20% of the total run time was used to calculate the ensemble averages.

4.3 Results and Discussion

4.3.1 Comparison of the classical GC theory and Monte Carlo simulations

Before studying the EDL structure inside nanopores with mixtures of trivalent and monovalent ions, we tested the CMC simulation scheme by comparing our results with the GC theory and Grand Canonical Monte Carlo (GCMC) simulation results (Yang et al., 2006). As shown in Figure 4.1, the ion concentration profiles obtained by the CMC simulation were compared with those predicted by the classical GC theory and GCMC simulations inside a 20-Å-diameter nanopore for a single 1:1 electrolyte—with an ionic diameter of 4.25 Å—at an ionic strength of 1.0 M, and with a surface charge density equivalent to -0.1 C/m^2 . When compared with the CMC and GCMC simulation results, the GC theory slightly overestimates the counterion concentration in the entire pore region because this theory does not consider ion size and ion-ion correlations. On the other hand, the EDL structure described by the CMC simulation is almost identical to that described by the GCMC simulation. The slight discrepancy, in which the CMC simulation predicts a lower counterion concentration than the GCMC simulation, is a consequence of the difference in the total number of ions inside the simulation box.

The limitation of CMC simulations is that the imposition of a closed system (i.e., constant number of ions inside the pore) may not allow the system to reach equilibrium with an outside bulk solution. In this regard, the GCMC method presents an advantage

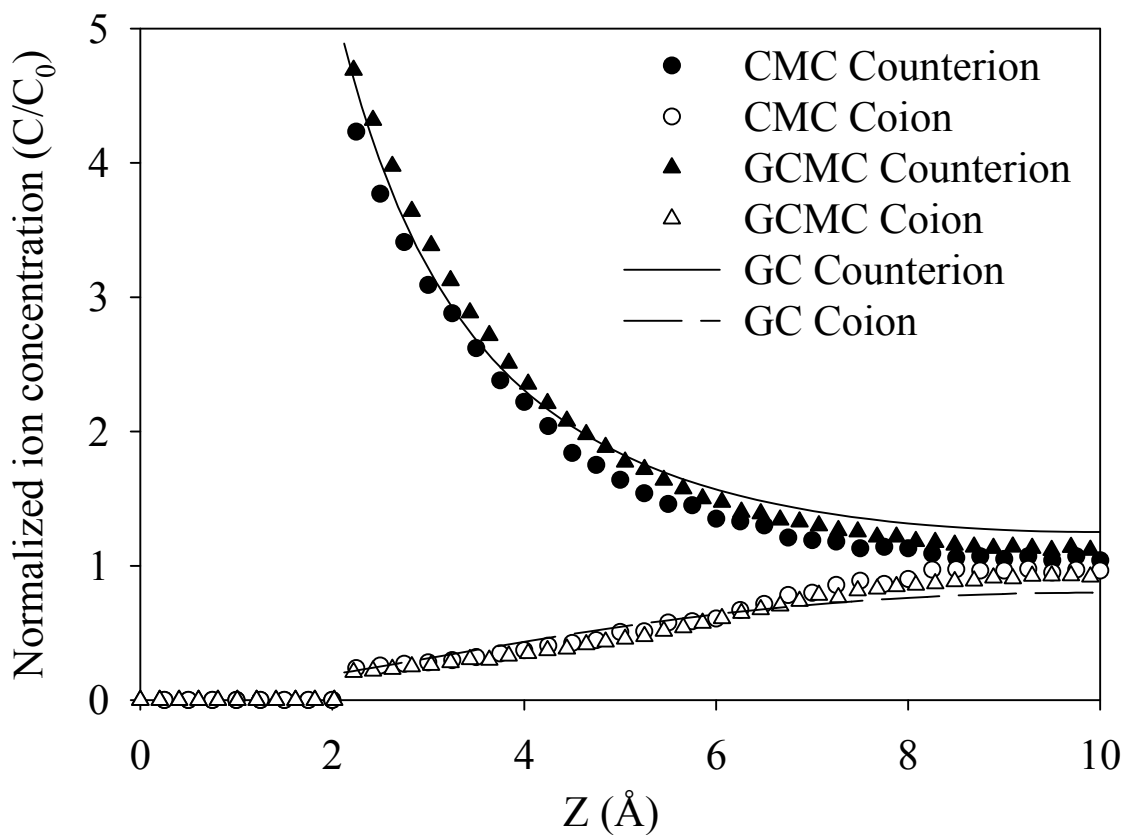


Figure 4.1 Comparison of ion concentration profiles in a slit-type nanopore of 20-Å diameter derived by the classical GC theory and Monte Carlo simulation techniques for a single 1:1 electrolyte of ionic strength of 1.0 M and a surface charge density of -0.1 C/m^2 . The value of C represents the local concentration of ions inside the pore. The value of C_0 is the average concentration of ions inside the pore in the absence of charge.

for EDL calculations inside confined spaces because the chemical potential remains constant providing an unambiguous way to determine the number of ions inside the pore in equilibrium with an outside solution (Valleau and Cohen, 1980; Yang et al., 2002). However, the absence of a method for the determination of a mean activity coefficient that includes the effects of ion size makes the application of the GCMC method difficult for mixtures of asymmetric electrolytes. Since our CMC simulations for the case of a 1:1 electrolyte inside a nanopore and the simulations reported in the literature (Yang et al., 2002) do not present dramatic differences, as shown in Figure 4.1, CMC simulations were used in this work to investigate the EDL formation inside nanopores. In the present work, the value of C_0 or “average concentration” was determined by independent CMC simulations of the electrolytes inside uncharged nanopores at identical conditions of ionic strength in each case. Therefore, C_0 should be regarded as an average concentration inside the pore in the absence of charge. This concentration may or may not coincide with the value of bulk concentration of a solution in equilibrium with the pore.

4.3.2 EDL behavior of a symmetric electrolyte in a nanopore

Figure 4.2(a) presents the concentration profiles for a single 1:1 electrolyte inside a 20-Å-diameter nanopore at an ionic strength of 0.5 M and a surface charge density equivalent to -0.05 C/m^2 . In this case, the monovalent coions and counterions have equal diameters of 4.25 Å. As shown in Figure 4.2(a), the local ion concentrations of coions and counterions at the center of the nanopore do not reach the average concentration, which indicates the occurrence of EDL overlapping. This is an extremely important feature of the EDL behavior in a charged nanopore under certain conditions of

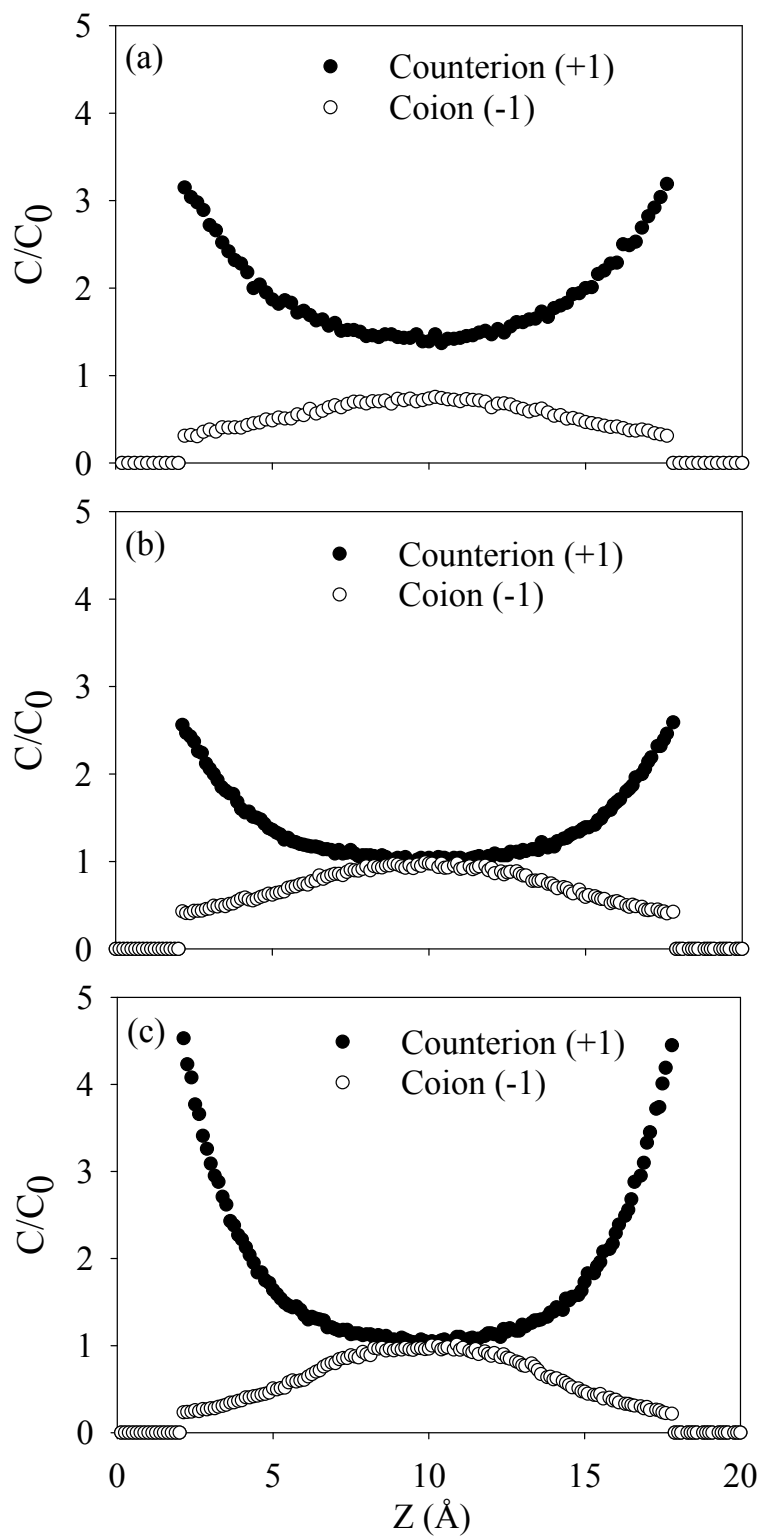


Figure 4.2 Counterion and coion concentration profiles in a 20-Å-diameter nanopore for a single 1:1 electrolyte at (a) ionic strength of 0.5 M and surface charge density of -0.05 C/m^2 , (b) ionic strength of 1.0 M and surface charge density of -0.05 C/m^2 , and (c) ionic strength of 1.0 M and surface charge density of -0.1 C/m^2 .

sufficiently low ionic strength and surface charge density. As a result of the strong electrostatic force and confinement effects, the coions are excluded from the charged pore space and the counterions dominate the EDL structure (Vlachy and Haymet, 1990). Therefore, the counterion concentration is higher than the coion concentration throughout the entire pore region, as shown in Figure 4.2(a).

The occurrence of EDL overlapping depends on ionic strength and surface charge density (Hou et al., 2006). When the ionic strength of electrolyte increases from 0.5 M to 1.0 M, as depicted in Figure 4.2(b), both the coion and counterion concentrations achieve the average concentration at the central region of the nanopore. In addition, the effect of EDL overlapping can be reduced by increasing the surface charge, as can be observed for the case of a higher surface charge density (-0.1 C/m^2), depicted in Figure 4.2(c). The maximum concentration of counterions next to the surface is approximate 1.8 times the value of that in Figure 4.2(b). It is energetically favorable for counterions to accumulate closer to the charged surface and, thus, to form compact EDLs.

Consequently, the occurrence of EDL overlapping is a function of ionic strength and surface charge density, and ultimately determines the accessibility of nanopores to ionic species. Coions are expelled from the pores, while counterions become the predominating ionic species in the EDL.

4.3.3 EDL Behavior of an Asymmetric Electrolyte in Nanopores

Figures 4.3(a) and 4.3(b) present the simulation results of EDL formation in a nanopore of 20-Å diameter with a single 3:1 electrolyte at an ionic strength of 1.0 M and a surface charge density of -0.025 C/m^2 . When the trivalent counterions and monovalent

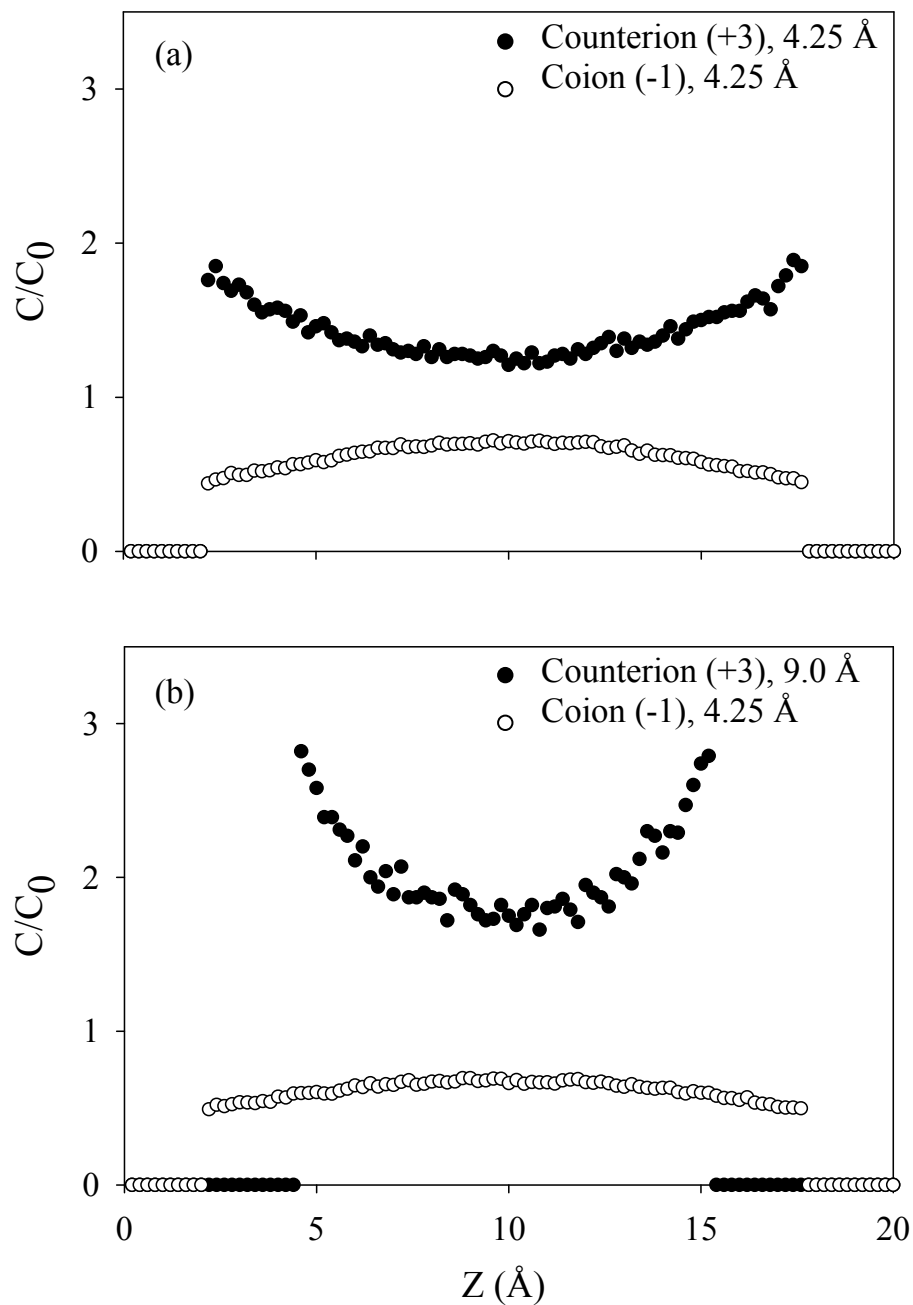


Figure 4.3 EDL structure in a 20-Å-diameter nanopore for an asymmetric 3:1 electrolyte at an ionic strength of 1.0 M and a surface charge density of 0.025 C/m^2 for (a) monovalent coions and trivalent counterions that have diameters of 4.25 Å and (b) monovalent coions and trivalent counterions that have diameters corresponding to 4.25 and 9.0 Å, respectively.

coions have an equal size (4.25 Å), as shown in Figure 4.3(a), the double layer extends throughout the entire pore region, resulting in mild EDL overlapping. In Figure 4.3(b), the trivalent counterions and monovalent coions have different diameters (9.0 and 4.25 Å, respectively). In this case, the marked ion-size asymmetry leads to high local concentrations of counterions adjacent to the charged surfaces. Although the concentration of counterions decays sharply towards the central region of the pore, a more pronounced EDL overlapping effect takes place. The EDL structure becomes dominated by the counterions present in solution. Furthermore, due to the competition between ion-charge and confinement effects, the ion distribution in such a confined space is sensitive not only to the pore size but also to the dimension of the ions.

4.3.4 EDL Behavior of Mixtures of Symmetric and Asymmetric Electrolytes in Nanopores at Low Surface Charge Density

To examine the effect of ion size on the EDL behavior in the presence of mixtures of symmetric and asymmetric electrolytes, CMC simulations were performed under three conditions: (i) trivalent and monovalent counterions of equal size (4.25-Å diameter), (ii) trivalent counterions having a larger diameter (9.0 Å) than monovalent ones (4.25-Å diameter), and (iii) trivalent counterions of 4.25-Å diameter and monovalent counterions having a diameter of 9.0 Å. For all three conditions, the diameter of monovalent coions was fixed at a 4.25 Å and the number of trivalent counterions was the same as that of monovalent counterions inside the simulation box.

Simulation results for a mixture of 1:1 and 3:1 electrolytes confined in a 20-Å pore at an ionic strength of 1.0 M and a surface charge density of -0.04 C/m^2 are

presented in Figure 4.4(a). When the difference in ion size is not taken into account, the distribution of ionic species is determined mainly by their ionic valences in terms of the electrostatic interaction with the charged surfaces. Due to their lower charge, the concentration profile for monovalent counterions is much less concave than that for trivalent counterions resulting in mild EDL overlapping. Figure 4.4(b) presents the case of ions of different diameters. In this case, the local concentration of monovalent counterions adjacent to the surface increases slightly, resulting in a more concave counterion concentration profile, and a milder EDL overlapping effect compared to the one observed in Figure 4.4(a). Moreover, due to their higher valence and larger size, the trivalent counterions present a high value of maximum local concentration at a larger distance than in Figure 4.4(a), accompanied by overlapping at the central region of the nanopore. In the case depicted in Figure 4.4(c), the trivalent counterions have a diameter of 4.25 Å (i.e., they are smaller than the 9.0-Å-diameter monovalent counterions). Because of their smaller size and higher valence, the trivalent counterions in this case present energetic advantages in terms of preferential surface charge screening over the monovalent counterions. Although both counterion species present a similar magnitude of local maximum concentration closest to the surfaces, the monovalent counterions exhibit a larger ion-exclusion volume and are distributed in a comparably reduced confined space. Thus, the concentration profile of monovalent counterions shifts towards higher positive values than in the previous cases, and these counterions become responsible for EDL overlapping.

Because of the size asymmetry, trivalent and monovalent counterions have different distances of closest approach to the surface in this study: larger ions cannot

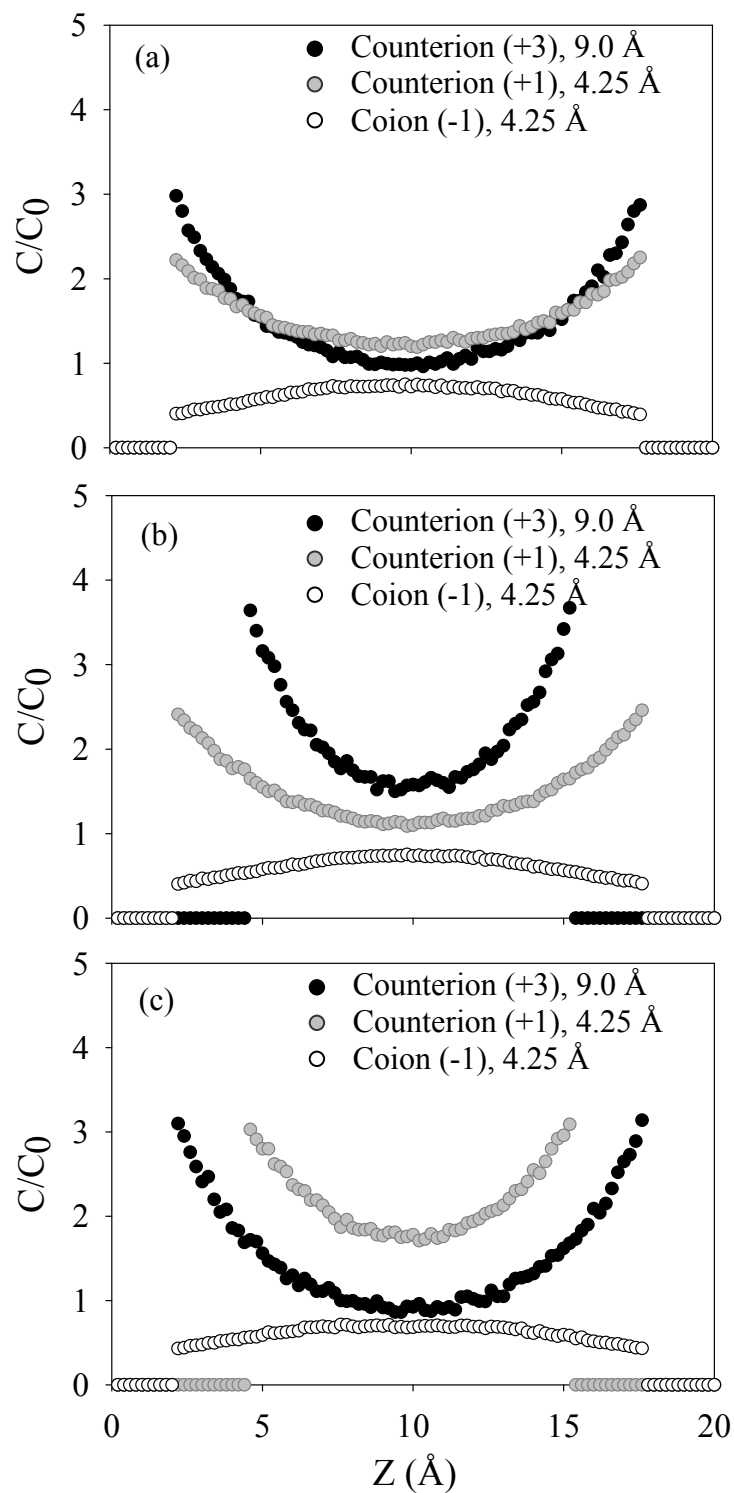


Figure 4.4 EDL structure in a nanopore of 20-Å diameter for a mixture of 1:1 and 3:1 electrolytes at an ionic strength of 1.0 M and a surface charge density equivalent to -0.04 C/m^2 . The sizes of the ions selected are as follows: (a) trivalent and monovalent counterions with equal diameters (4.25 Å), (b) 9.0-Å-diameter trivalent counterions and 4.25-Å-diameter monovalent counterions, and (c) 4.25-Å-diameter trivalent counterions and 9.0-Å-diameter monovalent counterions.

approach as close to the charged surface as smaller ions. At the same time, high-valence counterions preferentially screen the surface charge, which results in an overall lower potential energy. These competitive effects result in the “inversion” of the order between monovalent and trivalent counterions observed in Figure 4.4(c) with respect to Figure 4.4(b). In fact, the ion size affects not only the steepness of the concentration profiles and the composition of the layer of fluid adjacent to the charged wall, but also the nature of EDL overlapping and which ions will be excluded from the porous space.

4.3.5 EDL behavior of mixture electrolytes in nanopores at high surface charge density

In addition to the phenomena discussed in the previous section at conditions of low surface charge, charge inversion is expected to take place under conditions of high surface charge density and high electrolyte concentration. Martín-Molina and coworkers (2005; 2006) predicted charge inversion in a planar EDL with a mixture of electrolytes containing multivalent and monovalent ions. Vlachy (2001) also found a concentration of coions in the micropore larger than the concentration of the equilibrium bulk conditions for a 3:3 electrolyte. Usually, a rise in the surface charge density involves an increase in the magnitude of electrolyte concentration inside nanopores. Figure 4.5(a) presents the EDL structure of a mixture of electrolytes at a high surface charge density (-0.16 C/m^2) and an ionic strength of 5.0 M in a 100-Å-diameter nanopore. All ions have a diameter of 4.25 Å. The layer of counterions next to the surface creates a locally charged plane that is responsible for the occurrence of a maximum in the coion concentration. At a location of 5 Å from the surface, the distributions of trivalent and monovalent counterions exhibit a

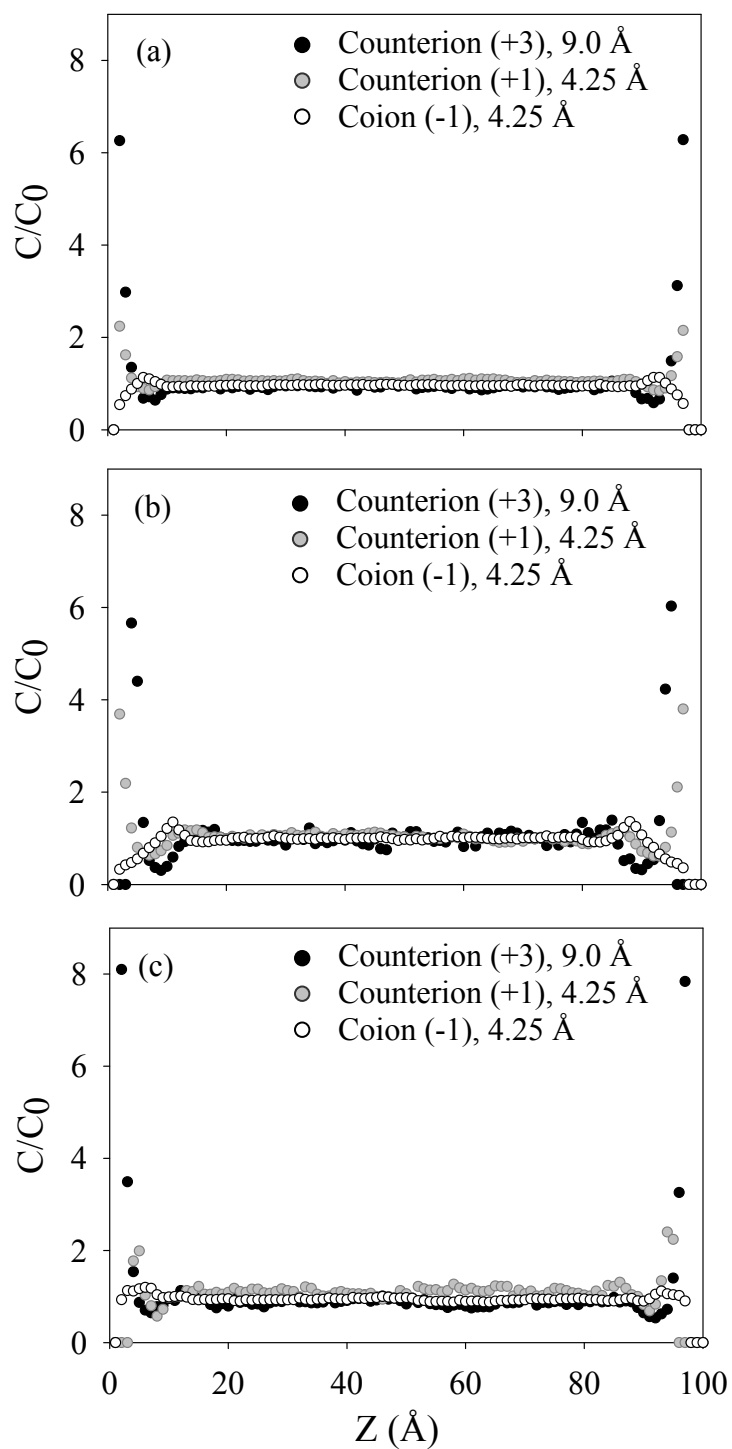


Figure 4.5 EDL structure in a nanopore of 100-Å diameter at a high surface charge density (-0.16 C/m^2) for a mixture containing 1:1 and 3:1 electrolytes at an ionic strength of 5.0 M. The sizes of the ions selected are as follows: (a) trivalent and monovalent counterions with equal diameters (4.25 Å), (b) 9.0-Å-diameter trivalent counterions and 4.25-Å-diameter counterions, and (c) 4.25-Å-diameter trivalent counterions and 9.0-Å-diameter monovalent counterions.

minimum after their maximum concentrations, whereas the coion distribution presents a maximum at the same location. This finding implies that both counterions approaching toward the surface draw a considerable quantity of coions because of the strong ion–ion interactions, resulting in what is known as planes of charge inversion.

Ion size plays a role in the onset and characteristics of charge inversion as it does during the phenomenon of EDL overlapping. As shown in Figure 4.5(b), the monovalent counterions tend to replace the larger trivalent counterions close to the surface, because the closest distance to the surface at which trivalent counterions can accumulate increases. Therefore, the plane of charge inversion (i.e., the plane at which the maximum in coion concentration occurs) is displaced further away from the charged surface. On the other hand, as depicted in Figure 4.5(c), the most preferential accumulation of smaller trivalent counterions next to the surface results in a “region” of charge inversion rather than the distinctive planes observed in Figures 4.5(a) and 4.5(b). The ion distribution profiles also demonstrate the direct effect of ion size on the magnitude of charge inversion. As shown in Figure 4.5(b), by considering the size-exclusion effect, the value of the maximum in the counterion concentration profiles increases from $C/C_0=1.13$ to $C/C_0=1.35$.

Figure 4.6(a) presents the behavior of a mixture containing 1:1 and 3:1 electrolytes in a 20-Å-diameter nanopore, in which the ionic strength and surface charge density correspond to 5.0 M and -0.16 C/m^2 , respectively. Because of the combined effects of confinement and high surface charge, the trivalent counterions populate a dense layer adjacent to the surface but achieve only a fraction of the average concentration, C_0 , in the central region of the pore. On the other hand, the monovalent counterions and

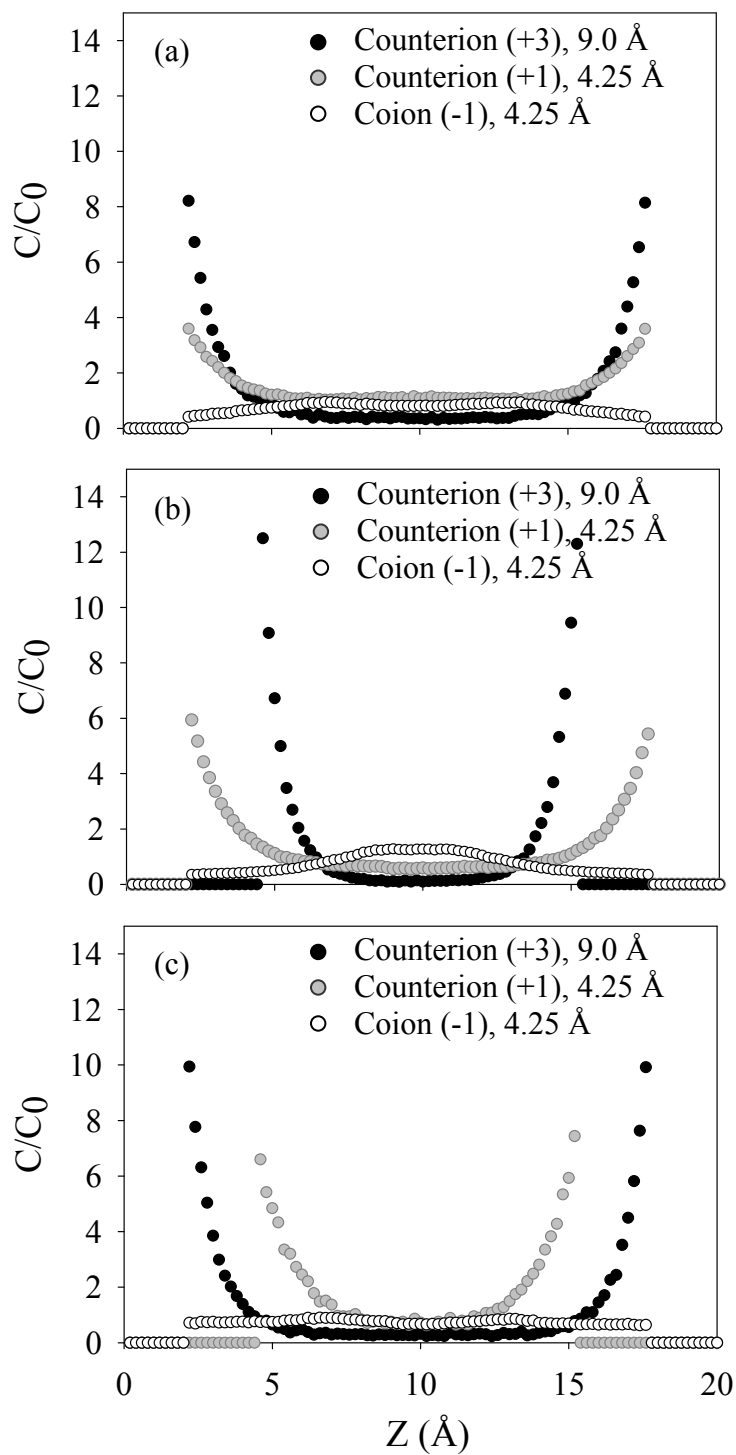


Figure 4.6 EDL structure in a nanopore of 20-Å diameter at a high surface charge density (-0.16 C/m^2) for a mixture containing 1:1 and 3:1 electrolytes at an ionic strength of 5.0 M. The sizes of the ions selected are as follows: (a) trivalent and monovalent counterions with equal diameters (4.25 Å), (b) 9.0-Å-diameter trivalent counterions and 4.25-Å-diameter monovalent counterions, and (c) 4.25-Å-diameter trivalent counterions and 9.0-Å-diameter monovalent counterions.

coions approximately reach their average concentrations at the central region of the pore. In this case, charge inversion is insignificant. In Figure 4.6(b), different ion sizes were taken into account (i.e., trivalent counterions have a diameter of 9 Å). As can be seen, the concentration profile of coions significantly peaks at the center of the pore, i.e., charge inversion occurs in the central region of the pore. The magnitude of the maximum peak of coion concentration corresponds to $C/C_0=1.27$ in the center of the pore. The trivalent and monovalent counterions present minimum local concentrations corresponding to $C/C_0=0.10$ and $C/C_0=0.59$, respectively, in the center of the pore. The concentration of trivalent counterions tends to peak as close to the surface as possible to compensate for the increase in the overall potential energy that results from the preferential surface charge screening next to the surface by the smaller monovalent counterions. Hence, the distributions of both counterion species closest to the surface shift towards higher concentrations. Figure 4.6(c) shows a mixture of electrolytes containing large monovalent counterions (with a diameter of 9.0 Å) and small trivalent counterions (with a diameter of 4.25 Å). Because of the competitive effects of ion size vs ion charge that determine which species will preferentially screen the surface charge, smaller trivalent counterions present a comparative advantage. This behavior leads to a high local concentration of trivalent counterions in the first layer of fluid next to the surface. However, the maximum peak of coion concentration becomes less apparent and the magnitude of charge inversion is reduced.

To further illustrate the confinement effect on the EDL structure inside nanopores, we can compare the specific distributions of trivalent counterions depicted in Figures 4.5(b) and 4.6(b). In a large nanopore with a 100-Å diameter, the larger size of trivalent

counterions prevents them from approaching closer to the surface, resulting in lower local concentrations adjacent to the surface. On the other hand, when the separation distance between the two charged surfaces is reduced and the double layers overlap, the concentration profile of trivalent counterions reveals an extreme distribution: most of the trivalent counterions are likely to accumulate at the closest distance. Moreover, the two planes of charge inversion detected in the wider nanopore merge into a single region of charge inversion at the center of the pore, as the pore size decreases. One should note that this phenomenon is most evident when the larger counterion bears the higher charge. Therefore, competitive effects between ion-size and ion-charge enhance the effects of confinement along with the effects of increase in surface charge.

4.4 Summary

In the present study, the EDL behavior in the presence of mixtures of symmetric and asymmetric electrolytes confined to a slit-type nanopore was investigated via CMC simulations using a primitive model. The EDL structure is determined not only by the ionic strength or the surface charge in the system, but also by the ion size and charge. Furthermore, confinement effects on EDL structure are enhanced by size and charge asymmetries.

The electrolyte distribution within small nanopores is sensitive to the size of ionic species present in solution. At low surface charge, strong EDL overlapping with obvious exclusion of the larger counterion from the porous space takes place. In addition, under certain conditions of high ionic strength and high surface charge density, the coions present local values of concentration higher than those of the counterions. This

phenomenon, which can be described as charge inversion, is a result of strong ion–ion correlations. The occurrence of charge inversion becomes most apparent in the presence of trivalent counterions with a large diameter. Additionally, a central region instead of individual planes of charge inversion can be observed as the pore diameter decreases in the presence of large, high-valence counterions.

Finally, in light of the results discussed in this work, we would recommend to consider ion-size effects when dealing with the identification of factors affecting ion selectivity, ion separation, and energy storage using nanostructured materials, processes which are highly governed by the EDL structure inside the pores.

Although the present work raises some important issues in terms of ion-size effects, it is desirable to overcome the limitations of the CMC simulations for further studies. In this regard, we are currently developing the means to overcome the difficulties in the application of an improved GCMC method to this problem. The new approach is expected to yield additional insights in terms of ion selectivity, EDL capacitance, and electrosorption inside nanopores.

CHAPTER 5

THE SIZE-EXCLUSION EFFECT ON PORE ACCESSIBILITY OF NANOPOROUS CARBON MEMBRANES

The electrochemical experiments and modeling studies in Chapters 3 and 4 showed that the properties of ionic species can significantly influence the electrical double-layer formation associated with the transport and sorption of ions inside nanopores. Therefore, this chapter is focused on the study of the size-exclusion effect within a nanoporous carbon membrane whose size-sieving properties were studied via molecular permeation and cyclic voltammetry experiments. Two phenomena, simple diffusion and electrochemically-aided diffusion, were tested. Molecular diffusion through the membrane was caused by a concentration gradient across the membrane, and was facilitated by electrosorption of ions under an externally applied electric field. The diffusion behavior of molecules transported through the membrane was characterized by the values of the diffusion coefficient. Because larger molecules are strongly restricted in terms of penetrating the pores, the molecular-size based selectivity of the mesoporous carbon membrane could be readily observed. In the bi-molecular permeation experiments, the transport of larger molecules through the membrane showed a more extensive retardation, resulting from the competitive mechanism between the two kinds of molecules in accessing the pore. A series of voltammetric experiments involving a mesoporous carbon membrane immersed in various electrolytes with ions of different sizes allowed the observation of ion-exclusion phenomena. It was found that the ion-size

effect is significant for electrochemically-aided diffusion and electrosorption processes. The number of cations inside the pores of the membrane decreases with increasing cation size.

5.1 Introduction

Carbon materials of porous structure such as activated carbon, carbon fiber, carbon aerogel, and graphite are ubiquitous and indispensable in various technologies. Because of their high surface area and unique physicochemical properties, porous carbons constitute very attractive materials for many applications, such as separation processes, water purification, catalysis support, and energy storage. When pore sizes approach molecular dimensions, activated carbons and carbon molecular sieves can provide selective separation of molecules via differences in their adsorption capacity or diffusion rates (Koresh and Soffer, 1980; Koresh and Soffer, 1983; Koresh and Soffer, 1987; Karanfil et al., 2006). In fact, the molecular size effect is one of the critical factors for the performance of porous carbon materials.

The size-based selectivity of molecules transported through a membrane represents a possible separation mechanism within various chemical and biological systems (Jirage et al., 1997; Martin et al., 2001; Yu et al., 2001; Wirtz et al., 2002; Yamaguchi et al., 2004; Li et al., 2004; Snyder and Tsapatsis, 2007). For example, Jirage et al. (1997) reported selective membranes containing an ensemble of gold nanotubes to selectively separate small molecules on the basis of molecular-sieving effects, in which transport selectivity increased as the inner diameter of the nanotubes decreased. Electrosorption, defined as the accumulation of ions next to a charged surface without

triggering electrochemical reactions, is another promising application of porous carbon materials in energy storage and capacitive desalination (Farmer et al., 1996; Frackowiak and Béguin, 2001; Ying et al., 2002). In electrosorption processes, porous carbon materials can be considered as electrical double-layer capacitors (EDLCs), characterized via a double-layer capacitance at the interface of the carbon and the electrolyte (Yang et al., 2003; Hou et al., 2006). A number of studies have reported that porous carbon materials with very small pores exhibit limitations for molecule penetration, and thus, they do not contribute to the double-layer capacitance because of the molecular-sieving effect (Koresh and Soffer, 1983; Lin et al., 1999; Salitra et al., 2000; Eliad et al., 2001; Barbieri et al., 2005). Therefore, porous carbon materials could be potentially used to estimate effective ion dimensions of aqueous and organic electrolytes, as well as ionic liquids (Eliad et al., 2001; Ania et al., 2006; Eliad et al., 2006).

The property of porous carbon materials that is indicative of their molecular-sieving capability is the corresponding pore-size distribution. The pore-size distribution affects not only the surface area available for sorption, but also the accessibility of molecules (Endo et al., 2001; Hou et al., 2006; Raymundo-Piñero et al., 2006; Salitra et al., 2006). According to the nomenclature of the International Union of Pure and Applied Chemistry (IUPAC), the pore size can be classified as micropores (pore diameter < 2 nm), mesopores (2 nm < pore diameter < 50 nm), and macropores (pore diameter > 50 nm). Conventional porous carbon materials usually exhibit broad pore-size distributions, ranging from micropores to macropores, and the corresponding pores are randomly connected. The presence of micropores is an essential feature in the high specific surface area for porous carbon materials. However, there is a conflict between enhancing surface

area of pores and improving the pore accessibility; micropores exhibit slow molecular motion and low conductivity, and their porous structures collapse during high-temperature treatments (Lin et al., 1999; Yoon et al., 2000; Yang et al., 2003; Hou et al., 2006; Liang et al., 2007). By contrast, mesopores show a fast mass transfer rate of molecules (Yoon et al., 2000; Yang et al., 2003; Hou et al., 2006). Therefore, ordered mesoporous carbons, which have narrow pore size distributions and less micropores present, are much desirable materials in numerous applications (Liang et al., 2007). The relationship between the pore size of porous carbon materials and the molecular dimensions has a profound effect on transport and sorption of molecules confined in a small space.

Recently, mesoporous carbon materials with ordered structures have been synthesized by us and other research groups using the self-assembly synthesis method via soft templates through co-condensation and carbonization (Liang et al., 2004; Tanaka et al., 2005; Meng et al., 2005; Lu, 2006; Rodriguez et al., 2006; Hu et al., 2007; Liang et al., 2007). Triblock copolymers were used as structure-directing agents. Phloroglucinol can form triple hydrogen bonding to the polyethylene chains of triblock copolymer. The hydrogen bonding between soft templates and carbon precursors is the key to the successful self-assembly synthesis of highly ordered mesoporous carbons (Liang et al., 2004; Laing et al., 2006). In addition, mesoporous carbon materials have been made with different morphologies, such as monoliths, films, fibers, and micro/nano wires (Liang et al., 2006; Steinhart et al., 2007).

The objective of the present work is to examine the molecular-sieving properties of the mesoporous carbon materials with well defined porous structures that have been

synthesized. Two phenomena, simple diffusion and electrochemically-aided diffusion and electrosorption, are tested with a specific focus on size-exclusion effects. First, diffusion of different-size molecules through the pores, caused by a concentration gradient, is studied. Second, diffusion and electrosorption of different-size ionic species into the pores due to an applied electric field is studied. The experimental results obtained in this work can provide a better understanding of the capabilities of these novel mesoporous carbon materials and contribute to assessing their potential applications, especially for separation technologies and energy storage.

5.2 Materials and Methods

5.2.1 Preparation and Characterization of Carbon Materials

Mesoporous carbon membranes were prepared via self-assembly of block copolymer and phenolic resin (Liang et al., 2006). Typically, 6.3 g of phloroglucinol (Aldrich) and 6.3 g of F127 (EO₁₀₆PO₇₀EO₁₀₆, Aldrich) were dissolved in 45 g of ethanol-water mixture (10:9 in mass ratio) containing 0.5 g of concentrated HCl (Aldrich). An amount of 6.5 g of formaldehyde (37 % in water, Sigma) was then added to the solution. The mixture was stirred at room temperature and turned cloudy after about 17 min, indicating the occurrence of phase separation. After stirring for another 13 min, the polymer-rich phase was separated out by centrifuge at 9500 rpm for 4 min. The polymer phase collected in the bottom of the centrifuge tube was re-dissolved in 10 g of ethanol. After removal of any air bubbles, the clear ethanolic solution of polymer was then loaded on a substrate via the tape-casting technique, giving a homogeneous and clear polymer film on the substrate. The film was dried in the air at room temperature overnight and

subsequently cured in an oven at 80 °C for 24 h. The self-standing polymer film was detached from the substrate and cut into desired sizes. Carbonization was carried out in a tubular furnace under inert atmosphere (e.g. N₂) at 400 °C for 2 h with a heating ramp of 1 °C/min and then at 850 °C for another 2 h with a ramp of 5 °C/min from 400 °C. The nitrogen sorption isotherm of mesoporous carbon membrane was recorded on a Micromeritics Gemini 2375 analyzer at 77 K. The specific surface area was calculated using the Brunauer-Emmett-Teller (BET) method from the nitrogen adsorption data in the relative pressure range (P/P_0) of 0.05-0.30. The pore size distribution plot was derived from the adsorption branch of the isotherm based on the Barrett–Joyner–Halenda (BJH) method.

5.2.2 Permeation Experiment

The permeation experiments were carried out using a measuring cell as shown in Figure 5.1. The permeation cell consisted of the source and receiver solutions, which were separated by a mesoporous carbon membrane with a permeation area of 0.5 cm². Before any experiments were performed, the carbon membrane was immersed in deionized water to ensure proper wetting conditions. The source solution was an aqueous solution containing the probe species. The receiver solution initially contained deionized water. The volumes of source and receiver solutions were 0.8 cm³ and 16.8 cm³, respectively. In each experiment, the receiver solution was continuously pumped through the flow cell installed in the circuiting line. The concentration of probe species in the receiver solution was measured in the flow-through cell as a change in spectroscopic absorbance using an ultraviolet-visible (UV-VIS) spectrophotometer (Cary 5000, Varian

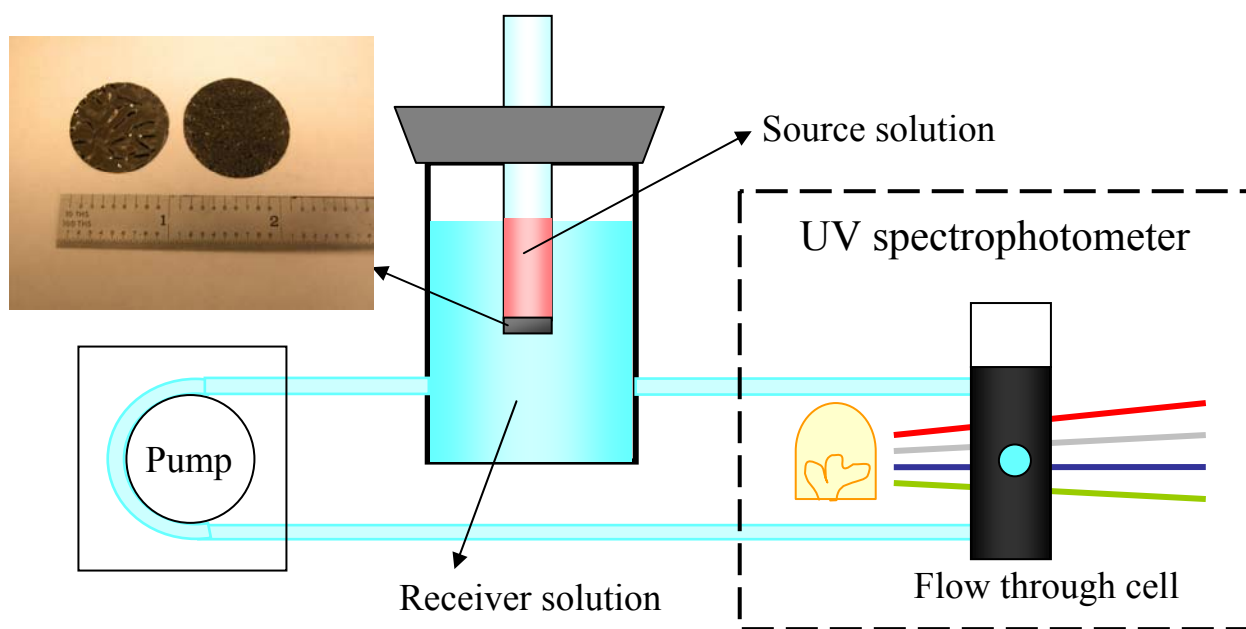


Figure 5.1 Schematic of the setup for permeation experiments with the carbon membrane. A UV-VIS spectrophotometer was used to measure the concentration of probe molecule in the receiver solution as a function of time. A photograph image reveals the size of our membranes synthesized for our experiments.

Inc.). Calibration of the optical absorbance of the molecules was made by measuring the absorbance of a series of dilution solutions over a wide range of concentrations. For the permeation experiments, two test molecules, anilinium (97%, Sigma-Aldrich, molecular weight 94) and rhodamine B (95%, Sigma-Aldrich, molecular weight 479), were chosen in order to examine the effect of molecular dimension on the transport of species through the mesoporous carbon membrane. The reproducibility of the results was confirmed by repeating several permeation experiments under identical conditions. All experiments were carried out at room temperature.

5.2.3 Electrochemical Measurement – Cyclic Voltammetry

Cyclic voltammetry experiments were performed using a CH Instruments model 604B electrochemical analyzer in conjunction with a Bioanalytical Systems model C-2 electrochemical cell. A three-electrode system was used for these experiments; the working electrode was a small piece of carbon clipped to a platinum wire in the aqueous solution. The counterelectrode was a large piece of carbon material, and the reference electrode was an Ag/AgCl electrode immersed in a 3 M NaCl electrolyte solution (Bioanalytical Systems). The electric current, obtained in the original experimental data, was normalized as the specific capacitance in Farads per gram of carbon material and per unit scan rate. The range of potentials applied to the system was +0.6 to -0.4 V within a pure EDL window where faradaic reactions do not take place. Thus, the specific capacitance may be basically attributed to the EDL capacitance as a result of electrosorption of ions (Yang et al., 2003; Hou et al., 2006). Aqueous solutions used in cyclic voltammetry experiments were prepared using deionized water (Millipore) and

sodium chloride (NaCl, >99%), magnesium chloride (MgCl₂, 98%) and tetrahexylammonium chloride (THACl, 96%) obtained from Sigma-Aldrich.

5.3 Results and Discussion

5.3.1 Characterization of Carbon Membranes

Figure 5.2 presents the nitrogen adsorption/desorption isotherms and the pore size distribution of the carbon membrane. The transmission electron micrograph (TEM) image showed the highly ordered porous structure of the carbon membrane and its BET surface area was determined to be 332.1 m²/g. The contribution of micropores to surface area was 78.1 m²/g, and a large portion of the pores was in the mesoporous range of 5 to 10 nm.

5.3.2 Molecular-Sieving Effect

Figure 5.3(a) presents the absorbance of UV spectra for the single-component permeation of 5 mM anilinium chloride solution transported through the membrane to deionized water. The absorbance at a wavelength of 230 nm was used for measuring the anilinium concentration in the receiver solution. Neutral aniline absorbed light at a wavelength of 280 nm (Katakura et al., 1994). Comparing the absorbance changes at 230 nm and 280 nm indicates that anilinium is the predominant species in the solution. Moreover, the pH values were measured in the source and receiver solutions to ensure that the proportion of neutral aniline and anilinium cation was kept constant during the experiment. The chemical structure of anilinium is also shown on Figure 5.3. As shown in Figure 5.3(b), the experimental data are represented as plots of moles of the probe

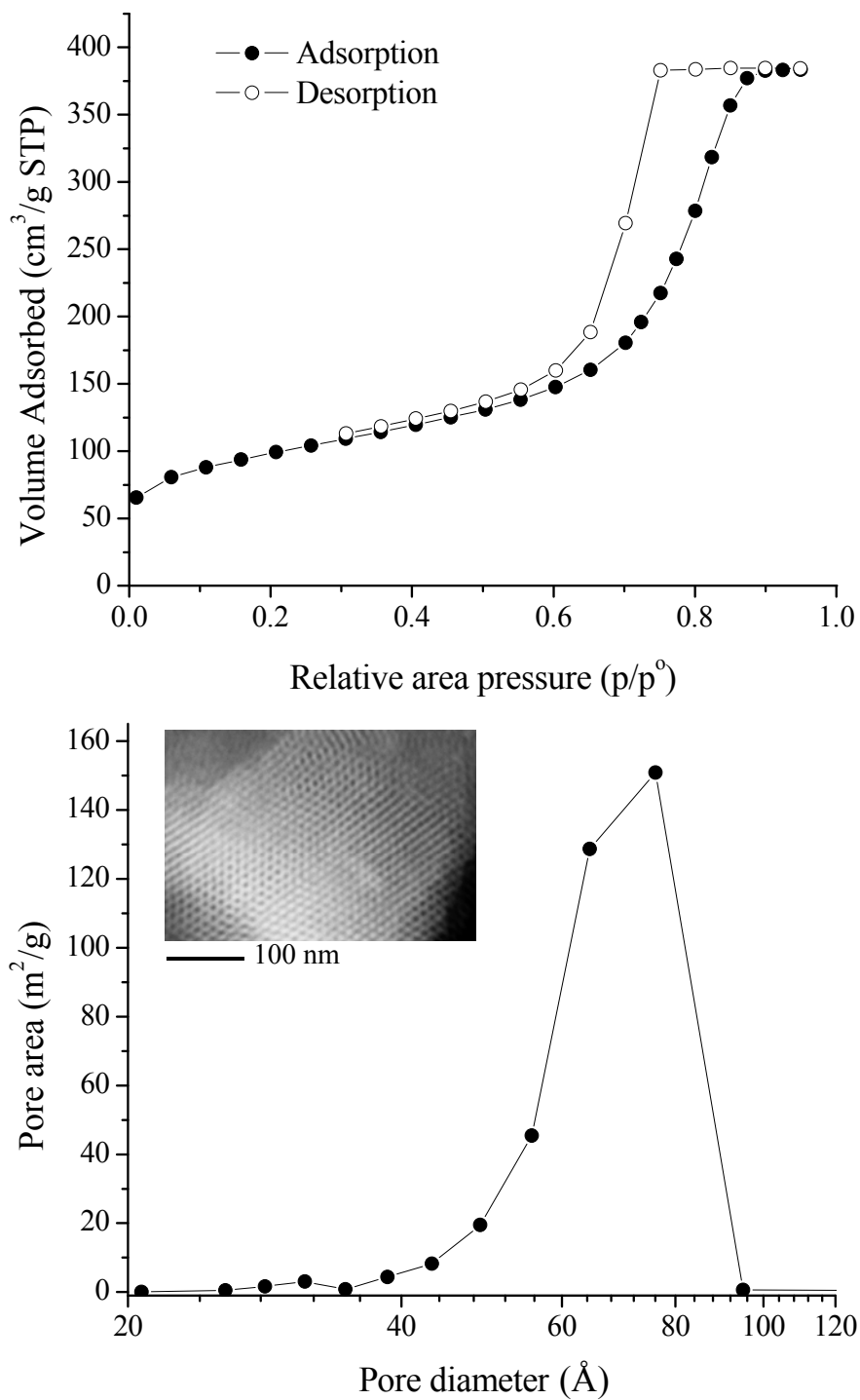


Figure 5.2 (a) Nitrogen adsorption/desorption isotherms and (b) the pore size distribution plot of the mesoporous carbon membrane (STP, standard temperature and pressure).

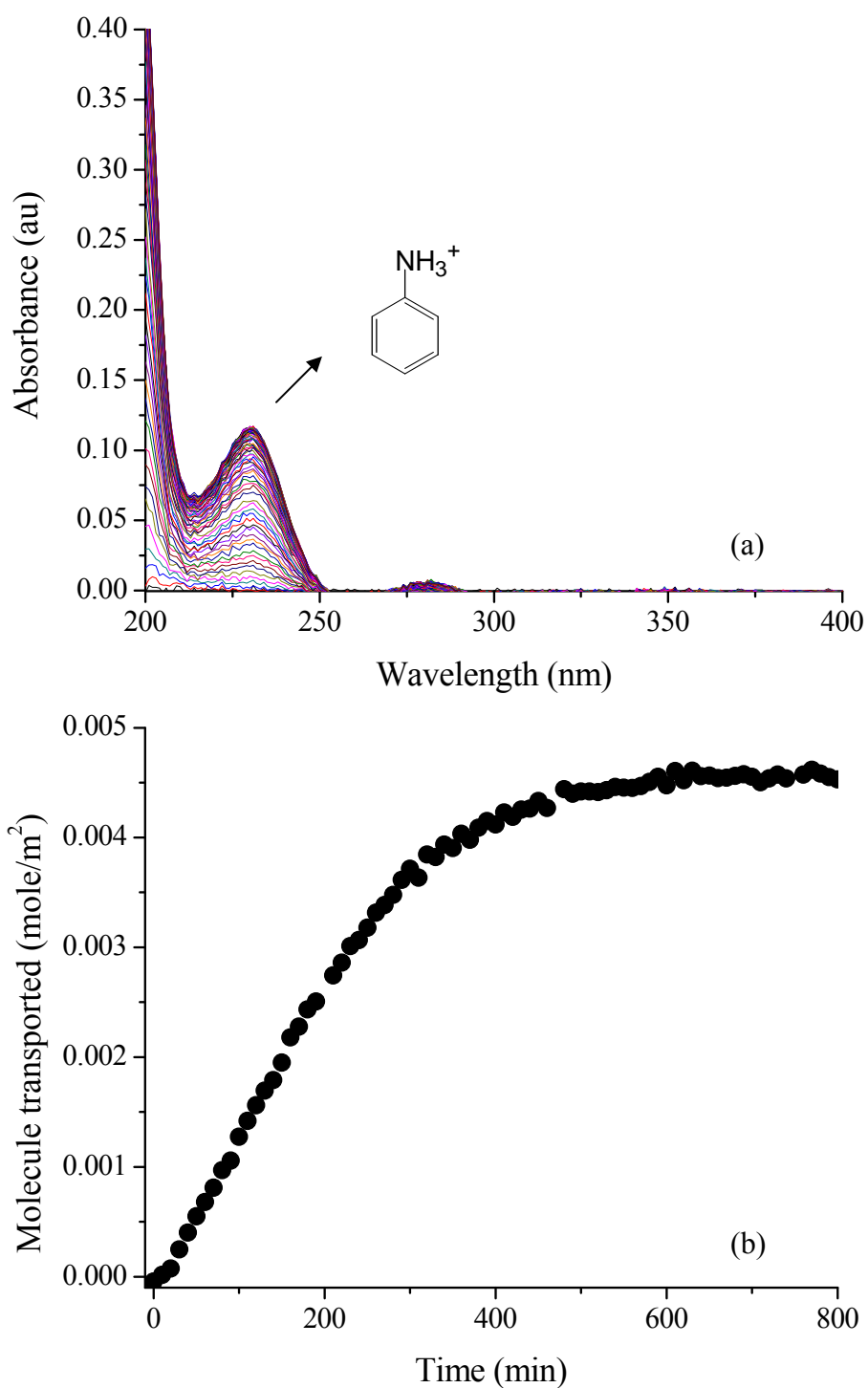


Figure 5.3 Single-component experiment for a source solution of 5 mM anilinium chloride transported through the mesoporous carbon membrane. (a) Absorbance spectra of anilinium recorded at the interval of 10 min. (b) Concentration of anilinium in the receiver solution as a function of time.

substance transported per unit area (in square meters) of membrane vs. permeation time. Because the transport of anilinium through the membrane is a result of the concentration gradient between the source and receiver solutions, the concentration initially increases linearly as a function of time and finally reaches a plateau. Figure 5.4 shows the data in the single-component experiment for a source solution of 5 mM rhodamine B and a receiver solution of deionized water. In the beginning of the experiment, the absorbance change of rhodamine B was insignificant in the receiver solution. After a retention time of approximate 180 minutes, the rhodamine B molecules penetrated through the membrane and the linear increase of concentration in the receiver solution was observed. This time lag for the transport of rhodamine B through the membrane, forming the steady-state concentration gradient, may result from the combination of sorption onto the pore walls and diffusion through the membrane. As a result, the molecular-transport rate decreases as the size of molecule increases (Jirage et al., 1997). Rhodamine B molecules have larger size than anilinium molecules, thus there are more restrictions for Rhodamine B molecules in penetrating the pores, leading to slow permeability.

Since the volume of the receiver solution was much larger than that of the source solution, the decrease concentration in the source solution was small and the change in concentration of probe molecules is typically linear in the initial permeation step. The concentration difference between the two solutions can be initially approximated as constant in each permeation experiment. One can calculate the flux of component i , J_i , through the membrane obtained from the slope of the straight line shown in Figures 5.3(b) and 5.4(b). The effective diffusion coefficient ($D_{i,\text{eff}}$), which is defined by

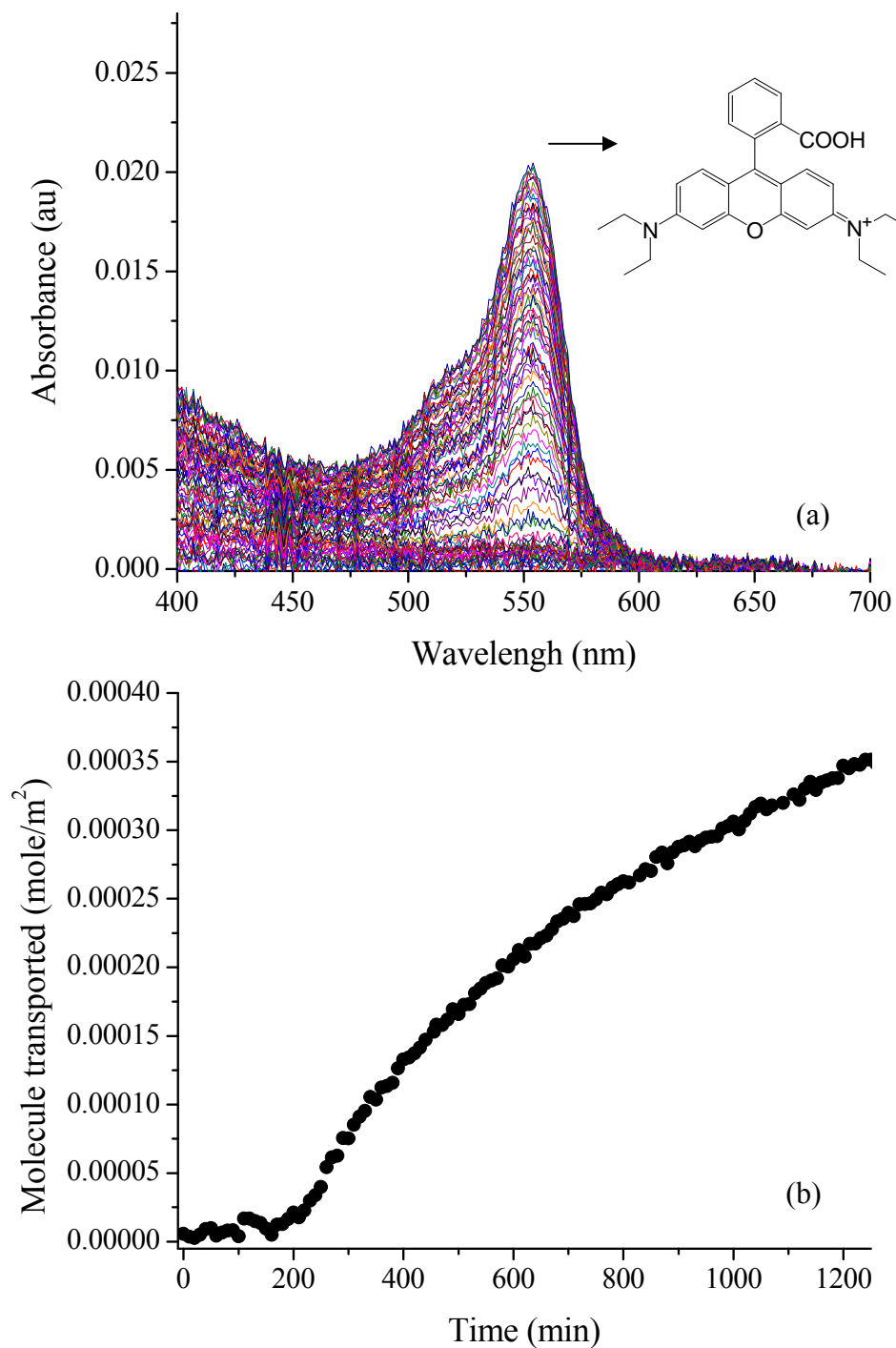


Figure 5.4 Single-component experiment for a source solution of 5 mM rhodamine B transported through mesoporous carbon membrane. (a) Absorbance spectra of rhodamine B recorded at the interval of 10 min. (b) Concentration of rhodamine B in the receiver solution as a function of time.

considering a linear dependence of the diffusion rate and the composition gradient of component i , can be expressed as (Taylor and Krishna, 1993):

$$J_i = -D_{i,\text{eff}} \frac{dC_i}{dx} \quad (5.1)$$

where dC_i / dx is the concentration gradient of component i and x is the diffusion coordinate across the membrane thickness. In the present work, the effective diffusion coefficient was used to characterize the diffusivity of molecules transported from the source solution through the membrane and to prove the size-sieving properties of the carbon membrane. For experimental data, the effective diffusion coefficients for anilinium and rhodamine B were calculated as $1.38 \times 10^{-6} \text{ cm}^2/\text{s}$ and $5.39 \times 10^{-8} \text{ cm}^2/\text{s}$, respectively. The result indicates that the size-exclusion effect decreases the transport rate of rhodamine B, much more than that of anilinium. Due to confinement, the diffusion rate of molecules is greatly affected by their size. This observation demonstrates the molecular sieving capabilities of the mesoporous carbon membrane.

The diffusivity of component i in bulk solution (water) can be characterized by the diffusion coefficient, $D_{i,0}$, which can be approximated using the Stokes-Einstein equation (Bird et al., 2002):

$$D_{i,0} = \frac{kT}{6\pi\eta r} \quad (5.2)$$

where k is the Boltzmann constant, T is the Kelvin temperature, η is the viscosity of water, and r is the radius of the diffusing molecule. When taking the radii of anilinium and rhodamine B as 2.9 Å and 8.0 Å, respectively, the diffusion coefficients for anilinium and rhodamine B in bulk solution are $8.45 \times 10^{-6} \text{ cm}^2/\text{s}$ and $3.06 \times 10^{-6} \text{ cm}^2/\text{s}$, respectively.

The diffusive-transport selectivity of the membrane (α) can be defined by the ratio of the diffusion coefficients of anilinium to that of rhodamine B. The selectivity of $\alpha = 25.6$ within the mesoporous carbon membrane was significantly enhanced from that of $\alpha = 2.8$ in bulk solution. The experimental result demonstrates that the mesoporous carbon-based membrane shows the ability to separate the molecules via molecular-size selectivity.

According to the Renkin equation, the diffusion coefficient of component i confined to the pore, $D_{i,\text{pore}}$, is determined by the ratio of the molecular radius (a) to the pore radius (r) (Rekin, 1954; Kathawalla et al., 1989):

$$\frac{D_{i,\text{pore}}}{D_{i,0}} = \left(1 - \frac{a}{r}\right)^2 \left[1 - 2.104 \frac{a}{r} + 2.09 \left(\frac{a}{r}\right)^3 - 0.95 \left(\frac{a}{r}\right)^5\right] \quad (5.3)$$

Theoretically, the restriction factor ($D_{i,\text{pore}} / D_{i,0}$) can be quantified using the Renkin equation. When one takes into account the radius of anilinium as 2.9 Å, the restriction factors are 0.59, 0.70, and 0.78 for the pore size of 5 nm, 7 nm, and 10 nm, respectively. The values of 0.18, 0.32, and 0.47 represent the theoretical restriction factors of rhodamine B in the pore size of 5 nm, 7 nm, and 10 nm. Theoretically calculated values correspond to selectivity coefficients $\alpha = 9.0$, 6.0, and 4.6 for the 5-nm,

7-nm, and 10-nm mesopores, respectively. However, a selectivity coefficient $\alpha = 25.6$ was obtained from the permeation experiment. While a six-fold decrease in diffusivity with respect to bulk conditions inside the mesopores was observed for anilinium, a two-order-of-magnitude decrease in diffusivity was observed for rhodamine B. Although the theoretical prediction clearly underestimates the membrane selectivity obtained by the permeation experiments, it provides consistent description of permeability characteristics. The difference between experimental and theoretical values may be caused from the simplifications introduced in the Renkin equation by ignoring the interaction between molecule and pore surface, the nonparallel alignment and nonuniformity of pores, and the irregular pore connections which decrease the molecular motions.

Figure 5.5 illustrates the absorbance changes and the molecule-transported histories for anilinium and rhodamine B in the receiver solution during two-component permeation experiments. As expected, the anilinium molecules are of smaller size and can easily pass through the membrane with less pore restriction. On the contrary, larger rhodamine B molecules, with a slow transport rate, cannot be detected by the UV-VIS instrument until a permeation time of 500 minutes. In comparison with the results in single-component experiments, the effective diffusion coefficient for anilinium slightly increases to $1.57 \times 10^{-6} \text{ cm}^2/\text{s}$. On the other hand, the diffusivity of rhodamine B in a mixture (i.e., $D_{i,\text{eff}} = 2.76 \times 10^{-8} \text{ cm}^2/\text{s}$) is much slower than that in single-component solution. The carbon membrane shows greater selectivity of smaller anilinium over large rhodamine, $\alpha = 56.9$. It is also noted that the retention time of rhodamine B extends from 180 minutes, in the single-component experiments, to 500 minutes, in the two-component experiments. These data suggest that these two molecules not only interact with the pore

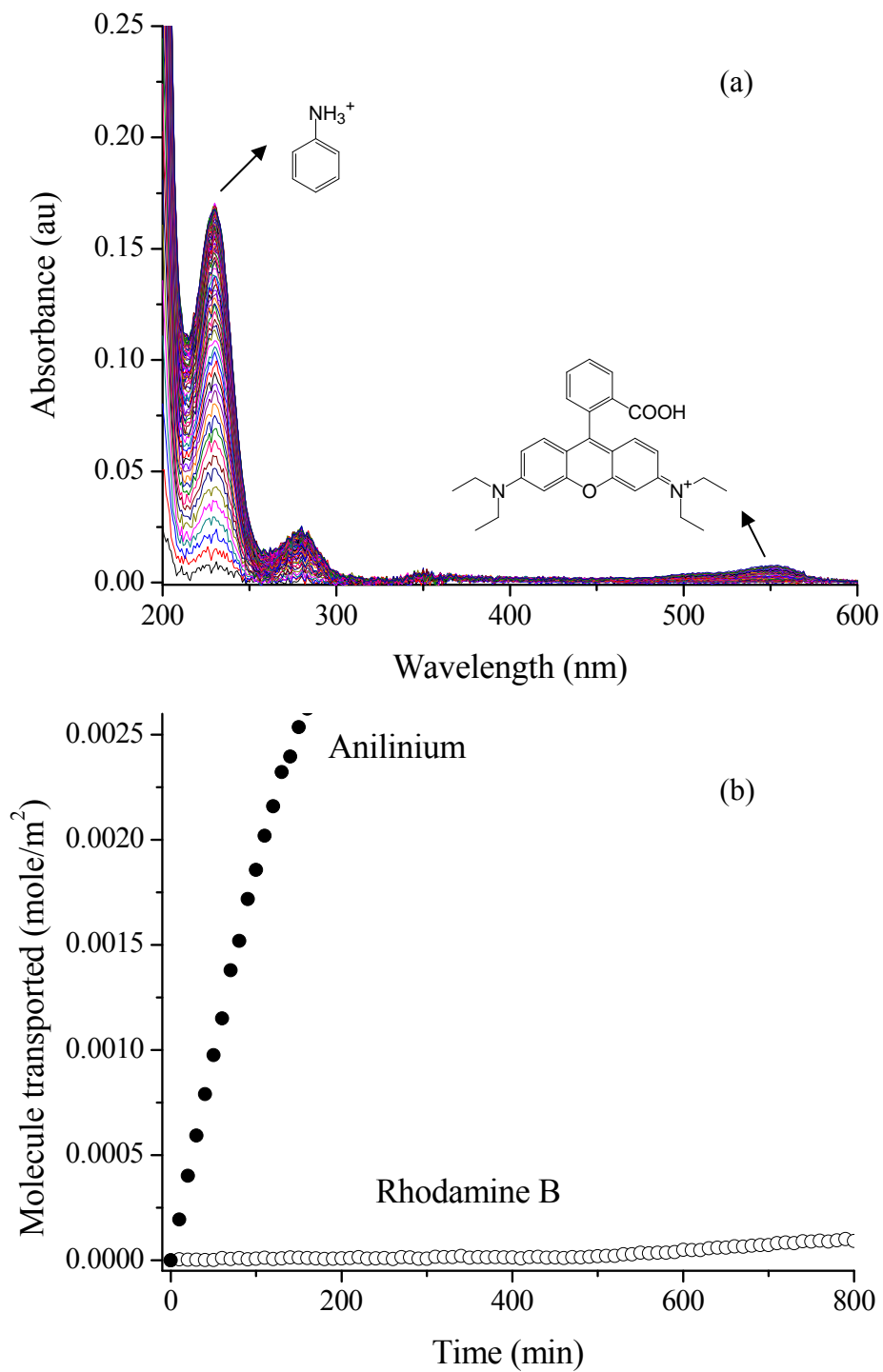


Figure 5.5 Two-component experiment for a source solution of the mixture of 5 mM anilinium chloride and 5 mM rhodamine B transported through mesoporous carbon membrane. (a) Absorbance spectra of anilinium and rhodamine B recorded at the interval of 10 min. (b) Concentration of test molecules in the receiver solution as a function of time.

wall of the membrane but also with each other. The transport of large rhodamine B through the membrane is limited by the presence of small anilinium. When both anilinium and rhodamine B exist in the solution, they compete with each other for access into the pores. Initially, the pores are only accessible to the smaller anilinium molecules, while at the same time, larger rhodamine B molecules are excluded from the pores. When the concentration gradient of anilinium decreases sufficiently, the driving force of rhodamine B is able to overcome the competitive size effect, allowing this species to pass through the pores. Therefore, the mesoporous carbon membrane can separate larger rhodamine B molecules from smaller anilinium molecules in a mixture solution.

In general, diffusion due to concentration gradients is responsible for the movement of the permeate molecule from the source solution through the carbon membrane and into the receiver solution. Three factors can explain the mechanisms behind the retardation of diffusive transport of larger molecules within pores. First, the steric hindrance effect plays a determining role in the molecular accessibility at the entrance of pores (Kathawalla et al., 1989). Because the accessible cross-sectional area of pores decreases with increasing molecular size, there is higher restriction for a larger molecule to enter the pores. Second, the motion of a molecule through a small pore is significantly affected by the interaction in terms of friction resistance between the molecule and the pore surfaces (Martin et al., 2001; Kathawalla et al., 1989). Finally, a larger molecule with associated large exclusion volume from the pore wall decreases the average concentration inside the pore and reduces the average flux density (Cervera et al., 2003). Furthermore, when dealing with a mixture of species, a competitive behavior between molecules that have different sizes can be observed. Because of the confinement

effect, the transport of larger molecules may be impeded by the transport of smaller molecules, leading to a more extensive retardation during the permeation process.

5.3.3 Ion-Size Effect

The investigation of the ion-size effect on EDL formation during electrosorption by the mesoporous carbon membrane was carried out using cyclic voltammetry experiments. Figures 5.6 and 5.7 present the cyclic voltammograms of the mesoporous carbon membranes in various electrolyte solutions using a slow scan rate (1 mV/s) and a fast scan rate (10 mV/s). The electrolyte solutions studied in comparative series were sodium chloride, magnesium chloride, and tetrahexylammonium chloride. All electrolyte solutions that contained the same amount of chloride anions had the same charge capacity in each experiment.

The point of zero charge (pzc) is the value of the electrical potential at which the surface charge density is zero. Previous studies have shown that the specific capacitance at a slow scan rate goes through a minimum around the point of zero charge (pzc) for both positive and negative scans (Yang et al., 2003). As shown in Figure 5.6, the pzc of the mesoporous carbon membrane in a 0.1 M sodium chloride solution can be estimated as 0.06 V (*vs.* Ag/AgCl in 3 M NaCl). When a potential range is chosen on either side of the pzc, electrosorption of counterions that have an opposite charge to that of the charged surface takes place in the EDL, resulting from the electrostatic interactions of ionic species and the charged surface. For example, Figure 5.6 shows that the cyclic voltammogram of NaCl exhibits a rectangular shape of the curve with increasing capacitance towards positive and negative potentials. Because of their similar hydrated

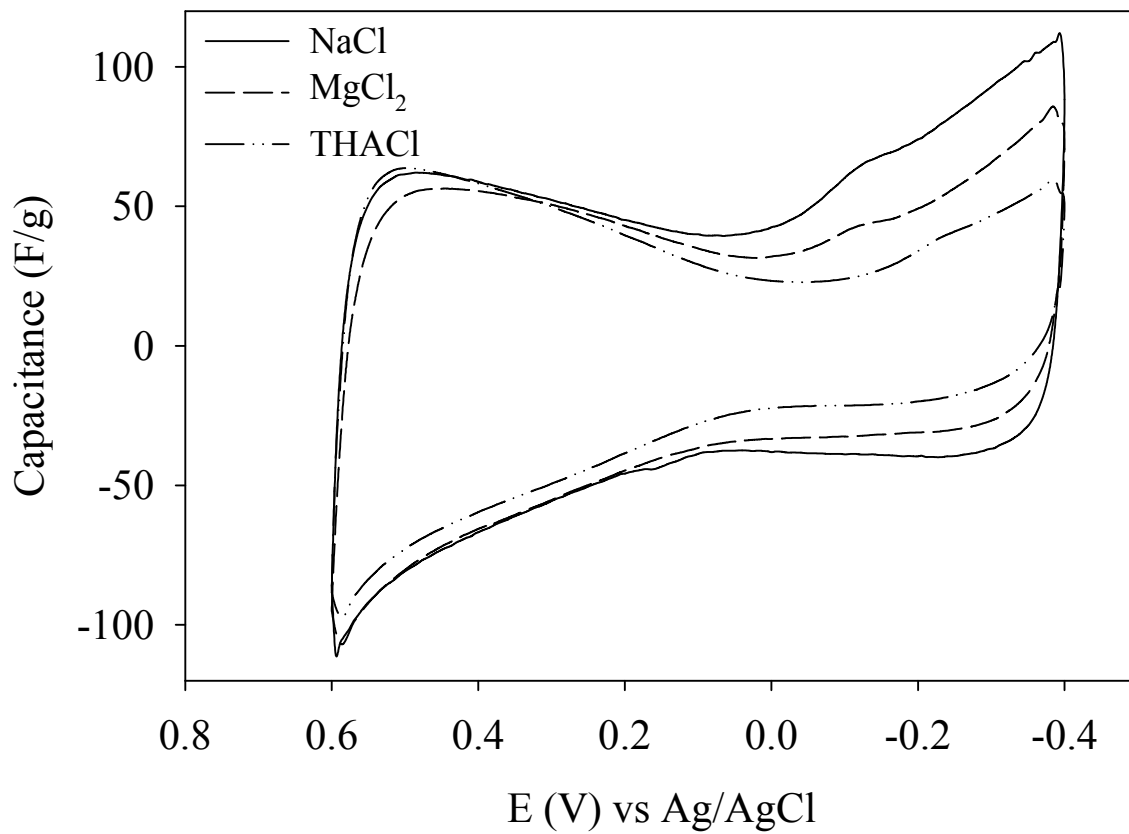


Figure 5.6 Cyclic voltammety experiments with the mesoporous carbon membrane immersed in various electrolyte solutions, including 0.1 M NaCl, 0.05 M MgCl₂, and 0.1 M THACl. The data were obtained at a slow scan rate of 1 mV/s.

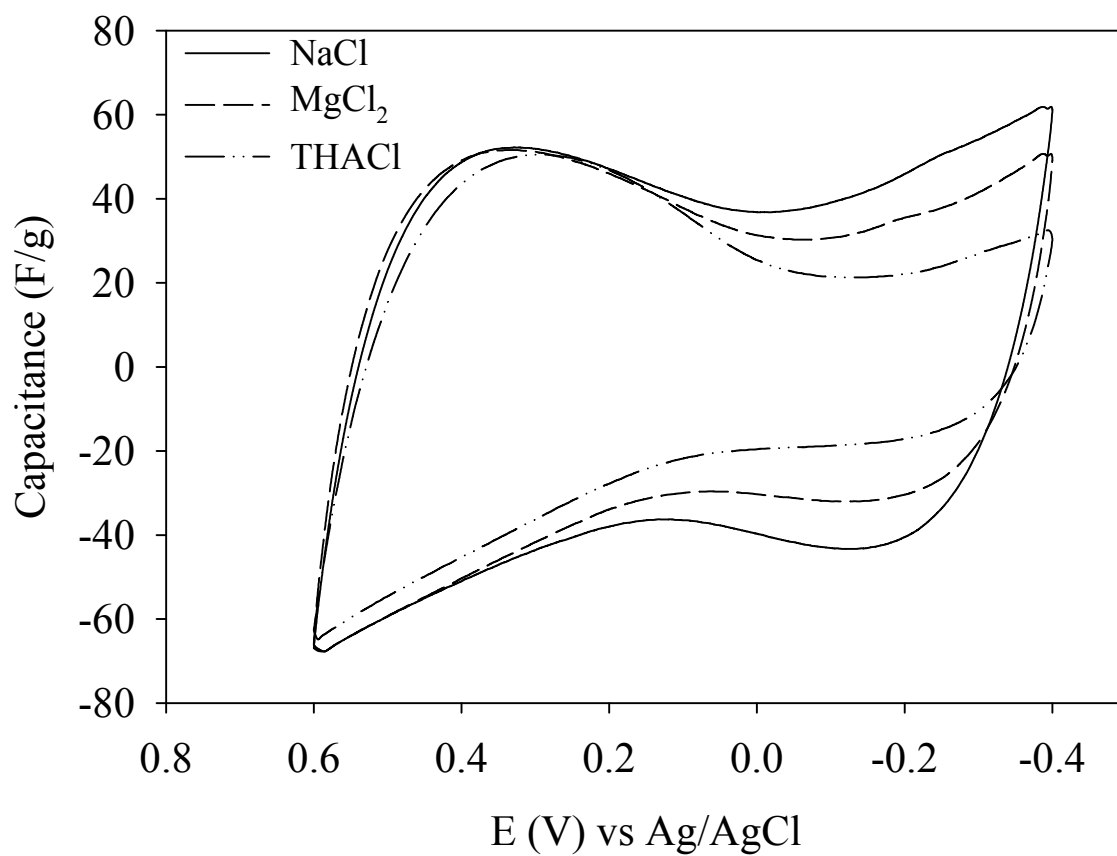


Figure 5.7 Cyclic voltammety experiments with the mesoporous carbon membrane immersed in various electrolyte solutions, including 0.1 M NaCl, 0.05 M MgCl₂, and 0.1 M THACl. The data were obtained at a fast scan rate of 10 mV/s.

ion size of 4.25 Å, the sodium cation (Na^+) and chloride anion (Cl^-) have a symmetric response during the electrosorption process (Salitra et al., 2000; Eliad et al., 2001). At negative potentials with respect to the pzc, the electrosorption of Na^+ cations dominates the EDL formation in order to neutralize the charged surfaces. At the same time, Cl^- anions are excluded from the charged pores. On the other hand, Cl^- anions provide the major contribution toward electroneutrality within the EDL at positive potentials with respect to the pzc.

For a magnesium-chloride electrolyte solution, the ion-size effect of the mesoporous carbon membrane on the voltammetric behavior can be observed in Figures 5.6 and 5.7. For example, a comparison of cyclic voltammograms in 0.1 M NaCl and 0.05 M MgCl_2 solutions at a slow scan rate (1 mV/s) indicates that the capacitance of magnesium ion (Mg^{2+}) drops to 73.1 F/g at the potential of -0.4 V, which is only 83 % of the capacitance of Na^+ ion. On the other hand, Cl^- ions present in these two solutions have the same magnitude of capacitance at the potential positive to the pzc. Because Mg^{2+} and Na^+ cations provide the same charge capacity in each system, the EDL capacitance can be independent of ion charge. Therefore, the loss of the double-layer capacitance can be mainly attributed to the size-exclusion effect of Mg^{2+} ions, which have a larger hydrated diameter of 8.0 Å, by the micropores of the carbon membrane. This result, furthermore, implied the successful development of EDL in the mesoporous region for large hydrated cations.

The voltammetric behavior of tetrahexylammonium ion (THA^+), which has tetraalkyl chains of about 8.6-Å radius, can further demonstrate the size effect on ion electrosorption. It can be seen that the cyclic voltammogram of tetrahexylammonium

chloride shows an asymmetric response at the potential window between -0.4 V and 0.6 V. As shown in Figure 5.6, the capacitance value decreases from 88.5 F/g for Cl^- anion to 50.0 F/g for THA^+ cation. This considerable loss (44 %) of double-layer capacitance may result from the poor micropore accessibility for larger THA^+ ions. Moreover, an increase in ionic dimension results in a decrease of double-layer capacitance. For instance, when using a slow scan rate (Figure 5.6), the values of the capacitance measured at -0.4 V for Na^+ , Mg^{2+} , and THA^+ cations are 86.7 , 73.1 , and 50.0 F/g, respectively. The explanation is that larger ions have larger limitations in terms of pore accessibility and tend to be excluded from the micropores, and at the same time, the density of ion accumulation inside the charged mesopores decreases with increasing ion size. Thus, the mesoporous carbon membrane exhibits significant ion-size properties for ion electrosorption, which is affected by the size of ionic species involved in the EDL formation.

Overall, the electrosorption behavior of porous carbon materials depends on two factors: (i) mass transfer rate of ions to access the pores, and (ii) concentration of ions inside the pores at equilibrium with bulk solution. As known from our previous studies (Yang et al., 2003; Hou et al., 2006), mesopores are much easily and rapidly penetrated by ions, leading to good electrochemical accessibility. Therefore, the equilibrium state in mesopores can be reached at a slow scan rate (e.g., 1 mV/s), and the concentration of ions inside the pores will be the factor determining the capacitance measured in this experiment. When the pore size and the dimension of ionic species are comparable, the confinement effect becomes important and affects the concentration and distribution of ions inside a charged pore. This phenomenon is much related to the EDL formation,

which is highly dependent on the characteristics of the ionic species present, such as ion charge and size. Due to the difference in ion charge, exclusion of coion from charged pores can be expected, while, at the same time, counterions become the predominating species contributing towards electroneutrality in the EDL. However, when the size of the counterion is comparable to the size of the pores, the EDL formation becomes sensitive to the size of ionic species in the confinement space. EDL formation may be distorted by steric effects, because larger ions associated with a stronger size-exclusion effect cannot approach the pore surface as close as smaller ions. A larger ion-exclusion volume causes a decrease in the average concentration of ions in the charged pores. This feature explains the asymmetric curves obtained in cyclic voltammetry experiments when the ion-size effect occurs. The selectivity of ion electrosorption of mesoporous carbon could be achieved according to the affinity of ions of smaller size.

5.4 Summary

The present work demonstrates the molecular size-based sieving effect of mesoporous carbon membranes on molecules transported through the pores. The relationship between the pore size and the molecule size plays an extremely important role in the determination of transport and sorption behavior of mesoporous carbon membranes in aqueous solutions. One of the consequences is that molecular transport rates through a membrane, induced by a concentration gradient, can be decreased by the molecule-size effect. The restriction to penetrate the pore increases with increasing molecule size, and at the same time, the average concentration of molecules in the pore solution can be further reduced by their larger exclusion volume. When dealing with a

mixture of solutions, molecules associated with different sizes present competition in accessing the pores, resulting in a more extensive retardation of larger molecules transported through the membrane.

When an external electric field is imposed, the ion-size effect on electrosorption of ions by the mesoporous carbon membrane is observed. Then ions can develop a double layer in the region of mesopores, and the properties of the ions determine the double-layer capacitance. While symmetry in electrosorption of cations and anions takes place for small, symmetric electrolytes, for asymmetric electrolytes involving unequal ion size, ions of larger size have more distance of closest approach to pore surface. Hence, larger ions are more easily excluded from the charged pores, resulting in asymmetric electrosorption behavior. This also suggests that ion accumulation in a charged pore, in which EDL forms, can determine the pore occupancy. As a result, the density of ions inside the pores decreases with increasing ion size. This observation is important because it plays a central role in ion selectivity. Membrane selectively allows the permeation of smaller ions with their size affinity. Selective separation of ions of different sizes may be achieved via the application of an external electric field on mesoporous membranes.

Consequently, the size-exclusion effect is one of the most important properties to be considered when dealing with the physical chemistry of porous materials in aqueous solutions and their possible applications in separation processes. The findings of this work can provide fundamental knowledge for the utilization of nanoporous carbon materials in separation processes, energy storage, or removal of contaminant from aqueous solutions.

CHAPTER 6

ELECTROSORPTION SELECTIVITY OF IONS FROM MIXTURES OF ELECTROLYTES INSIDE NANOPORES

In Chapter 4, the electrical double layer (EDL) formation in a slit-type nanopore was simulated via the canonical Monte Carlo (CMC) method. The simulation results indicated that ion charge and size have a significant influence on the ion distribution in the restricted space of pores. Furthermore, the experimental data shown in Chapter 5 provided supporting evidence on the occurrence of size exclusion effects determining pore accessibility in terms of transport and sorption of ions in a realistic system.

In this chapter, grand canonical Monte Carlo (GCMC) simulations are employed to study the selective electrosorption of ions from a mixture of symmetric and asymmetric electrolytes confined in the pores. GCMC simulations have the advantage over other Monte Carlo methods of unambiguously quantifying the total number of ions in the pore solution. In the present work, the exclusion parameter and the selectivity factor are used to evaluate the selective capacity of pores towards different ionic species under various conditions. As a result, the number of coions inside the pore solution is determined by the proportion of different counterions present in the double-layer region. Because of the competitive effects resulting from asymmetries in charge and size associated with different ions, the electrosorption selectivity of small monovalent over large divalent counterions first decreases with increasing surface charge, passes through a

minimum, and then increases with further increase of the surface charge. At low and moderate surface charge densities, the fact that large divalent counterions preferentially screen the surface charge has a large effect on pore occupancy; whereas, at a very high surface charge density, size exclusion effects dominate and determine the accessibility of different ions into the pores. Therefore, electrosorption selectivity of ions from a mixture of electrolytes can be achieved via manipulation of the EDL formation inside the pores. The findings of this work provide important information relevant to ion selectivity during separation processes and energy storage in supercapacitors.

6.1 Introduction

Electrosorption, defined as potential-induced sorption on a surface, is an important process taking place in many physical, chemical, and biological systems. One of the examples in terms of direct application of electrosorption is the utilization of nanoporous carbon materials as electrodes for electrical double layer capacitors (EDLCs) for purposes of energy storage (Frackowiak and Béguin, 2001). Electrosorption by nanoporous carbon materials is also used in separation processes, especially for water purification and desalination (Farmer et al., 1996; Gabelich et al., 2002; Ying et al., 2002). The mechanism behind electrosorption is based on the formation of the electrical double layer (EDL), i.e., the formation of a region with increased accumulation of counterions while the coions are driven away from the electrode/electrolyte interface. Moreover, the formation of EDL inside nanopores, in terms of the electrical potential distribution and the double-layer thickness, plays a central role in the selective transport of ions through

nanopores such as ionic channels and biological membranes (Jirage et al., 1997; Weetman et al., 1997; Kuo et al., 2001).

It has long been suggested that selective electrosorption of ions, depending on the surface properties of electrodes and the properties of ions, could potentially be achieved inside nanopores (Koresch and Soffer, 1983). During electrosorption, the relationship between ion size and pore size is one of the most important properties when dealing with nanoporous materials immersed in electrolyte solutions. For example, it has been shown that small micropores are not accessible to electrolyte ions, and thus, do not significantly contribute to the double-layer capacitance (Lin et al., 1999; Yang et al., 2001, Hou et al., 2006). The study by Eliad et al. (2001) demonstrated that common cations (e.g., alkali metals and alkaline earth metals) could not enter pores smaller than their hydrated size within the EDL range of potential. More specifically, it was suggested that when multiple ions are present in a mixture of electrolytes, ion selectivity based on the size, charge, and degree of complexation of the different ions may occur (Farmer et al., 1996). Gabelich et al. (2002) reported that the hydrated size of the ions in solution determined the electrosorption selectivity in a competitive environment, in which monovalent ions (e.g., sodium) with smaller hydrated size were preferentially removed from aqueous solutions over multivalent ions (e.g., calcium).

Monte Carlo simulation methods have been successfully utilized for the calculation of EDL formation next to a single planar charged surface within the primitive electrolyte system (Torrie and Valleau, 1980). Additionally, another important interfacial phenomenon, the problem of single, symmetric electrolyte distribution between two charged surfaces has been successfully studied using Monte Carlo simulations (van

Megen and Snook, 1980; Yang et al., 2002). Vlachy and co-workers studied single charge-symmetric (1:1 and 2:2) and single, charge-asymmetric (1:2 and 2:1) electrolytes confined in charged cylindrical capillaries and in thermodynamic equilibrium with an external bulk electrolyte of the same chemical composition (Vlachy and Haymet, 1989; Vlachy and Haymet, 1990; Jamnik and Vlachy, 1993; Hribar et al., 2000). They found that exclusion of electrolytes increases, reaches a maximum, and then decreases with increasing surface charge density, depending on ion valence. Calculations of thermodynamic parameters of different electrolytes were also reported (Vlachy and Haymet, 1989; Vlachy and Haymet, 1990; Jamnik and Vlachy, 1993). In the case of a 3:3 electrolyte present in solution, a higher average concentration of coions inside the pore than the one in the bulk solution at equilibrium was predicted (Vlachy et al., 2001). Jamnik and Vlachy (1995) analyzed the exclusion behavior of a mixture of 1:1 and 2:1 electrolytes between a porous phase and a bulk solution. The results indicated that the selectivity for separating divalent and monovalent counterions increases with increasing surface charge density. All the studies reported above considered only ion-valence effects. No ion-size effects were considered.

Recently, Monte Carlo studies on the competition between size and charge of counterions, involved in the EDL formation, raised important issues in terms of our lack of understanding of phenomena related to ion selectivity. In the presence of a mixture of electrolytes, for example, under certain conditions, ion-size effects can dominate the distribution of ions in the EDL of one charged planar surface, specifically in the presence of multivalent counterions with larger diameters (Taboada-Serrano et al., 2005; Quesada-Pérez et al., 2005; Martín-Molina et al., 2006). In general, preferential accumulation and

electrosorption of multivalent counterions over monovalent ones is expected at one charged planar interface. Interestingly, a number of studies have reported that, under certain conditions (e.g., high surface charge density), smaller monovalent counterions can replace larger multivalent counterions close to the surface (Valiskó et al., 2004; Taboada-Serrano et al., 2005; Biesheuvel and Soestbergen, 2007; Valiskó et al., 2007). Then, electrosorption selectivity of ions of different diameters and charges could in principle be achieved via manipulation of the EDL formation. In fact, it has been reported that narrow pores or ionic channels are able to select ions, depending on their ionic dimensions as well as size-exclusion effects (Goulding et al., 2000; Roth and Gillespie, 2005). Recent works by Boda and coworkers have studied the competition of sodium and calcium in a biological pore channel using a cylindrical simulation cell, in which all cations occupy about the same dimension (Boda et al., 2000; Boda et al., 2006; Boda et al., 2007). They found that ion selectivity of calcium over sodium results from a charge/space competition mechanism because calcium ions of a higher valence more effectively neutralize the charges inside the pores. Moreover, our previous work showed that these competitive effects between ion charge and size not only determine the screening of surface charge by the counterions, but also significantly affect the electrolyte distribution within charged pores (Hou et al., 2008).

In our previous work, canonical Monte Carlo (CMC) simulations were conducted to study the EDL formation from mixtures of electrolytes inside nanopores (Hou et al., 2008). The CMC method, however, comes with the limitation that the imposition of a closed system (i.e., constant number of ions inside the pore) may not allow the system to reach equilibrium with an external bulk solution. Therefore, in the present work, the

Grand Canonical Monte Carlo (GCMC) method was used to relate the system to a bulk electrolyte solution at equilibrium. Then, number of ions inside the pore can be unambiguously quantified. The main objective of the present work is to elucidate the fundamental mechanisms behind electrosorption selectivity of mixtures of symmetric and asymmetric indifferent electrolytes inside the pores. The focus of this work is to examine the competitive effects of charge and size asymmetry in the presence of mixtures of electrolytes with counterions of different properties and a single type of coions in all cases. The choice of the characteristics of the ions for this study (i.e., charge and hydrated size) was based on a real system. The monovalent counterions chosen for this work were: potassium (K^+) with a 3.62-Å diameter and lithium (Li^+) with a 4.25-Å diameter. The divalent counterion selected was calcium (Ca^{2+}) with a 5.8-Å diameter, and the common monovalent coion with a 4.25-Å diameter that corresponds to chloride (Cl^-) (Eliad et al., 2001). In addition, cyclic voltammetry and batch equilibrium experiments of electrosorption of these ionic species were conducted to evaluate the competitive effects, as well as to support the simulation calculations. The results provide important insight into the tailoring of EDL formation as a separation strategy, targeting ionic species.

6.2 Experimental Methods

6.2.1 Electrochemical Experiments

Cyclic voltammetry measurements were performed using a Bioanalytic Systems (BAS, West Lafayette, IN) voltammetric analyzer (CV-50W) connected to a BAS C-2 electrochemical cell. A three-electrode system was used for these experiments: (1) the working electrode was a platinum wire attached to a small piece of carbon aerogel; (2)

the counterelectrode was a large piece of carbon aerogel clipped onto another platinum wire; and (3) the reference electrode was the BAS Model RE-1 (Ag/AgCl electrode immersed in a 3 M NaCl electrolyte solution). The potential range applied to the system was +0.6 to -0.4 V within a pure EDL window, i.e., the potential window in which oxidation/reduction reactions do not take place. Aqueous solutions used in the voltammetry experiments were prepared using triply distilled 18-M Ω deionized water, and potassium chloride (KCl), lithium chloride (LiCl), and calcium chloride (CaCl₂) obtained from Sigma-Aldrich. All the voltammetry experiments in the aqueous system were carried out under a flow of nitrogen gas to avoid the experimental noise caused by the dissolved gases.

6.2.2 Equilibrium Experiments of Electrosorption

Batch electrosorption experiments were conducted using a three-electrode electrosorption cell, as shown in Figure 6.1. The electrosorption cell consisted of a pair of carbon aerogel electrodes attached to titanium plates, as well as a working electrode and a counterelectrode. A separation distance of 2.5 cm between the two electrodes was maintained by using a central hollow piece of Plexiglas, in which the reference electrode (BAS Model RE-1) was inserted. The assembly of one half of the cell followed this sequence: Plexiglas cover, titanium plate, carbon aerogel, Viton gasket with hole, and central hollow Plexiglas. The titanium plates were connected to a potentiostat (BAS Model LC-3E). The applied potentials varied from 0 to -0.6 V to evaluate the electrosorption of cations such as K⁺, Li⁺, and Ca²⁺. In each experiment, the aqueous solution was continuously pumped through the electrosorption cell by a peristaltic pump

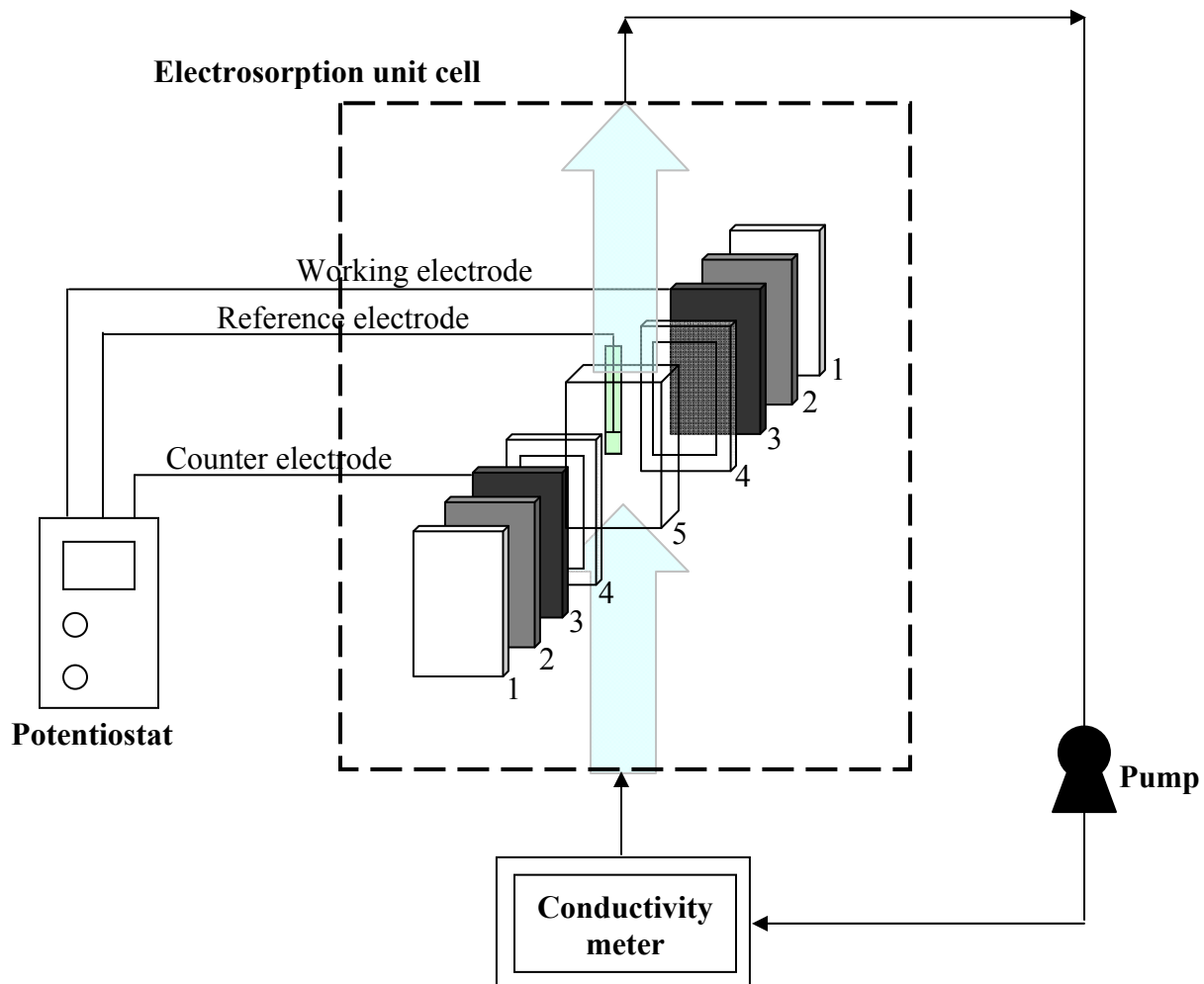


Figure 6.1 Schematic of the setup for batch electroadsorption equilibrium experiments. The electroadsorption unit cell (detailed inset) consisted of: (1) a Plexiglas cover, (2) a titanium plate, (3) a carbon aerogel electrode, (4) a Viton gasket with hole, and (5) a central Plexiglas with hole for spacing between the two electrodes.

with a flow rate of around 10 mL/min. The solution conductivity was monitored at the outlet of the cell by using a conductivity meter model 3200 (YSI, Yellow Springs, OH). The system had reached electrosorption equilibrium when the solution conductivity became a constant. The concentration was analyzed by using an inductively couple plasma spectrometer (ICP), Elan 6000 (Perkin-Elmer, Waltham, MA), in the Laboratory for Environmental Analysis, University of Georgia, Athens, GA.

6.3 Grand Canonical Monte Carlo Simulation

In the GCMC simulation method, the chemical potential (μ) of the system is fixed for a constant volume (V) and a constant temperature (T). In this regard, GCMC simulations present comparative advantages over CMC simulations for the study of the properties of an electrolyte distributed between charged surfaces because the electrolyte system is kept at a constant chemical potential and is, therefore, allowed to reach equilibrium with an external bulk electrolyte solution (Valleau and Cohen, 1980; William and Snook, 1980; Jamnik and Vlachy, 1993; Hribar et al., 2000; Yang et al., 2002). The GCMC simulation method can provide an unambiguous way to determine the total number of ions involved in the EDLs inside a pore at equilibrium with an outside bulk solution.

The dimension of the central simulation box used in this work (see Figure 6.2) is $W \times W \times L$ in the x , y , and z directions. Two impenetrable walls of surface charge density, σ_0 , are located in the xy planes at $z = 0$ and $z = L$. The primitive model was used in this work, i.e., the ions were treated as charged hard spheres in a dielectric continuum (water). Therefore, the potential energy of interaction between ions is composed of hard sphere

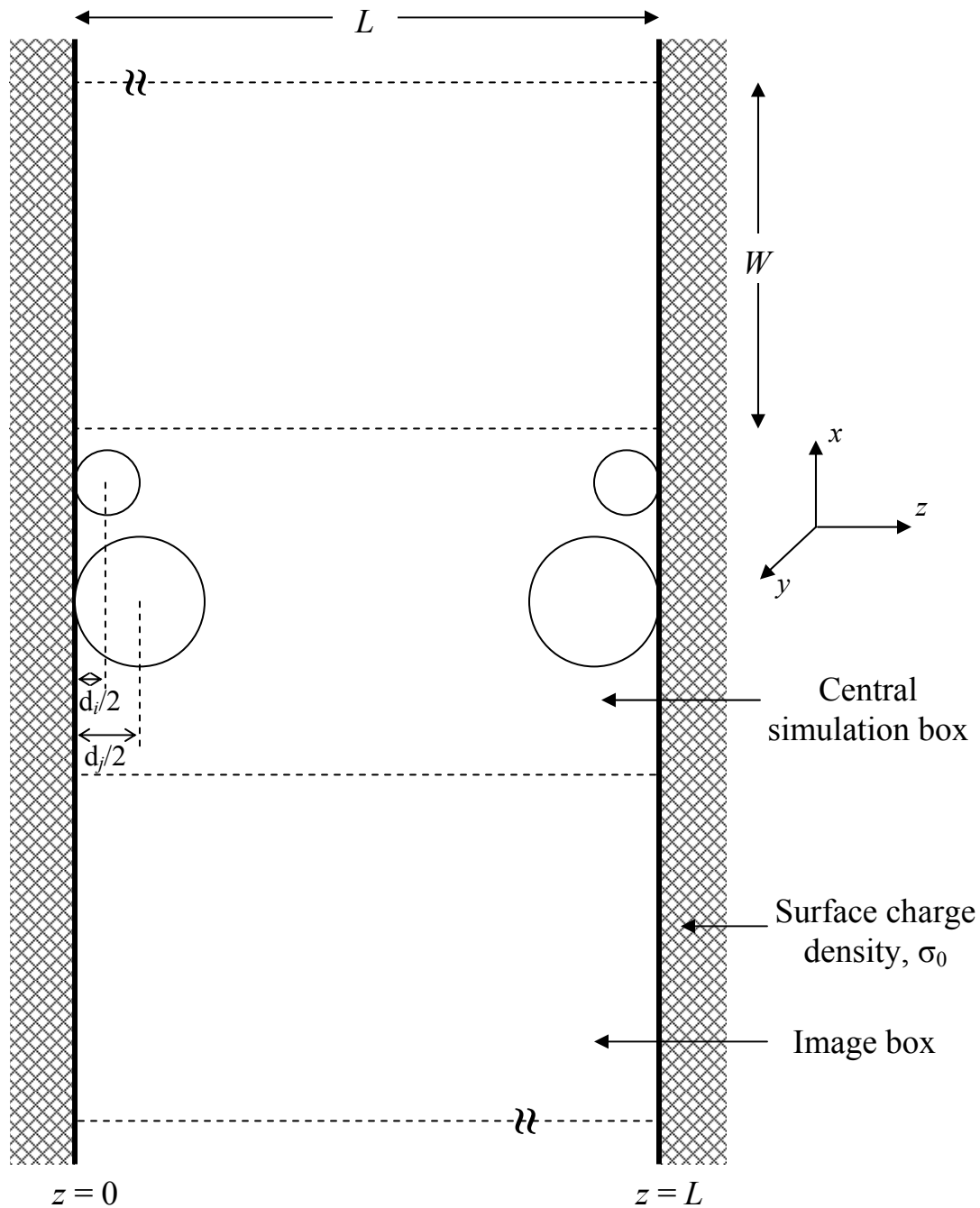


Figure 6.2 Schematic showing the geometry of the xz cross section of the simulation cell. The dimension of the simulation box is $W \times W \times L$ in the x, y, z directions, respectively. A surface charge density, σ_0 , is located in the xy planes at $z = 0$ and $z = L$. d_i and d_j correspond to the diameters of ions of different sizes. The system is periodic in the x and y directions, and the minimum image convention is employed in the x and y directions.

and Coulombic terms. The long-range interactions, representing the image electrostatic interactions of each ion outside the central simulation box, in compliance with the minimum image convention, were calculated based on the method employed by Boda et al (1998). In this method, each ion inside the central simulation box possesses an associated charge sheet of infinite dimensions minus the central square hole occupied by the central simulation box. Details on the calculation of potential energy can be found in our previous work (Yang et al., 2002; Taboada-Serrano et al., 2005; Hou et al., 2008).

Three kinds of moves are attempted during a GCMC simulation: (1) displacement of a randomly selected ion to a new random position, (2) insertion of a neutral pair of ions, and (3) removal of a neutral pair of ions. The acceptance probability, f_{ij} , for the displacement of an ion is given by the canonical probability distribution function (Valleau and Cohen, 1980; Allen and Tildesley, 1987):

$$f_{ij} = \min\{1, \exp[-\beta(U_j - U_i)]\} \quad (6.1)$$

where $\beta = (kT)^{-1}$, and U_i and U_j correspond to the configurational energy of the states i and j . The addition and deletion of a neutral pair of ions are treated similarly in terms of probability. In the state i , the numbers of counterions and coions are $N_{i^{+x}}$ and $N_{i^{-}}$, respectively. The j^{th} state will consist of $N_{j^{+x}}$ counterions and $N_{j^{-}}$ coions, in which $N_{j^{+x}} = N_{i^{+x}} + v_{+x}$ and $N_{j^{-}} = N_{i^{-}} + v_{-}$. The associated probabilities for addition and deletion of ions are given as (Valleau and Cohen, 1980; Jamnik and Vlachy, 1995):

$$f_{ij} = \min\{1, f_{ij} / f_{ji}\} \quad \text{for addition} \quad (6.2)$$

$$f_{ji} = \min\{1, f_{ji} / f_{ij}\} \quad \text{for deletion} \quad (6.3)$$

$$f_{ij} / f_{ji} = \frac{N_{i^-}! \prod N_{i^{+x}}!}{N_{j^-}! \prod N_{j^{+x}}!} \exp[B - \beta(U_j - U_i)] \quad (6.4)$$

$$B = \beta(\mu - \mu_{ideal}) + \ln(N_{-}^v \prod N_{+x}^{v_{+x}}) \quad (6.5)$$

where N_{-} and N_{+x} represent the bulk electrolyte concentrations of coions and counterions, respectively. Detailed descriptions of the GCMC method can be found in the open literature (Valleau and Cohen, 1980; Jamnik and Vlachy, 1993; Jamnik and Vlachy, 1995). The parameter B , fixed as a constant during the simulation, is related to the chemical potential of the external bulk electrolyte solution. Therefore, the simulation starts with a predetermined parameter B that corresponds to a certain bulk electrolyte concentration. The bulk concentration, determining the parameter B , can be estimated from independent GCMC simulations at bulk conditions.

6.4 Results and Discussion

6.4.1 Effects of Ion Properties on Electrosorption Behavior

Before performing the GCMC simulations, electrosorption experiments were conducted using carbon aerogel to study the effects of ion charge and size on electrosorption behavior. The carbon aerogel (Marketech, Port Townsend, WA) used in the experiments has a Brunauer-Emmett-Teller (BET) surface area of 691 m²/g, 85% of which is contributed by micropores (< 2nm) and 15% of which is contributed by mesopores (2–50 nm).

Figure 6.3 presents cyclic voltammetry curves of carbon aerogel using a slow scan rate of 1.0 V/s within the potential range of EDL (-0.4 to +0.6V), in which electrosorption of ions is a result of the electrostatic interactions of ions and charged pore surfaces. The electrolyte solutions used in a comparative series were composed of different cations (i.e., K^+ , Li^+ , and Ca^{2+}), with a common anion of Cl^- . The sequence of hydrated ion size is: $K^+ < Li^+ < Ca^{2+}$ (Eliad et al., 2001). Usually, when pore sizes are considerably larger than the ion size, the cyclic voltammetry curves of rectangular shape and the electrosorption capacitance is independent of the charge and size of the ions that are present in the solution (Salitra et al., 2000; Eliad et al., 2001, Eliad et al., 2006). However, because the dimensions within the pore size distribution for carbon aerogel have the same order of magnitude as the EDL thickness, ion-size effects during electrosorption can be observed in Figure 6.3. For example, at the potential of -0.4V, the EDL capacitances for K^+ , Li^+ , and Ca^{2+} cations, referred to as counterions, are 109.0, 87.6, and 53.0 F/g, respectively. The capacitance of cations decreases in the order of increasing ion size (i.e., $K^+ < Li^+ < Ca^{2+}$). At the same time, the Cl^- anions present in these three electrolyte solutions contribute with approximately the same capacitance value at the positive potential of +0.6 V. Additionally, the number of counterions involved in the formation of the EDL inside the pores significantly affects the electrosorption capacitance (Hou et al., 2006). Therefore, the ions of larger size result in a lower value of EDL capacitance because of a decrease in the average concentration of counterions inside the pores.

Table 1 and Figure 6.4 show experimental data obtained from the equilibrium experiments with carbon aerogel and mixtures of electrolytes, containing two different

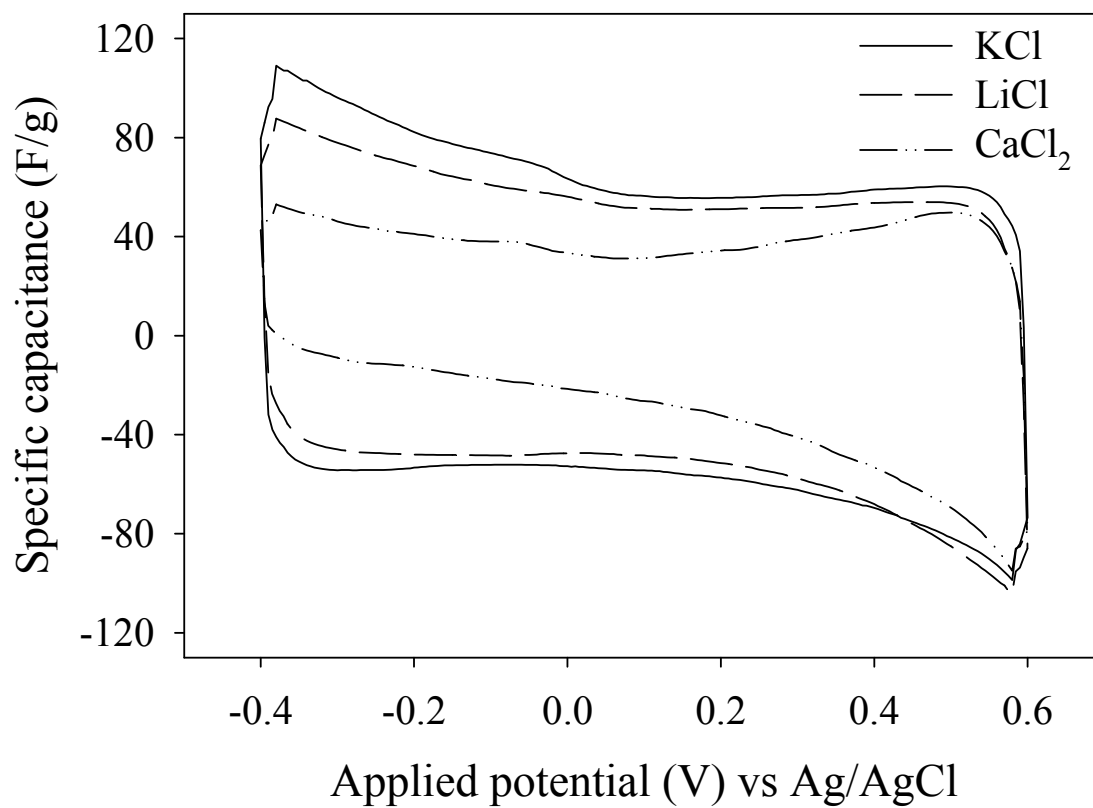


Figure 6.3 Specific capacitance of carbon aerogel measured by cyclic voltammetry using a slow scan rate of 1 mV/s for electrolyte solutions of 1.0 M KCl, 1.0 M LiCl, and 0.5 M CaCl₂.

Table 6.1 Experimental data obtained from the batch equilibrium experiments using carbon aerogel. The electrosorption experiments were performed in the following competitive environment of an electrolyte mixture of: (a) KCl and LiCl, and (b) KCl and CaCl₂.

(a)

E (V)	Initial concentration (mM)		Final concentration (mM)		Electrosorption Capacity ($\mu\text{mol/g}$)		Percent removal (%)	
	K ⁺	Li ⁺	K ⁺	Li ⁺	K ⁺	Li ⁺	K ⁺	Li ⁺
0	0.8773	0.6992	0.8722	0.6969	1.19	0.54	0.58	0.33
-0.1	0.8977	0.7428	0.7827	0.6612	26.83	19.03	12.82	10.99
-0.2	0.8798	0.7343	0.7366	0.6204	33.39	26.56	16.28	15.51
-0.4	0.8798	0.7343	0.6624	0.5693	50.69	38.45	24.71	22.46

(b)

E (V)	Initial concentration (mM)		Final concentration (mM)		Electrosorption Capacity ($\mu\text{mol/g}$)		Percent removal (%)	
	K ⁺	Ca ²⁺	K ⁺	Ca ²⁺	K ⁺	Ca ²⁺	K ⁺	Ca ²⁺
0	0.8926	0.5782	0.8773	0.5696	3.57	1.99	1.72	1.48
-0.1	0.9796	0.6373	0.8389	0.5474	32.80	20.97	14.36	14.11
-0.2	0.9361	0.6014	0.8006	0.5165	31.61	19.77	14.48	14.10
-0.4	0.8926	0.57822	0.6931	0.4446	46.51	31.16	22.35	23.11

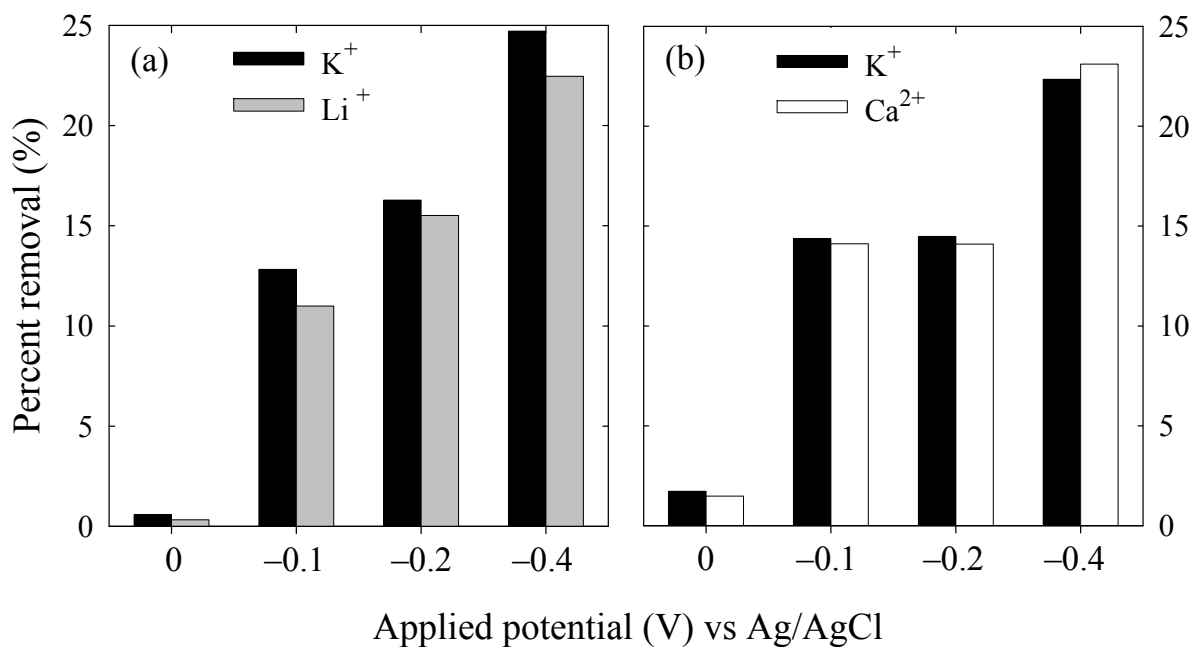


Figure 6.4 Percent removal of ions from aqueous solutions obtained via batch equilibrium experiments using carbon aerogel. The study of electrosorption selectivity was based on ion properties in a mixture of electrolytes containing a common anion Cl^- and: (a) monovalent cations K^+ and Li^+ , and (b) monovalent cation K^+ and divalent cation Ca^{2+} . All experiments were conducted using a three-electrode electrosorption cell.

cations at a time from the three cations under study (K^+ , Li^+ , and Ca^{2+}) with a common anion (Cl^-). The percent removal of ions from the aqueous solutions was determined as the difference between the initial and final concentrations in the bulk solution divided by the initial concentrations in the bulk solution. As expected, the amount of ions removed by the electrosorption process increased with increasing applied potential. In the presence of the two monovalent cations K^+ and Li^+ , smaller K^+ cations are more efficiently removed from the solutions than larger Li^+ cations because size effects dominate the removal process. When both K^+ and Ca^{2+} cations coexist in the solution, preferential electrosorption of Ca^{2+} cations was expected because the electrosorption of divalent counterion (Ca^{2+}) is thermodynamically favorable. However, no such favorable electrosorption of Ca^{2+} ions could be observed in any of the experiments summarized in Figure 6.4. This finding implies that the electrosorption of divalent cations may be limited because of the selectivity imposed by the difference in hydrated size of the ions (Gabelich et al., 2002).

The experimental data have demonstrated that, when the pore size approaches the magnitude of the ion size, ion-size effects occur during electrosorption. Furthermore, the electrosorption behavior of ions within nanoporous carbon materials during such processes as charging of EDLCs and removal of ions from aqueous solutions could be affected by the competition between the effects of charge and size of ions involved in the EDL.

6.4.2 Effects of Counterion Properties on Coion Exclusion in Single Electrolytes

Electrostatic interactions between ionic species and charged surfaces are responsible for the EDL formation inside pores, resulting in accumulation of counterions within the double-layer region, while coions are excluded from the charged pores. Vlachy and coworkers first reported on the electrolyte exclusion from pores in solutions containing symmetric and asymmetric electrolytes of the same size, at various surface charge densities, observed during GCMC simulations (Vlachy and Haymet, 1989; Vlachy and Haymet, 1990; Jamnik and Vlachy, 1993). In their studies, they defined the exclusion parameter as (Vlachy and Haymet, 1989):

$$\Gamma = \frac{C_0 - C_{pore}}{C_0} \quad (6.6)$$

where C_0 is the concentration of coions present in the bulk solution and C_{pore} is the average concentration of ions inside the pore, respectively. This definition is adopted in this work for discussion purposes.

Figure 6.5(a) presents the exclusion parameter of coions rejected from pores of different diameters for a symmetric 1:1 electrolyte at a concentration of 1 M and at a surface charge density of -0.05 C/m^2 . In this case, the coions and counterions have an equal size of 4.25 \AA . As expected, the exclusion of coions is strongly dependent on the pore size. Pores with a smaller size have a greater ability to exclude coions from the double-layer region. Increasing the surface charge density enhances coion exclusion from the charged pores, as shown in Figure 6.5(b). Also, the exclusion parameter tends to reach a plateau, in which the coion exclusion cannot be efficiently improved by further

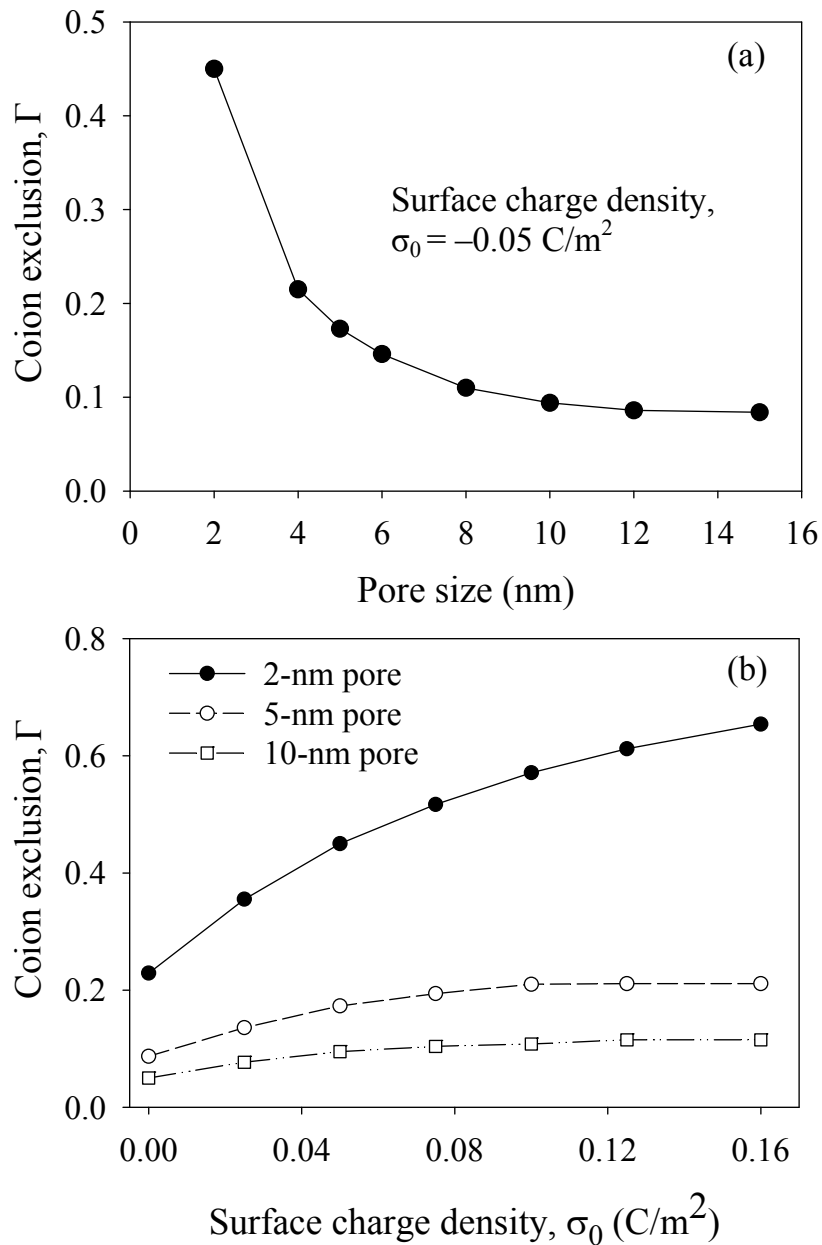


Figure 6.5 Exclusion parameter of coions from nanopores containing a 1:1 symmetric electrolyte: (a) as a function of pore size, and (b) as a function of surface charge density. The bulk electrolyte solution in each case has a concentration of 1 M. All coions and counterions have an equal size of 4.25-Å in all cases.

increasing the surface charge. It should be noted that, for uncharged pores, the coion exclusion is also a function of the pore size. Because of steric effects, the average concentration of electrolyte inside smaller pores is lower than that inside larger pores.

Figure 6.6 presents the effects of charge and size asymmetry of counterions on the behavior of coion exclusion from a 2-nm-diameter pore for various surface charge densities. The external bulk solutions correspond to a single symmetric (1:1) or to a single asymmetric (2:1) electrolyte at a concentration of 1 M. The electrolytes have identical monovalent coions of 4.25-Å diameter. When the smallest monovalent counterions (with a diameter of 3.62 Å) are present in solution, the curve of exclusion coefficient as a function of surface charge density shifts to lower values than the curve corresponding to larger monovalent counterions of 4.25-Å diameter. The explanation for this behavior is that the average concentration of counterions in the pore solution increases with decreasing ion size, which translates into the fact that the corresponding coions are excluded to a lesser degree from the charged pore. In other words, more ions are required inside the pores to ensure electroneutrality in cases where larger counterions are present at higher concentrations, which means lower Γ (see eq. 6.6). In the case of divalent counterions of 5.8-Å diameter, the coion exclusion becomes less sensitive to the surface charge density. This can be explained by the fact that one divalent counterion provides twice the positive charge to neutralize the negative charges inside the pore.

In summary, the exclusion of coions from pores is determined by the efficiency of the counterion in neutralizing the surface charge, and the counterion concentration achievable inside the pores as determined by size effects (i.e., counterion size as compared to pore size).

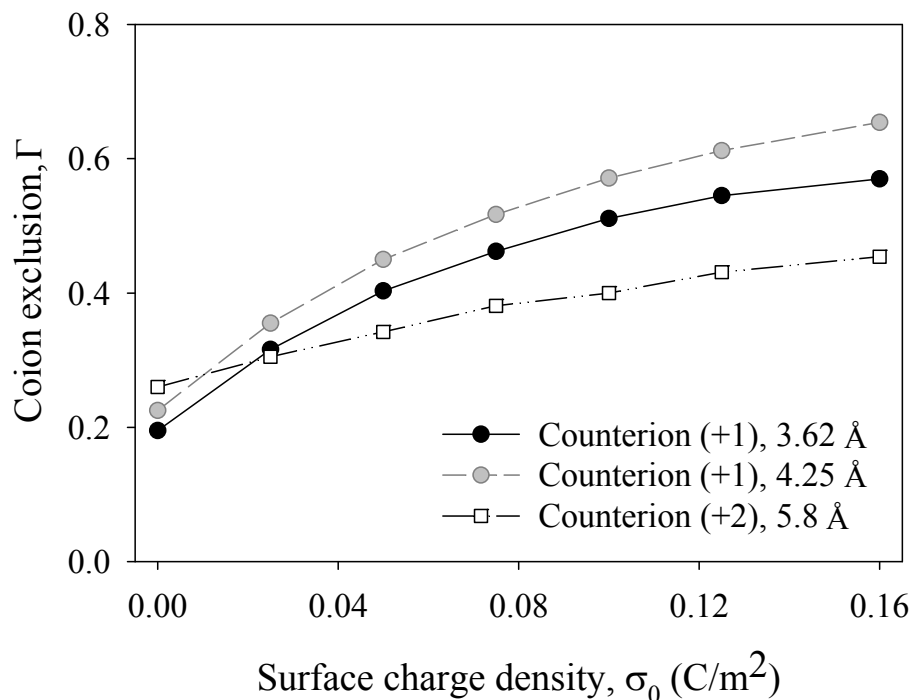


Figure 6.6 Effects of size and charge asymmetry of counterions on coion exclusion from a 2-nm nanopore for symmetric and asymmetric electrolytes. The bulk electrolyte solutions contained the following species: (1) a 1:1 electrolyte with monovalent counterions and monovalent coions that have diameters corresponding to 3.62 and 4.25 Å, respectively, (2) a 1:1 electrolyte with monovalent counterions and monovalent coions that have diameters of 4.25 Å, or (3) a 1:2 electrolyte with divalent counterions and monovalent coions that have diameters corresponding to 5.8 and 4.25 Å, respectively. The bulk concentration of each of the counterions is 1 M in every case. The size of ions corresponds to: K^+ for 3.62 Å, Li^+ for 4.25 Å, and Ca^{2+} for 5.8 Å.

6.4.3 Ion-Size Effects on Ion Selectivity in Mixtures of Electrolytes

In a mixture of symmetric and asymmetric electrolytes, the selectivity factor can be used in addition to the exclusion parameter to characterize the electrosorption of different counterions (i.e., asymmetry in size and charge) in the pore solution at equilibrium with an external bulk electrolyte. The selectivity factor, α , is defined as (Jamnik and Vlachy, 1995):

$$\alpha = \frac{C_i / C_j}{C_{i,0} / C_{j,0}} \quad (6.7)$$

where C_i and C_j represent the average concentrations of counterions i and j inside the pore. $C_{i,0}$ and $C_{j,0}$ are the concentrations of ions i and j present in an external solution, respectively. In the case of a mixture of two 1:1 electrolytes, ions i and j are the small and large monovalent counterions (with diameters equal to 3.62 and 4.25 Å), respectively. For a mixture of 1:1 and 2:1 electrolytes, ion i is the small monovalent counterion of 3.62-Å diameter and ion j is the large divalent counterion of 5.8-Å diameter, respectively.

Figures 6.7 (a) and 6.7(b) show the GCMC simulation results for the selectivity factor and exclusion parameter inside the pores for a mixture of 1:1 electrolytes, containing two types of counterions with size asymmetry. The pore solution is assumed to be in equilibrium with an external bulk electrolyte, which has an equivalent concentration of 0.5 M of small and large monovalent counterions (with diameters equal to 3.62 and 4.25 Å, respectively) and 1 M concentration of monovalent coions of 4.25-Å diameter. As expected, reducing the pore size from 5 nm to 2 nm enhances both the selectivity factor and the exclusion parameter. With regard to electrolyte exclusion, the

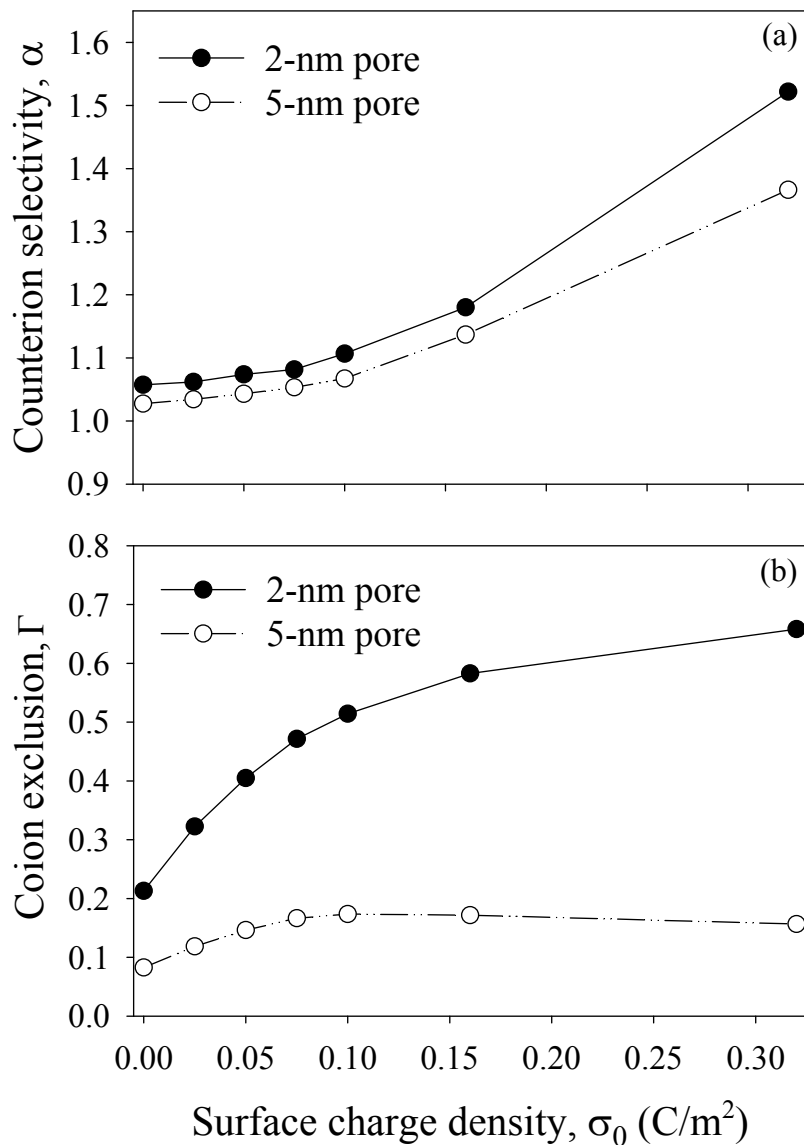


Figure 6.7 Effect of surface charge density on (a) counterion selectivity and (b) coion exclusion for a mixture of two 1:1 electrolytes inside the pores. The equilibrium bulk electrolyte consists of 0.5 M smaller monovalent counterions of 3.62 Å, 0.5 M larger monovalent counterions of 4.25 Å, and 1.0 M monovalent coions of 4.25 Å.

exclusion parameter of coions increases as the surface charge density is increased, following the trend observed for single electrolytes. To better examine the effects of ion size, we characterize the number of counterions located inside the pore by the selectivity factor. It is evident that a larger selectivity for smaller counterions (3.62 Å) over larger counterions (4.25 Å) is observed in the restricted space of the pores, i.e., smaller counterions penetrate the pore more easily. At higher surface charge densities, the electrosorption of smaller counterions is more energetically favorable than that of larger counterions. For instance, when the surface charge density increases from 0 to 0.32 C/m², the selectivity of smaller counterions over larger ones (α) is significantly improved from 1.05 to 1.52 for a 2-nm-diameter pore. Small-counterion selectivity is a direct result from ion-size (steric) effects on the formation of the EDL inside the pores.

To obtain an insight into the selectivity of ions during electrosorption, the ion concentration profiles for a mixture of 1:1 electrolytes confined in a 2-nm-diameter pore are illustrated in Figure 6.8. The local concentration of ions inside the pore is normalized with respect to the bulk electrolyte concentration, i.e., it is expressed as C/C_0 . In the absence of surface charge, ions randomly scatter over the space inside the pores, and the local concentration of ions is equal to the bulk concentration ($C/C_0 = 1.0$). Under this condition, ion selectivity is mainly determined by the difference in hydrated radius (3.62 and 4.25 Å) between the two counterions. Because the smaller counterions can get closer to the surface, they are more widely distributed over the effective pore width, which translates into their presenting higher average concentrations inside the pore. At low surface charge densities (e.g., equivalent to -0.05 C/m²) the onset of double layers results in the accumulation of counterions inside the pore; and the coions are partially excluded

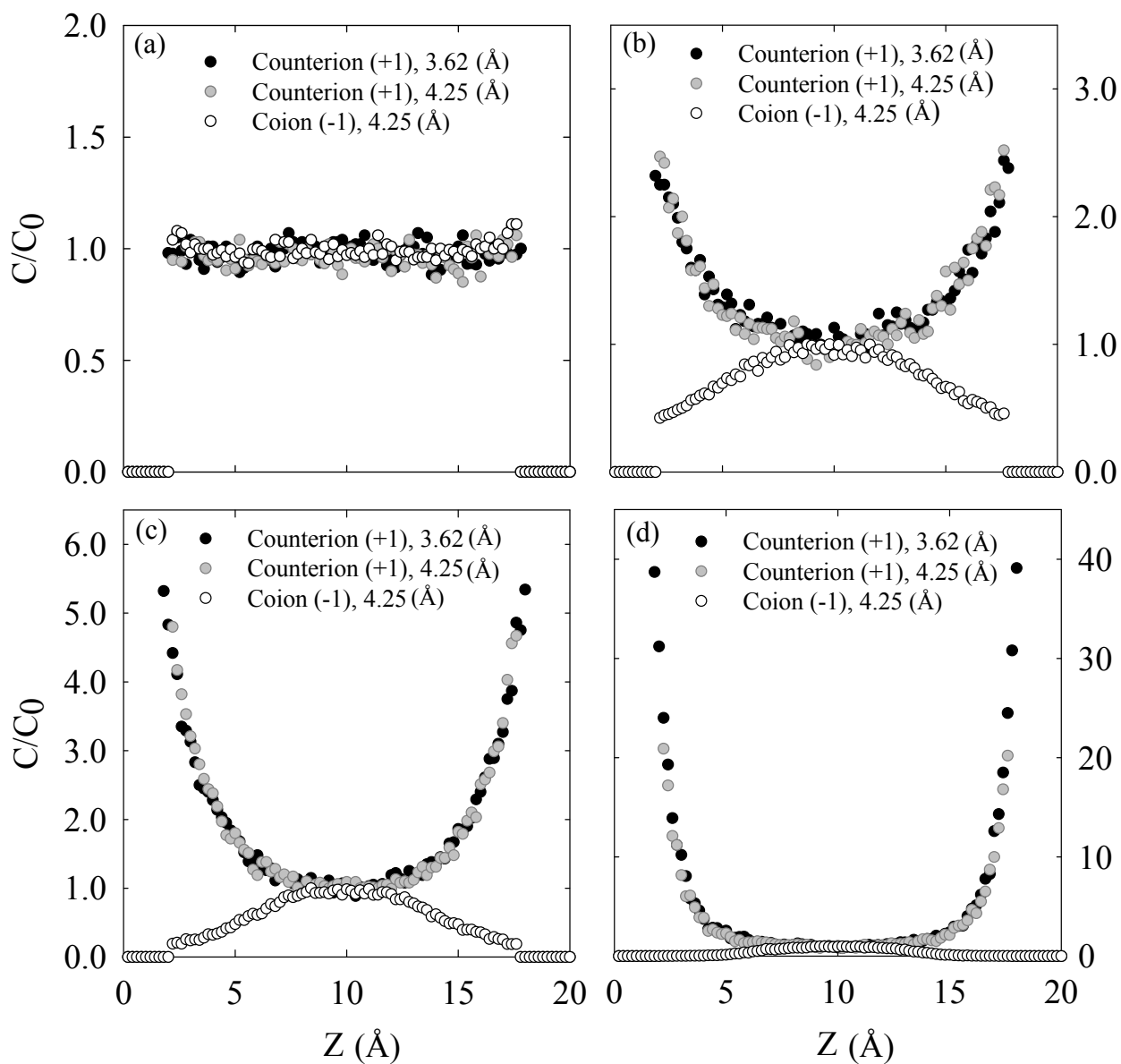


Figure 6.8 Ion concentration profiles for a mixture of two 1:1 electrolytes inside a slit-type nanopore of 2-nm diameter at surface charge densities of (a) 0 C/m^2 , (b) -0.05 C/m^2 , (c) -0.1 C/m^2 , and (d) -0.32 C/m^2 . The equilibrium bulk electrolyte consists of 0.5 M smaller monovalent counterions of 3.62-Å diameter, 0.5 M larger monovalent counterions of 4.25-Å diameter, and 1.0 M monovalent coions of 4.25-Å diameter.

from the pores ($\Gamma = 0.40$). In this case, smaller and larger counterions present approximately the same magnitude of local concentration next to the surface, and the selectivity based on ion size is not very evident ($\alpha = 1.08$). In the case of a high surface charge of -0.32 C/m^2 , the local concentration of counterions present in the EDL is much higher than that in the external solution. Moreover, the 3.62-\AA -diameter counterions present an almost twice higher local concentration next to the surface than the 4.25-\AA -diameter counterions, which is evidenced by a selectivity factor, α , equal to 1.52. The reason for the large selectivity factor in this case is because ions that occupy less space are more effective at screening the surface charge. The electrosorption of smaller counterions and their inclusion in the EDL becomes more energetically favorable with increasing surface charge.

Overall, in a mixture of small and large counterions of the same valence, the nanopores show ion selectivity because smaller counterions favorably neutralize the surface charge while occupying a smaller volume. Smaller ions present comparative advantages to access the restricted space of the pores, and to be electrosorbed in the double-layer region. At even higher surface charge densities than the ones discussed in this study, small counterions could further outcompete large counterions and become the dominant species in the EDL inside the pores.

6.4.4 Charge/Size Competitive Effects on Ion Selectivity in Mixtures of Electrolytes

Figure 6.9(a) shows the counterion selectivity, α , as a function of the surface charge density for a mixture of 1:1 and 2:1 electrolytes enclosed in pores. The equilibrium bulk solution has equimolecular mixture of 0.5 M smaller monovalent (with

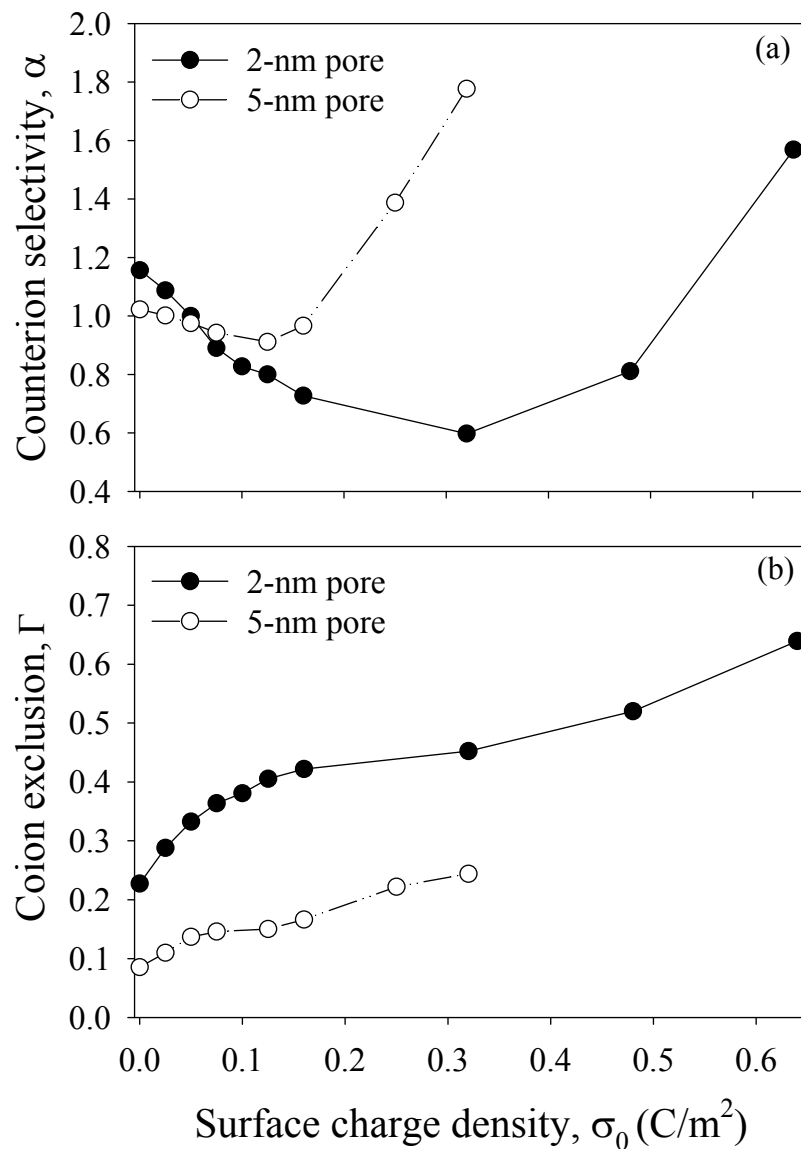


Figure 6.9 Effect of surface charge density on (a) counterion selectivity and (b) coion exclusion for a mixture of 1:1 and 1:2 electrolytes inside pores. The equilibrium bulk electrolyte consists of 0.5 M smaller monovalent counterions of 3.62-Å diameter, 0.5 M larger divalent counterions of 5.8-Å diameter, and 1.5 M monovalent coions of 4.25-Å diameter.

a diameter of 3.62 Å) and 0.5 M larger divalent counterions (with a diameter of 5.8 Å), and 1.5 M monovalent coions (with a diameter of 4.25 Å). The selectivity factor of monovalent counterions over divalent ones first decreases with increasing surface charge density, passes through a minimum (maximal selectivity of divalent counterions over monovalent ones), and then increases with further increase of the surface charge. In conditions of zero or low surface charge density, the pore presents greater selectivity for smaller monovalent counterions because smaller ions have less restriction to access the pore than larger ions. As surface charge density increases, the affinity of the pores for larger divalent counterions increases because of the energetic advantage of screening the surface charge with higher-valence ions. Importantly, a turning point in the behavior of ion selectivity of the pore as a function of surface charge is observed with further increases in surface charge density. The reason is that increasing the surface charge density enhances ion-size effects (Taboada-Serrano et al, 2005). At very high surface charge densities, when large amounts of counterions are required to achieve electroneutrality inside the pores, monovalent counterions of smaller size are preferentially electrosorbed close to the surface, while larger divalent counterions tend to be excluded from the EDL region.

It must also be noted that the tendency toward coion exclusion of charge-asymmetric mixtures (1:1 and 2:1 electrolytes) is different with that of size-asymmetric mixture (two 1:1 electrolytes). The behavior of coion exclusion depends on the composition of the EDL in terms of the predominant counterion. As shown in Figure 6.9(b), when the affinity for divalent counterions is larger, the exclusion parameter for coions increases until reaching a plateau that corresponds to the minimum in counterion

selectivity. Subsequently, when the turning point in counterion selectivity takes place, the number of smaller monovalent counterions strongly increases with further increase of the surface charge, while coions are increasingly excluded from the pore to satisfy electroneutrality. In other words, the affinity of the pore that switches from large divalent counterions to small monovalent counterions results in two stages of coion exclusion.

Figure 6.10 presents the ion distribution of mixtures of 1:1 and 2:1 electrolytes in a slit-type nanopore of 2-nm diameter at different surface charge densities. For the uncharged pore, the local concentrations of both counterions correspond to their bulk concentrations [Figure 6.10(a)]. Still, because the accessible cross-sectional area increases with decreasing ion size, a slight selectivity for smaller monovalent counterions (3.62 Å) over large divalent counterions (5.8 Å) can be expected ($\alpha = 1.15$). In the case of surface charge density equivalent to -0.05 C/m^2 , the two counterions are present in equal proportions in the pore solution, and $\alpha = 1.0$. However, due to their higher valence and larger size, the distribution of divalent counterions is more concave, which translates into higher local concentrations of divalent counterions in a comparable reduced space next to the charged walls of the pore (Hou et al., 2008). Moreover, the higher the surface charge, the greater the selectivity of the pores for divalent counterions until the selectivity for divalent counterions reaches a maximum. At the surface charge density of -0.125 C/m^2 , the accumulation of divalent counterions in the EDL region to neutralize surface charge presents an energetic advantage over the accumulation of monovalent counterions ($\alpha = 0.80$). Charge inversion also takes place in the central region of the pore because of strong ion-ion correlations and size-exclusion effects towards coions exerted by the counterions close to the pore walls, as shown in Figure 6.10(c). The phenomenon of

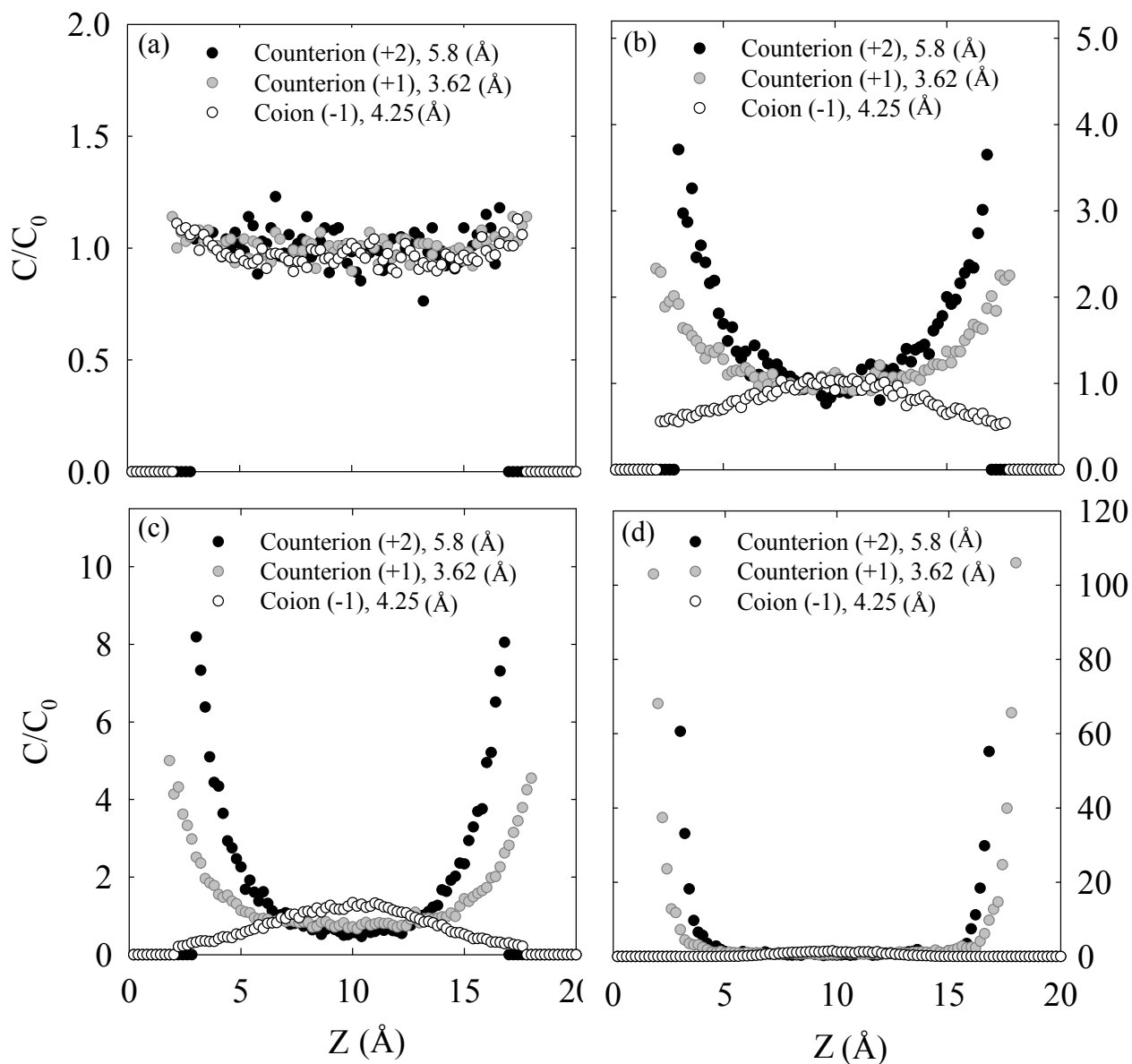


Figure 6.10 Ion concentration profiles for a mixture of 1:1 and 1:2 electrolytes inside a slit-type nanopore of 2-nm diameter at surface charge densities of (a) 0 C/m^2 , (b) -0.05 C/m^2 , (c) -0.125 C/m^2 , and (d) -0.64 C/m^2 . The equilibrium bulk electrolyte consists of 0.5 M smaller monovalent counterions of 3.62-Å diameter, 0.5 M larger divalent counterions of 5.8-Å diameter, and 1.5 M monovalent coions of 4.25-Å diameter.

charge inversion has also been reported in our earlier studies (Hou et al., 2008). At the very high surface charge density of -0.64 C/m^2 , monovalent counterions present the advantage of greater proximity to the surface, resulting in large monovalent counterion selectivity over divalent counterions ($\alpha = 1.57$). In this case, the smaller monovalent counterions become the predominant ionic species in the EDL, replacing the large divalent counterions. Most of the screening of the surface charge is performed by the smaller counterions.

A comparison between experimental data and simulation results shows good qualitative agreement. As one can see from the results in Figures 6.4(a) and 6.7(a), small monovalent counterions (K^+) are preferentially removed from the bulk solution and held in the double-layer region of the pores. In comparison, selectivity of small monovalent counterions (K^+) over large monovalent counterions (Li^+) was found in simulations. In the case of mixtures of charged-asymmetric electrolytes, the experimental data in Figure 6.4(b) do not show pore affinity for either large divalent counterions (Ca^{2+}) or small monovalent counterions (K^+). This implies a competitive behavior between these two counterions for accessing the pores in electrosorption processes, which can be explained by simulation results [Figure 6.9(a)], where the ion selectivity is based on the competitive effects of pore size, surface charge density, and characteristics of counterions.

In light of the results discussed above, one concludes that the competition of charge and size asymmetry plays an important role on selective electrosorption of ions in a confined space like pores. In a mixture of electrolytes, counterions associated with different properties (i.e., size and charge) compete to access the pores. Selectivity of the pores for counterions, i.e., which ions will be preferentially electrosorbed in the double-

layer region, is defined by a counterbalance between minimization of potential energy and size exclusion effects (Taboada-Serrano et al, 2005; Valiskó et al., 2007; Hou et al., 2008). At low and moderate surface charges, the energetic advantage of predominant divalent counterions inside the pores overcomes the size exclusion effects. On the other hand, at very high surface charge densities, size-exclusion effects dominate the selectivity of the pores towards different ions, resulting in the preferential accumulation of monovalent counterions with a better “size affinity”. Additionally, when the separation distance between the two charged surfaces diminishes (i.e., for smaller pore sizes), the confinement effect enhances the selectivity of divalent counterions over monovalent counterions at low charge densities. This behavior may be explained by the distortion of the EDL structure because two double layers strongly overlap within smaller pores. As EDL overlap occurs when pore size diminishes, energetic effects become more predominant than ion-size effects.

6.5 Summary

In this work, experiments and GCMC simulations were performed to study the fundamental aspects of electrosorption selectivity in the presence of symmetric and asymmetric indifferent electrolytes. Electrochemical experiments indicate that the electrosorption behavior is significantly dependent on the properties of electrolytes. Competitive effects take place inside the pores. Simulation results are in qualitative agreement with the results obtained via electrosorption experiments.

In the case of single electrolytes, the exclusion of coion from the pores increases with increasing surface charge density. Additionally, due to confinement effects, the

coion exclusion dramatically increases as the pore size approaches molecular dimensions. Moreover, the behavior of coion exclusion is determined by the size and valence of the counterions in the EDL formation.

When dealing with mixtures of electrolytes, the competitive effects of asymmetries of ion charge and size determine the pore accessibility. Divalent counterions present the energetic advantage of preferential screening the surface charge due to their higher valence. On the other hand, small counterions present “size affinity” to access the pores and to approach closer to the charged surfaces. These two competitive effects result in the electrosorption selectivity of small monovalent over large divalent ions being highly dependent on the magnitude of surface charge. As surface charge density increases, the preferential selectivity of the pores for large divalent counterions increases, reaches a maximum and then turns into a preferential selectivity for small monovalent counterions. This can be easily visualized by analyzing the EDL structure inside the pores. The population of ions within the EDL inside the pores switches from being predominant in divalent counterions to being predominant in monovalent counterions. Therefore, manipulation of electrosorption selectivity to separate ions from an electrolyte mixture could in principle be achieved via tuning the EDL structure inside the pores through the regulation of surface charge, tailored for different ion characteristics. The results of this work have several significant implications in terms of development of technologies for ion separations and energy storage, and in terms of providing insights into ion selectivity phenomena in natural systems.

CHAPTER 7

CONCLUSIONS AND RECOMMENDATIONS

This research combines experiments and theories on the electrical double layer (EDL) formation, and was conducted to examine the electrosorption behavior of ions in the restricted space of nanoporous carbon materials. The main contribution of this research lies on improving the current state of knowledge with respect to the fundamental aspects of the EDL formation and its use for the separation of ions via electrosorption by nanoporous carbon materials.

The fundamental aspects of this research have significance in several disciplines. The knowledge obtained on the voltammetric characteristics using cyclic voltammetry has significance in the characterization of the electrosorption behavior of nanoporous carbon materials. The data obtained by simple diffusion and electrically-aided diffusion experiments demonstrate the exclusion-size effect on pore accessibility of nanoporous carbon materials. Equilibrium electrosorption experiments indicated that ions of different characteristics, such as charge and size, can be selectively electrosorbed in the double-layer region in a competitive environment. The knowledge gained from molecular simulations using Monte Carlo methods has significance in the understanding of EDL formation in a mixture of symmetric and asymmetric electrolytes, especially the competitive effects of asymmetries of ion charge and ion size. The model developed for the electrosorption of ions by nanoporous materials under the influence of an electric

field can provide insight into the design of better materials for use in separations. Based on the experimental data and modeling results, the following specific conclusions can be drawn:

- It was shown in the cyclic voltammetry experiments that the presence of micropores results in the occurrence of double-layer overlapping, which has a pronounced effect on electrosorption performance using nanoporous carbon materials. Because of EDL overlapping, mesopores (pore width between 2 and 50 nm) and micropores (less than 2nm) manifest different behaviors in electrosorption processes; mesopores show good electrochemical accessibility and micropores lead to a considerable loss of double-layer capacitance. EDL overlapping decreases not only the transport rate of ions diffusing into the pores, but also the number of ions in the pore solution at equilibrium. It implies that manipulation of EDL formation could control ion transport and sorption inside nanopores.
- An extended EDL model based on the classical Gouy-Chapman (GC) theory was developed by taking into consideration the double-layer overlapping. It indicated that there is a close relationship between pore size distribution and double-layer capacitance of nanoporous carbon materials. Pore accessibility by ions can be determined by the rate of ions diffusing into pores and the total number of ions inside the pores at equilibrium with a bulk solution. However, the classical GC theory does not take into account the ion-size effect on the EDL formation.
- By using a series of voltammetric experiments for various electrolytes that contain a marked difference in size of cations, the size-exclusion effect of ions can be observed;

an increase in ion size results in a lower value of double-layer capacitance. Larger counterions have more restriction to access the pores and to be electrosorbed in the double-layer region. A larger exclusion volume causes a decrease in the average concentration of larger counterions inside the nanopores. Therefore, electrosorption selectivity of ions in nanoporous carbon materials could take place based on the ion-size effect in an external electric field.

- In the bi-molecular permeation experiments, molecular transport rates through a mesoporous carbon membrane (synthesized at Oak Ridge National Laboratory) showed that the transport of large molecules was impeded by the transport of small molecules in a competitive environment. Because of the competitive mechanisms between the two molecules for accessing the pores, large molecules tend to be excluded from the pores, while small molecules present “size affinity” to penetrate into pores. Therefore, the size-exclusion effect causes a more extensive retardation of large molecules transported through the membrane.
- Based on the batch electrosorption experiments, the competition between ions that have different characteristics (i.e., charge and size) can further be observed using nanoporous carbon materials in an external electric field. When dealing with a mixture of electrolytes, monovalent counterions with small hydrated size are more preferentially removed from aqueous solution, and at the same time, electrosorption of multivalent counterions with large hydrated size is limited. It implies ion selectivity for nanoporous carbon materials could occur based on the different properties of ions present in the double-layer region during electrosorption processes.

- Because the canonical Monte Carlo (CMC) simulations of the primitive EDL model consider the ions as charged hard spheres with a selected size, the effects of asymmetries of ions on the ion distribution in the confined nanopores could be investigated. It was found that the EDL formation is not only determined by the ionic strength or the surface charge, but also by the ion size and charge. The competitive behaviors between ion charge and size could result in the “inversion” of the order between monovalent and multivalent counterions present in a mixture of electrolytes. This result indicated that these competitive effects not only determine the screening of surface charge but also significantly affect the electrolyte distribution within charged pores. Moreover, charge inversion takes place in the central region of nanopores because of the strong ion-ion correlations and the asymmetries in size and charge of ions, especially in the case of multivalent counterions with large size. It is also suggested that taking into consideration the ion-size effect is very essential for elucidating the fundamental mechanisms of ion transport and sorption at the nanoscale.
- Further modeling investigations were carried out using the grand canonical Monte Carlo (GCMC) simulation method, where the total number of ions can be unambiguously quantified in the pore solution at equilibrium with an external bulk electrolyte. In the case of mixtures of electrolytes, the competitive effects of asymmetries of charge and size of ions can determine the pore accessibility. Electrosorption selectivity of small monovalent versus large multivalent ions strongly depends on the magnitude of surface charge. With increasing surface charge density, the preferential selectivity of the pores for large multivalent counterions is transferred

to that of small monovalent counterions because of the competitive effects of electrostatic potential and size exclusion. In addition, the population of ions present in the double-layer region of the pore not only affects the screening of surface charge but also dominates the pore occupancy (i.e., accumulation of different counterions and exclusion of coions).

In summary, the combination of experimental data and molecular simulations provides a more realistic approach in identifying the mechanisms of phenomena inside nanopores. This research has two significant contributions: (i) understanding of mechanisms behind EDL formation of a mixture of electrolytes inside nanopores, and (ii) devising advanced techniques for electric field application of ion separation. The knowledge on the EDL formation at the nanoscale is important for many interfacial phenomena occurring in physical, chemical, and biological systems.

Since these findings are significant in the design of novel, intensified separations processes, it is suggested that a laboratory-scale selective separation of ions using a nanoporous membrane can be conducted to prove that membranes containing ionic channels have the ability to separate ions of different characteristics from a mixture of electrolytes, via manipulation of EDL formation inside nanopores. The direct observation will enable us to evaluate the accuracy of Monte Carlo simulations using a primitive model as well. Moreover, because a primitive model means that the solvent (water) is treated as a continuum of constant electrical permittivity, the use of the nonprimitive model is more desirable. In this case, water molecules can be considered as individual molecules instead of a continuum in order to simulate a more realistic system. Parallel to

experimental studies, we would recommend the development of a transport model for ion separation by nanoporous membranes in electrosorption processes. The utilization of dynamic molecular modeling information will allow the enrichment of the thermodynamic and transport properties of electrolytes through pore channels. On the other hand, the model developed for transport properties of electrolytes for nanoporous materials under the influence of an electric field can provide insight into the design of better materials for use in separations.

REFERENCES

Allen, M. P.; Tildesley, D. J., *Computer simulation of liquid*, Oxford University Press, New York, **1987**.

Ania, C. O.; Pernak, J.; Stefaniak, F.; Raymundo-Pinero, E.; Beguin, F., Solvent-free ionic liquids as in situ probes for assessing the effect of ion size on the performance of electrical double layer capacitors, *Carbon* **2006**, 44, (14), 3126-3130, 2006.

Barbieri, O.; Hahn, M.; Herzog, A.; Kotz, R., Capacitance limits of high surface area activated carbons for double layer capacitors, *Carbon* **2005**, 43, (6), 1303-1310.

Biesheuvel, P. M.; van Soestbergen, M., Counterion volume effects in mixed electrical double layers, *Journal of Colloid and Interface Science* **2007**, 316, (2), 490-499.

Bird, R. B.; Stewart, W. E.; Lightfoot, E. N., *Transport phenomena*, Wiley, New York, **2002**.

Boda, D.; Chan, K. Y.; Henderson, D., Monte Carlo simulation of an ion-dipole mixture as a model of an electrical double layer, *Journal of Chemical Physics* **1998**, 109, (17), 7362-7371.

Boda, D.; Busath, D. D.; Henderson, D.; Sokolowski, S., Monte Carlo simulations of the mechanism for channel selectivity: The competition between volume exclusion and charge neutrality, *Journal of Physical Chemistry B* **2000**, 104, (37), 8903-8910.

Boda, D.; Fawcett, W. R.; Henderson, D.; Sokolowski, S., Monte Carlo, density functional theory, and Poisson-Boltzmann theory study of the structure of an electrolyte near an electrode, *Journal of Chemical Physics* **2002**, 116, (16), 7170-7176.

Boda, D.; Valisko, M.; Eisenberg, B.; Nonner, W.; Henderson, D.; Gillespie, D., The effect of protein dielectric coefficient on the ionic selectivity of a calcium channel, *Journal of Chemical Physics* **2006**, 125, 034901.

- Boda, D.; Valisko, M.; Eisenberg, B.; Nonner, W.; Henderson, D.; Gillespie, D., Combined effect of pore radius and protein dielectric coefficient on the selectivity of a calcium channel, *Physical Review Letters* **2007**, 98, 168102.
- Cervera, J.; Garcia-Morales, V.; Pellicer, J., Ion size effects on the electrokinetic flow in nanoporous membranes caused by concentration gradients, *Journal of Physical Chemistry B* **2003**, 107, (33), 8300-8309.
- Eliad, L.; Salitra, G.; Soffer, A.; Aurbach, D., Ion sieving effects in the electrical double layer of porous carbon electrodes: Estimating effective ion size in electrolytic solutions, *Journal of Physical Chemistry B* **2001**, 105, (29), 6880-6887.
- Eliad, L.; Pollak, E.; Levy, N.; Salitra, G.; Soffer, A.; Aurbach, D., Assessing optimal pore-to-ion size relations in the design of porous poly(vinylidene chloride) carbons for EDL capacitors, *Applied Physics a-Materials Science & Processing* **2006**, 82, (4), 607-613.
- Endo, M.; Maeda, T.; Takeda, T.; Kim, Y. J.; Koshiba, K.; Hara, H.; Dresselhaus, M. S., Capacitance and pore-size distribution in aqueous and nonaqueous electrolytes using various activated carbon electrodes, *Journal of the Electrochemical Society* **2001**, 148, (8), A910-A914.
- Farmer, J. C.; Bahowick, S. M.; Harrar, J. E.; Fix, D. V.; Martinelli, R. E.; Vu, A. K.; Carroll, K. L., Electrosorption of chromium ions on carbon aerogel electrodes as a means of remediating ground water, *Energy & Fuels* **1997**, 11, (2), 337-347.
- Farmer, J. C.; Fix, D. V.; Mack, G. V.; Pekala, R. W.; Poco, J. F., Capacitive deionization of NaCl and NaNO₃ solutions with carbon aerogel electrodes, *Journal of the Electrochemical Society* **1996**, 143, (1), 159-169.
- Frackowiak, E.; Beguin, F., Carbon materials for the electrochemical storage of energy in capacitors, *Carbon* **2001**, 39, (6), 937-950.
- Gabelich, C. J.; Tran, T. D.; Suffet, I. H., Electrosorption of inorganic salts from aqueous solution using carbon aerogels, *Environmental Science & Technology* **2002**, 36, (13), 3010-3019.
- Golub, D.; Soffer, A.; Oren, Y., The electrical double layer of carbon and graphite electrodes: 5. Specific interactions with simple ions, *Journal of Electroanalytical Chemistry* **1989**, 260, (2), 383-392.

- Goulding, D.; Hansen, J. P.; Melchionna, S., Size selectivity of narrow pores. *Physical Review Letters* **2000**, 85, (5), 1132-1135.
- Grahame, D. C., Differential capacity of mercury in aqueous sodium fluoride solutions: 1. Effect of concentration at 25 degrees, *Journal of the American Chemical Society* **1954**, 76, (19), 4819-4823.
- Greberg, H.; Kjellander, R., Charge inversion in electric double layers and effects of different sizes for counterions and coions, *Journal of Chemical Physics* **1998**, 108, (7), 2940-2953.
- Gryglewicz, G.; Machnikowski, J.; Lorenc-Grabowska, E.; Lota, G.; Frackowiak, E., Effect of pore size distribution of coal-based activated carbons on double layer capacitance, *Electrochimica Acta* **2005**, 50, (5), 1197-1206.
- Hamann, C. H.; Hamnett, A.; Vielstich, W., *Electrochemistry*, Wiley-VCH, New York, **1998**.
- Hou, C. H.; Liang, C. D.; Yiacoumi, S.; Dai, S.; Tsouris, C., Electrosorption capacitance of nanostructured carbon-based materials, *Journal of Colloid and Interface Science* **2006**, 302, (1), 54-61.
- Hou, C. H.; Taboada-Serrano, P.; Yiacoumi, S.; Tsouris, C., Monte Carlo simulation of electrical double-layer formation from mixtures of electrolytes inside nanopores, *Journal of Chemical Physics* **2008**, 128, 044705.
- Hribar, B.; Vlachy, V.; Bhuiyan, L. B.; Outhwaite, C. W., Ion distributions in a cylindrical capillary as seen by the modified Poisson-Boltzmann theory and Monte Carlo simulations, *Journal of Physical Chemistry B* **2000**, 104, (48), 11522-11527.
- Hu, Q. Y.; Kou, R.; Pang, J. B.; Ward, T. L.; Cai, M.; Yang, Z. Z.; Lu, Y. F.; Tang, J., Mesoporous carbon/silica nanocomposite through multi-component assembly, *Chemical Communications* **2007**, (6), 601-603.
- Hunter, R. J., *Foundations of Colloid Science*, second ed., Oxford University Press, New York, **2001**.

- Jamnik, B.; Vlachy, V., Monte Carlo and Poisson-Boltzmann study of electrolyte exclusion from charged cylindrical micropores, *Journal of the American Chemical Society* **1993**, 115, (2), 660-666.
- Jamnik, B.; Vlachy, V., Ion partitioning between charged micropores and bulk electrolyte solution: Mixtures of monovalent and divalent counterions and monovalent cations, *Journal of the American Chemical Society* **1995**, 117, (30), 8010-8016.
- Jirage, K. B.; Hulteen, J. C.; Martin, C. R., Nanotubule-based molecular-filtration membranes, *Science* **1997**, 278, (5338), 655-658.
- Johnson, A. M.; Newman, J., Desalting by means of porous carbon electrodes, *Journal of the Electrochemical Society* **1971**, 118, (3), 510-517.
- Karanfil, T.; Dastgheib, S. A.; Mauldin, D., Exploring molecular sieve capabilities of activated carbon fibers to reduce the impact of NOM preloading on trichloroethylene adsorption, *Environmental Science & Technology* **2006**, 40, (4), 1321-1327.
- Katakura, K.; Inaba, M.; Toyama, K.; Ogumi, Z.; Takehara, Z., Electrotransportation of aniline through a perfluorosulfonate ion-exchange membrane, *Journal of the Electrochemistry Society* **1994**, 141, (7), 1827-1831.
- Kathawalla, I. A.; Anderson, J. L.; Lindsey, J. S., Hindered diffusion of porphyrins and short-chain polystyrene in small pores, *Macromolecules* **1989**, 22, (3), 1215-1219.
- Kemery, P. J.; Steehler, J. K.; Bohn, P. W., Electric field mediated transport in nanometer diameter channels, *Langmuir* **1998**, 14, (10), 2884-2889.
- Kinoshita, K., *Carbon: Electrochemical and Physicochemical Properties*, Wiley, New York, **1988**.
- Koresh, J.; Soffer, A., Study of molecular-sieve carbons: 1. Pore structure, gradual pore opening and mechanism of molecular-sieving, *Journal of the Chemical Society-Faraday Transactions I* **1980**, 76, 2457-2471.
- Koresh, J.; Soffer, A., Stereoselectivity in ion electroadsorption and in double-layer charging of molecular-sieving carbon electrodes, *Journal of Electroanalytical Chemistry* **1983**, 147, (1-2), 223-234.

- Koresh, J. E.; Soffer, A., The carbon molecular-sieve membranes: General properties and the permeability of CH₄ and H₂ mixture, *Separation Science and Technology* **1987**, 22, (2-3), 973-982.
- Kuo, T. C.; Sloan, L. A.; Sweedler, J. V.; Bohn, P. W., Manipulating molecular transport through nanoporous membranes by control of electrokinetic flow: Effect of surface charge density and debye length, *Langmuir* **2001**, 17, (20), 6298-6303.
- Lamperski, S.; Bhuiyan, L. B., Counterion layering at high surface charge in an electric double layer: Effect of local concentration approximation. *Journal of Electroanalytical Chemistry* **2003**, 540, 79-87.
- Li, S.; Wang, X.; Beving, D.; Chen, Z. W.; Yan, Y. S., Molecular sieving in a nanoporous b-oriented pure-silica-zeolite MFI monocrystal film, *Journal of the American Chemical Society* **2004**, 126, (13), 4122-4123.
- Liang, C. D.; Dai, S.; Guiochon, G., A graphitized-carbon monolithic column, *Analytical Chemistry* **2003**, 75, (18), 4904-4912.
- Liang, C. D.; Dai, S., Synthesis of mesoporous carbon materials via enhanced hydrogen-bonding interaction, *Journal of the American Chemical Society* **2006**, 128, (16), 5316-5317.
- Liang, C. D.; Hong, K. L.; Guiochon, G. A.; Mays, J. W.; Dai, S., Synthesis of a large-scale highly ordered porous carbon film by self-assembly of block copolymers, *Angewandte Chemie-International Edition* **2004**, 43, (43), 5785-5789.
- Liang, C. D.; Li, Z.; Dai, S., Mesoporous carbon materials: synthesis and modification, *Angewandte Chemie-International Edition*. **2007**, DOI: 10. 1002/anie.200.
- Lin, C.; Ritter, J. A.; Popov, B. N., Correlation of double-layer capacitance with the pore structure of sol-gel derived carbon xerogels, *Journal of the Electrochemical Society* **1999**, 146, (10), 3639-3643.
- Lo, W. Y.; Chan, K. Y.; Lee, M.; Mok, K. L., Molecular simulation of electrolytes in nanopores, *Journal of Electroanalytical Chemistry* **1998**, 450, (2), 265-272.
- Lozadacassou, M., A new method of deriving electrical double-layer equations from electrolyte theories, *Journal of Chemical Physics* **1981**, 75, (3), 1412-1421.

- LozadaCassou, M.; Olivares, W.; Sulbaran, B., Violation of the electroneutrality condition in confined charged fluids, *Physical Review E* **1996**, 53, (1), 522-530.
- Lozadacassou, M.; Saavedrabarrera, R.; Henderson, D., The application of the hypernetted chain approximation to the electrical double-layer: Comparison with Monte Carlo results for symmetric salts, *Journal of Chemical Physics* **1982**, 77, (10), 5150-5156.
- Lu, Y. F., Surfactant-templated mesoporous materials: From inorganic to hybrid to organic, *Angewandte Chemie-International Edition* **2006**, 45, (46), 7664-7667.
- Martin, C. R.; Nishizawa, M.; Jirage, K.; Kang, M., Investigations of the transport properties of gold nanotubule membranes, *Journal of Physical Chemistry B* **2001**, 105, (10), 1925-1934.
- Martin-Molina, A.; Quesada-Perez, M.; Galisteo-Gonzalez, F.; Hidalgo-Alvarez, R., Probing charge inversion in model colloids: electrolyte mixtures of multi- and monovalent counterions, *Journal of Physics-Condensed Matter* **2003**, 15, (48), S3475-S3483.
- Martin-Molina, A.; Quesada-Perez, M.; Hidalgo-Alvarez, R., Electric double layers with electrolyte mixtures: Integral equations theories and simulations, *Journal of Physical Chemistry B* **2006**, 110, (3), 1326-1331.
- Matlosz, M.; Newman, J., Experimental investigation of porous carbon electrode for the removal of mercury from contaminated brine, *Journal of the Electrochemical Society* **1986**, 133, (9), 1850-1859.
- Meng, Y.; Gu, D.; Zhang, F. Q.; Shi, Y. F.; Yang, H. F.; Li, Z.; Yu, C. Z.; Tu, B.; Zhao, D. Y., Ordered mesoporous polymers and homologous carbon frameworks: Amphiphilic surfactant templating and direct transformation, *Angewandte Chemie-International Edition* **2005**, 44, (43), 7053-7059.
- Nishizawa, M.; Menon, V. P.; Martin, C. R., Metal nanotubule membranes with electrochemically switchable ion-transport selectivity, *Science* **1995**, 268, (5211), 700-702.
- Oren, Y.; Soffer, A., Water desalting by means of electrochemical parametric pumping: 1. The equilibrium properties of a batch unit-cell, *Journal of Applied Electrochemistry* **1983**, 13, (4), 473-487.

- Pekala, R. W.; Farmer, J. C.; Alviso, C. T.; Tran, T. D.; Mayer, S. T.; Miller, J. M.; Dunn, B., Carbon aerogels for electrochemical applications, *Journal of Non-Crystalline Solids* **1998**, 225, (1), 74-80.
- Qu, D. Y.; Shi, H., Studies of activated carbons used in double-layer capacitors, *Journal of Power Sources* **1998**, 74, (1), 99-107.
- Quesada-Perez, M.; Martin-Molina, A.; Hidalgo-Alvarez, R., Simulation of electric double layers with multivalent counterions: Ion size effect, *Journal of Chemical Physics* **2004**, 121, (17), 8618-8626.
- Quesada-Perez, M.; Martin-Molina, A.; Hidalgo-Alvarez, R., Simulation of electric double layers undergoing charge inversion: Mixtures of mono- and multivalent ions, *Langmuir* **2005**, 21, (20), 9231-9237.
- Raymundo-Pinero, E.; Kierzek, K.; Machnikowski, J.; Beguin, F., Relationship between the nanoporous texture of activated carbons and their capacitance properties in different electrolytes, *Carbon* **2006**, 44, (12), 2498-2507.
- Renkin, E. M., Filtration, diffusion, and molecular sieving through porous cellulose membranes, *Journal of General Physiology* **1954**, 38, (2), 225-243.
- Rodriguez, A. T.; Chen, M.; Chen, Z.; Brinker, C. J.; Fan, H. Y., Nanoporous carbon nanotubes synthesized through confined hydrogen-bonding self-assembly, *Journal of the American Chemical Society* **2006**, 128, (29), 9276-9277.
- Roth, R.; Gillespie, D., Physics of size selectivity, *Physical Review Letters* **2005**, 95, 247801.
- Salitra, G.; Soffer, A.; Eliad, L.; Cohen, Y.; Aurbach, D., Carbon electrodes for double-layer capacitors - I. Relations between ion and pore dimensions, *Journal of the Electrochemical Society* **2000**, 147, (7), 2486-2493.
- Schmuhl, R.; Keizer, K.; van den Berg, A.; ten Elshof, J. E.; Blank, D. H. A., Controlling the transport of cations through permselective mesoporous alumina layers by manipulation of electric field and ionic strength, *Journal of Colloid and Interface Science* **2004**, 273, (1), 331-338.

- Shi, H., Activated carbons and double layer capacitance, *Electrochimica Acta* **1996**, 41, (10), 1633-1639.
- Snyder, M. A.; Tsapatsis, M., Hierarchical nanomanufacturing: From shaped zeolite nanoparticles to high-performance separation membranes, *Angewandte Chemie-International Edition* **2007**, 46, (40), 7560-7573.
- Steinhart, M.; Liang, C. D.; Lynn, G. W.; Gosele, U.; Dai, S., Direct synthesis of mesoporous carbon microwires and nanowires, *Chemistry of Materials* **2007**, 19, (10), 2383-2385.
- Taboada-Serrano, P.; Yiacoymi, S.; Tsouris, C., Behavior of mixtures of symmetric and asymmetric electrolytes near discretely charged planar surfaces: A Monte Carlo study, *Journal of Chemical Physics* **2005**, 123, (5).
- Tanaka, S.; Nishiyama, N.; Egashira, Y.; Ueyama, K., Synthesis of ordered mesoporous carbons with channel structure from an organic-organic nanocomposite, *Chemical Communications* **2005**, (16), 2125-2127.
- Taylor, R.; Krishna, R., *Multicomponent Mass Transfer*, Wiley, New York, **1993**.
- Torrie, G. M.; Valleau, J. P., Monte Carlo study of an electrical double-layer, *Chemical Physics Letters* **1979**, 65, (2), 343-346.
- Torrie, G. M.; Valleau, J. P., Electrical double layers: 1. Monte Carlo study of a uniformly charged surface, *Journal of Chemical Physics* **1980**, 73, (11), 5807-5816.
- Torrie, G. M.; Valleau, J. P.; Patey, G. N., Electrical double layers: 2. Monte Carlo and HNC studies of image effects, *Journal of Chemical Physics* **1982**, 76, (9), 4615-4622.
- Torrie, G. M.; Valleau, J. P., Electrical double layers: 4. Limitation of the Gouy-Chapman theory, *Journal of Physical Chemistry* **1982**, 86, (16), 3251-3257.
- Valisko, M.; Boda, D., Selective adsorption of ions with different diameter and valence at highly charged interfaces, *Journal of Physical Chemistry C* **2007**, 111, (43), 15575-15585.

- Valisko, M.; Henderson, D.; Boda, D., Competition between the effects of asymmetries in ion diameters and charges in an electrical double layer studied by Monte Carlo simulations and theories, *Journal of Physical Chemistry B* **2004**, 108, (42), 16548-16555.
- Valleau, J. P.; Cohen, L. K., Primitive model electrolytes: 1. Grand canonical Monte Carlo computations, *Journal of Chemical Physics* **1980**, 72, (11), 5935-5941.
- Valleau, J. P.; Torrie, G. M., The electrical double layer: 3. Modified Gouy-Chapman theory with unequal ion sizes, *Journal of Chemical Physics* **1982**, 76, (9), 4623-4630.
- van Megen, W.; Snook, I., The grand canonical ensemble Monte Carlo method applied to the electrical double layer, *Journal of Chemical Physics* **1980**, 73, (9), 4656-4662.
- Vlachy, V., Ion-partitioning between charged capillaries and bulk electrolyte solution: An example of negative "rejection", *Langmuir* **2001**, 17, (2), 399-402.
- Vlachy, V.; Haymet, A. D. J., Electrolyte in charged micropores, *Journal of the American Chemical Society* **1989**, 111, (2), 477-481.
- Vlachy, V.; Haymet, A. D. J., Salt exclusion from charged and uncharged micropores, *Journal of Electroanalytical Chemistry* **1990**, 283, (1-2), 77-85.
- Wang, J.; Angnes, L.; Tobias, H.; Roesner, R. A.; Hong, K. C.; Glass, R. S.; Kong, F. M.; Pekala, R. W., Carbon aerogel composite electrodes, *Analytical Chemistry* **1993**, 65, (17), 2300-2303.
- Weetman, P.; Goldman, S.; Gray, C. G., Use of the Poisson-Boltzmann equation to estimate the electrostatic free energy barrier for dielectric models of biological ion channels, *Journal of Physical Chemistry B* **1997**, 101, (31), 6073-6078.
- Wirtz, M.; Parker, M.; Kobayashi, Y.; Martin, C. R., Molecular sieving and sensing with gold nanotube membranes, *Chemical Record* **2002**, 2, (4), 259-267.
- Yamaguchi, A.; Uejo, F.; Yoda, T.; Uchida, T.; Tanamura, Y.; Yamashita, T.; Teramae, N., Self-assembly of a silica-surfactant nanocomposite in a porous alumina membrane, *Nature Materials* **2004**, 3, (5), 337-341.

- Yang, K. L.; Yiacoumi, S.; Tsouris, C., Monte Carlo simulations of electrical double layer formation in nanopores, *Journal of Chemical Physics* **2002**, 117, (18), 8499-8507.
- Yang, K. L.; Yiacoumi, S.; Tsouris, C., Electrosorption capacitance of nanostructured carbon aerogel obtained by cyclic voltammetry, *Journal of Electroanalytical Chemistry* **2003**, 540, 159-167.
- Yang, K. L.; Ying, T. Y.; Yiacoumi, S.; Tsouris, C.; Vittoratos, E. S., Electrosorption of ions from aqueous solutions by carbon aerogel: An electrical double-layer model, *Langmuir* **2001**, 17, (6), 1961-1969.
- Ying, T. Y.; Yang, K. L.; Yiacoumi, S.; Tsouris, C., Electrosorption of ions from aqueous solutions by nanostructured carbon aerogel, *Journal of Colloid and Interface Science* **2002**, 250, (1), 18-27.
- Yoon, S.; Lee, J. W.; Hyeon, T.; Oh, S. M., Electric double-layer capacitor performance of a new mesoporous carbon, *Journal of the Electrochemical Society* **2000**, 147, (7), 2507-2512.
- Yu, S. F.; Lee, S. B.; Kang, M.; Martin, C. R., Size-based protein separations in poly(ethylene glycol)-derivatized gold nanotubule membranes, *Nano Letters* **2001**, 1, (9), 495-498.

VITA

CHIA-HUNG HOU was born on March 20, 1976 in Taipei, Taiwan. He received a Bachelor of Science degree in Civil Engineering from the National Taiwan University, Taipei, Taiwan in 1998, and a Master of Science degree in Environmental Engineering from the National Taiwan University, Taipei, Taiwan in 2000. In Fall 2003, he joined the Georgia Institute of Technology, Atlanta, GA to pursue a doctorate in Environmental Engineering. In Spring 2004, the author joined the research group of Dr. Sotira Yiacoumi with a research focusing on advanced separation technologies at the nanoscale of environmental systems. The author completed his Ph.D. degree in March 2008.